# MICROSCOPIC STUDY OF THE HIGH – SPIN YRAST SPECTRA OF SOME DOUBLY EVEN NUCLEI IN THE MASS 60 TO 110 REGION IN A VARIATIONAL FRAMEWORK

*By*

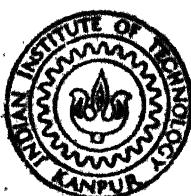PRAKASH NARAYAN TRIPATHI

PHY

1984

D

TRI

Mic

TH
PHY/1984/D
T738m

# MICROSCOPIC STUDY OF THE HIGH – SPIN YRAST SPECTRA OF SOME DOUBLY EVEN NUCLEI IN THE MASS 60 TO 110 REGION IN A VARIATIONAL FRAMEWORK

A Thesis Submitted
In Partial Fulfilment of the Requirements
for the Degree of

## DOCTOR OF PHILOSOPHY

*By*

PRAKASH NARAYAN TRIPATHI

*to the*

DEPARTMENT OF PHYSICS
INDIAN INSTITUTE OF TECHNOLOGY, KANPUR
JANUARY, 1984

PHY - 1984 - D - TRI-MIC

To

My Parents

# CERTIFICATE

Certified that the work presented in this thesis entitled, "Microscopic Study of the High-Spin Yrast Spectra of Some Doubly Even Nuclei in the Mass 60 to 110 Region in a Variational Framework", by Mr Prakash Narayan Tripathi has been carried out under my supervision and that this has not been submitted elsewhere for a degree.

January, 1984.

                              (S.K.SHARMA)
                           Assistant Professor
                          Department of Physics
                  Indian Institute of Technology, Kanpur
                          KANPUR-16 (India)

## ACKNOWLEDGEMENT

# TABLE OF CONTENTS

LIST OF TABLES

LIST OF FIGURES

# SYNOPSIS

P.N.TRIPATHI

Ph.D. (Physics)

Indian Institute of Technology Kanpur

JANUARY 1984

## MICROSCOPIC STUDY OF THE HIGH-SPIN YRAST SPECTRA OF SOME DOUBLY EVEN NUCLEI IN THE MASS 60 TO 110 REGION IN A VARIATIONAL FRAMEWORK

One of the important frontiers in nuclear research is the extension of our knowledge of the structure of nuclei to higher spins. In recent years the in-beam gamma-ray spectroscopy following heavy ion induced reactions has provided a wealth of experimental data regarding the spectroscopic properties of the Yrast bands (with $J^{\pi}_{max} = 16^{+}$) of a large number of nuclei in the mass range $A = 60-110$. The increased activity on the experimental side has triggered a large number of theoretical attempts. Apart from the usual shell model configuration mixing calculations which have been carried out for some light Ge isotopes, attempts have also been made to elucidate the structure of the levels in the Ge, Se and Kr isotopes by invoking the collective model as well as by coupling the valence particles and the collective excitations.

The various models, however, have been applied to specific nuclei and do not cover completely the doubly even

isotopes of Ge, Se, Kr and Sr. Further, arbitrary choices of the input parameters as well as the set of approximations involved have more often than not resulted in theoretical schemes which contradict each other.

It thus appears worthwhile to have a consistent description in the framework of a microscopic model involving a reasonably large configuration space in conjunction with realistic effective interactions. Further, it seems necessary to invoke a calculational procedure which not only permits a treatment of the pairing and the deformation degrees of freedom on the same footing but also allows for the possibility of having different intrinsic deformations for the various members of the Yrast cascade. The latter feature is necessitated by the fact that the observed excitation energies of the higher members $(J^{\pi} > 6^{+})$ of the Yrast cascades in a number of doubly even isotopes of Ge, Se and Kr display significant deviations from the $J(J+1)$-law.

A parameter-free, microscopic description of the Yrast states in the doubly even Ge, Se, Kr, Sr and Mo isotopes is the main theme of the present work; the approach followed here satisfies the criteria just mentioned.

Chapter I presents a survey of the existing experimental information. It also contains an overview of the various theoretical attempts that have been made in the recent past to elucidate the structure of the low-lying levels in the A=60-90 region.

In Chapters II and III we examine the high-spin Yrast levels in the nuclei $^{68-74}$Ge, $^{72-78}$Se, $^{74-82}$Kr and $^{80-84}$Sr in the framework of the variation-after-projection (VAP) method in conjunction with the Hartree-Fock-Bogoliubov (HFB) ansatz for the trial wavefunctions. Whereas the HFB form of the wavefunction permits a consistent treatment of the pairing and deformation effects, the VAP method helps in selecting the optimum intrinsic state for each J by minimizing the relevant projected energy. The calculations employ a valence space spanned by the $2p_{3/2}$, $2p_{1/2}$, $1f_{5/2}$ and $1g_{9/2}$ orbits. The doubly closed nucleus $^{56}$Ni is treated as an inert core. The relevant effective two-body interaction that we have employed is a renormalized G matrix due to Kuo which is the sum of $G_{bare}$, $G_{3p-1h}$, and $G_{2p-2h}$ in the $^{56}$Ni core. We have presented an extensive comparison of the theoretical Yrast spectra, static quadrupole moments as well as the inter-cascade E2 transition strengths with the available experimental results. The overall agreement between the observed and the calculated results is reasonably good. The results for the calculation of the occupation numbers of the various subshells involved in the ground states of the Ge and Se isotopes are also presented and compared with the transfer reaction data obtained from the studies of (d,p), (d,n), (p,d), and (t,$\alpha$) reactions. The study reveals that the observed large deviations from the quasi-rotational behaviour can be related, in most of the cases, to a systematic variation of the intrinsic quadrupole deformations along the Yrast cascade.

A new region of deformation has some time ago been discovered around mass number A=100; well-developed quasi-rotational spectra were observed in several highly neutron-rich isotopes (A >100) ·of Zr and Mo during a study of the fission fragments of $^{252}$Cf. The observed B(E2; $0^+ \rightarrow 2^+$) values were as enhanced as in the rare-earth and the actinide regions.

In Chapter IV we present a first-ever microscopic study of the quasirotational spectra in the isotopes $^{100-106}$Mo in the framework of the VAP method. Here we have employed the usual pairing-plus-quadrupole-quadrupole effective interactions operating in a valence space spanned by the $2p_{1/2}$, $3s_{1/2}$, $2d_{3/2}$, $2d_{5/2}$, $1g_{7/2}$, $1g_{9/2}$ and $1h_{11/2}$ orbits for protons as well as for neutrons. The nucleus $^{76}$Sr (N=Z=38) has been considered as an inert core. The calculated intrinsic quadrupole moments of the HFB states in the isotopes $^{94-102}$Zr and $^{92-106}$Mo are consistent with the observed deformation systematics. Further, the VAP spectra for the isotopes $^{102-106}$Mo are in reasonable agreement with the experiments. The self-consistent HFB wave-functions also explain satisfactorily the available B(E2;$0^+ \rightarrow 2^+$) values in a number of Mo isotopes provided reasonable effective charges ($1.35 \lesssim e_p < 1.50$, $0.35, < e_n < 0.50$) are used. The calculation reveals a number of interesting features associated with the observed phase transition in the Mo isotopes at A=102. The results indicate unambiguously that, in sharp contrast with the suggestions made in a number of recent investigations, the

onset of large deformations in the A > 100 nuclei in the Zr region is <u>not</u> compatible with the usual assumption of an inert $^{94}$Sr core. The role of the $1h_{11/2}$ orbit vis-a-vis the occurrence of large deformations in the heavier Mo isotopes is examined. The present work also suggests strongly the interesting possibility of observing the backbending effect in the nuclei $^{102-106}$Mo.

# CHAPTER I

## INTRODUCTION

Nuclei around the A ~ 70 mass region have attracted the attention of a large number of experimental groups in recent years[1-19]. Much of the nuclear structure information has been obtained through in-beam gamma-ray spectroscopy experiments with heavy ions ($A > \alpha$ -particle). The experiments have revealed a large number of highly collective band structures of the following types: (i) high-spin yrast bands, (ii) one or two even-spin, positive-parity bands with $8^+$ as band head, (iii) odd- and even-spin negative-parity bands, (iv) $\Delta J=1$ even-parity bands with $2^+$ as band heads, and (v) deformed bands built on the excited $0^+$ states.

A large number of theoretical calculations[20-23] involving microscopic as well as phenomenological models have recently been attempted to elucidate the structure of the low-lying levels in the A ~ 70 region. The complexity of the structure of the levels in this region arises from the fact that many protons and neutrons are distributed among several subshells without strong closure properties, between the well-established magic numbers 28 and 50. The relatively large number of valence particles and of possible configurations makes exact shell model calculations difficult. Recent theoretical studies have been carried out in the framework of the

shell model involving truncated configurational spaces, Hartree-Fock (HF) and Hartree-Fock-Bogoliubov (HFB) methods, collective phenomenological models, as well as models involving coupling of the single-particle and the collective excitations.

Most of the recent theoretical studies[20] have sought to examine the structure of the non-yrast bands and the anomalous excited $0^+$ levels. The available high-spin yrast spectra (with $J^{\pi}_{max} = 16^+$) have been studied mostly in the framework of phenomenological models such as the Interacting Boson Model[21-23]. Further, these models have been applied for specific nuclei and do not cover completely the doubly even isotopes of Ge, Se, Kr and Sr.

In Chapters II and III we present a microscopic description of the observed high-spin yrast levels in sixteen isotopes of Ge, Se, Kr and Sr in the mass range A=68-84. The high-spin yrast levels have been studied by selecting intrinsic states appropriate for each J by minimizing the expectation value of the Hamiltonian with respect to the states of definite angular momenta projected from HFB intrinsic states. The effective two-body interaction that we have employed is a G matrix due to Kuo[24] which is the sum of $G_{bare}$, $G_{3p-1h}$ and $G_{4p-2h}$ in the $^{56}Ni$ core. The calculations employ a valence space spanned by the $2p_{3/2}$, $2p_{1/2}$, $1f_{5/2}$ and $1g_{9/2}$ orbits.

The observed excitation energies of the higher
members ($J^\pi \geq 6^+$) of the yrast bands in most of the isotopes
of Ge, Se, Kr and Sr display significant deviations from the
$J(J+1)$-law. The calculational procedure employed in the
present work includes the possibility of large structural
changes along the yrast cascade. The use of the HFB ansatz
for the trial wavefunctions permits a consistent treatment
of the pairing and the deformation degrees of freedom.

The calculations presented in Chapters II and III
demonstrate that the variation-after-(angular momentum)
projection (VAP) technique, in conjunction with the HFB
ansatz for the trial wavefunctions, provides a reasonably
successful microscopic framework for correlating and inter-
preting the available data on the yrast energies, intercascade
E2 transition strengths as well as the subshell occupation
numbers.

A new island of large deformations around A=100 has
sometime ago been reported by Cheifetz et al.[25]  Well-
developed yrast spectra were observed in several highly
neutron-rich isotopes of Zr and Mo. The reduced transition
probabilities for E2 transitions between the yrast levels were
as large as in the rare-earth and the actinide regions.  In
Chapter IV we have studied the observed yrast spectra in the
isotopes $^{100,102,104,106}$Mo in the framework of the VAP
prescription.  We have employed the usual pairing-plus-
quadrupole-quadrupole interaction operating in a valence space

spanned by the $2p_{1/2}$, $3s_{1/2}$, $2d_{3/2}$, $2d_{5/2}$, $1g_{7/2}$, $1g_{9/2}$ and $1h_{11/2}$ orbits for protons as well as neutrons. The calculations[26] bring out the role of the $1h_{11/2}$ orbit vis-á-vis the observed dramatic onset of large deformations at A=100. Further, our VAP study of the yrast spectra suggests strongly the possibility of observing the backbending phenomenon in $^{102}$Mo.

Finally, in Chapter V we summarize the results obtained in, and wisdom gained from Chapters II, III and IV.

## REFERENCES

1. C.Morand et al., Phys. Rev. C13 (1976) 2182.

2. K.P. Lieb and J.J.Kolata, Phys. Rev. C15 (1977) 939.

3. A.P.de Lima et al., Phys. Lett. 83B (1979) 43.

4. C.Morand et al., Nucl. Phys. A313 (1979) 45.

5. C.Lebrum et al., Phys. Rev. C19 (1979) 1294.

6. R.B.Piercey et al., Phys. Rev. C19 (1979) 1344.

7. J.C.Wells, Jr., et al., Phys. Rev. C22 (1980) 126.

8. A.P. de Lima et al., Phys. Rev. C23 (1981) 23.

9. T.Matsuzaki and H.Taketani, Nucl. Phys. A390 (1982) 413.

10. R.B.Piercey, et al., Phys. Rev. Lett. 47 (1981) 1514;
    Phys. Rev. C25 (1982) 1941.

11. S.Matsuki et al., Nucl. Phys. A370 (1981) 1.

12. H.P.Hellmeister et al., Nucl. Phys. A332 (1979) 241;
    Phys. Lett. B85 (1979) 34.

13. L.Funke et al., Nucl. Phys. A355 (1981) 328.

14. D.L.Sastry et al., Phys. Rev. C23 (1981) 2086.

15. C.M.Cartwright et al., J. Phys. G7 (1981) 65.

16. C.A.Fields, F.W.N. De-Boer, E.Sugerbaker and P.M.Walker,
    Nucl. Phys. A363 (1981) 352.

17. C.J.Lister, B.J.Varley, H.G.Price and J.W.Olness,
    Phys. Rev. Lett. 49 (1982) 308.

18. T.Higo, S.Matsuki and T.Yanabu, Nucl. Phys. A393 (1983) 224.

19. A.Dewald et al., Phys. Rev. C25 (1982) 226.

20. M.Vergnes, in Proceedings of the Conference on the
    Structure of Medium-heavy Nuclei, Rhodes, 1979,
    edited by the 'Demokritos' Tandem Acclerator Group,
    Athens (Institute of Physics, Bristol, 1980) p.25,
    and the references contained therein.

21. U.Kaup and A.Gelberg, Z. Phys. A293 (1979) 311.

22. D.Bucurescu et al., Nucl. Phys. A401 (1983) 22.

23. R.Soundranayagam et al., Phys. Rev. C25 (1982) 2983.

24. T.T.S.Kuo, private communication to Professor K.H.Bhatt.

25. E.Cheifetz et al., Phys. Lett. 25 (1970) 38.

26. S.K.Khosa, P.N.Tripathi and S.K.Sharma, Phys. Lett. 119B (1982) 257.

# CHAPTER II

## HIGH-SPIN YRAST SPECTRA IN DOUBLY EVEN GERMANIUM
## AND SELENIUM ISOTOPES

## II.1 Introduction

The high-spin yrast spectra (with $J^\pi = 16^+$) in doubly
even Ge and Se isotopes have been the subject of a large number
of recent experimental studies[1-9] involving in-beam gamma-ray
spectroscopy.

The increased activity on the experimental side has
triggered a large number of theoretical studies which have
attempted a description of mostly the low-lying ($J^\pi \leq 6^+$) levels
in Ge and Se. These studies have been carried out in the frame-
work of the usual shell model[10] involving restricted configura-
tion mixing, self-consistent Hartree-Fock (HF) and Hartree-
Fock-Bogoliubov[11] (HFB) methods employing the Skyrme-3 as well
as the Gogny effective interactions[12], collective models[13,14]
as well as models involving an interweaving of the single-
particle and the collective modes[15-17]. Most of these investi-
gations have sought to examine the structure of the anomalous
excited $0^+$ levels in doubly even Ge and Se isotopes. These
calculations have been recently reviewed by Vergnes[18].

In contrast to the large-scale effort that has been
made to elucidate the structure of the low-lying states in the
Ge and Se isotopes, only a few calculations[2,6]— and these

involve phenomenological models such as the Interacting Boson Model (IBM) - presently exist as far as the yrast levels with $6^+ \leq J^\pi \leq 16^+$ are concerned. Further, these studies have been carried out for specific nuclei and do not cover completely the even-even isotopes of Ge and Se. A lack of microscopic descriptions involving the same calculational framework for various nuclei has prevented a clear understanding of the high-spin members of the yrast bands.

The available data on the high-spin yrast states in the nuclei $^{68,70,72,74}$Ge and $^{72,74,76,78}$Se suggests certain requirements that a consistent microscopic description of these isotopes must satisfy.

An important feature that characterizes the available data on Ge and Se isotopes is the indication concerning shape transition at N=40. A comparison of the (p,t) and (t,p) reactions on Ge isotopes (with N=36-40) by Vergnes et al.[19] suggests dramatic structural changes around N=40. This is also supported by a measurement of the ratio $[B(E2,4^+ \to 2^+)/B(E2, 2^+ \to 0^+)]$ by Lecomte et al.[20,21]; the ratio increases sharply in going from $^{70}$Ge to $^{72}$Ge. Since the onset of deformation at N=40 is expected to result from an excitation of nucleon pairs from 2p-1f Nilsson orbitals to $1g_{9/2\pm1/2}$ orbitals, it seems essential to invoke a calculational procedure which permits an interplay of the pairing and the deformation effects.

The observed excitation energies of the high-spin yrast levels in a number of doubly even Ge and Se isotopes show significant deviation from the $J(J+1)$-law. Thus the observed[6] yrast levels (with $J^{\pi}_{max} = 14^+$) in $^{72}$Se can be described reasonably well-with an average energy deviation of 29 keV-by the expression $(E_J - E_0) = (\hbar^2/2I) J(J+1) + a\, J^2 (J+1)^2$, where $(\hbar^2/2I) = 36.8 \pm 0.2$ keV and $a = -37 \pm 1$ eV. The yrast spectrum[7,22] (with $J^{\pi}_{max} = 16^+$) in $^{74}$Se translates into an $I$-$\omega^2$ curve that shows a break at $J^{\pi} = 10^+$. In view of these features, it seems essential to incorporate in the microscopic description the possibility of having different intrinsic states for various members of the yrast cascade.

The parameter-free microscopic description of the yrast levels in the nuclei $^{68,70,72,74}$Ge and $^{72,74,76,78}$Se presented in this Chapter satisfies the criteria just mentioned. We have examined the high-spin yrast levels in the framework of the variation-after-projection (VAP) technique in conjunction with the Hartree-Fock-Bogoliubov (HFB) ansatz[23] for the trial wavefunctions. Whereas the HFB form of the wavefunction permits a consistent treatment of the pairing and deformation degrees of freedom on the same footing, the VAP procedure helps in selecting an appropriate intrinsic state for each J through a minimization of the expectation value of the Hamiltonian with respect to the states of good angular momenta.

In section II.2 we present the calculational framework. Section II.3 contains an extensive comparison of the calculated

yrast spectra, static quadrupole moments as well as the intercascade E2 transition strengths with the available experimental results. The results for the calculation of sub-shell occupation numbers associated with the ground states of the Ge and Se isotopes are also presented and compared with the experimental values obtained by Rotbard et al.[24] It turns out that the observed large departures of the yrast energies as well as E2 transition strengths from the predictions based on the rotational model can be related, in most of the cases, to a systematic variation of the quadrupole deformation of the intrinsic states along the yrast cascade. Finally, section II.4 contains some concluding remarks.

## II.2  Calculational Framework

### II.2.1  The Hartree-Fock-Bogoliubov (HFB) Method

Consider the shell model Hamiltonian of the nucleus under consideration

$$H = \sum_{\alpha} <\alpha|\varepsilon|\alpha> \; C_{\alpha}^{\dagger} C_{\alpha} + (1/4) \sum_{\alpha\beta\gamma\delta} < \alpha\beta \; | V_A | \; \gamma\delta > \; C_{\alpha}^{\dagger} C_{\beta}^{\dagger} C_{\delta} C_{\gamma}$$

$$(II.1)$$

where $\varepsilon_{\alpha}$ are the spherical single-particle energies and $< \alpha\beta |V_A| \gamma\delta >$ is the antisymmetrized matrix element of an effective interaction. Here $C_{\alpha}^{\dagger}$ ($C_{\alpha}$) is the creation (annihilation) operator in the spherical basis $|\alpha>$. We wish to obtain a transformation from particle coordinates to quasiparticle coordinates such that the quasiparticles are relatively weakly

interacting:

$$H = E_o + H_{qp} + H_{qp-int} \qquad (II.2)$$

where $E_o$ is the energy of the quasiparticle vacuum, $H_{qp}$ describes the elementary quasiparticle excitations, and $H_{qp-int}$ is a (hopefully) weak interaction between the quasiparticles.

The Hamiltonian $(E_o + H_{qp})$ may not, in general, preserve all the symmetries of H. In HFB one imposes constraints via the use of Lagrange multipliers such that some of the observables possess desired expectation values. More specifically, we have

$$H' = H - \lambda_\pi N_\pi - \lambda_\nu N_\nu \qquad (II.3)$$

where the Lagrange multipliers are chosen so that the number operators $N_\pi = \sum_\alpha C_{\alpha\pi}^\dagger C_{\alpha\pi}$ and $N_\nu = \sum_\alpha C_{\alpha\nu}^\dagger C_{\alpha\nu}$ possess the expectation values

$$< \Phi_o | N_\pi | \Phi_o > = Z, \quad < \Phi_o | N_\nu | \Phi_o > = A-Z \qquad (II.4)$$

In the HFB theory one considers the general Bogoliubov transformation

$$q_\alpha^\dagger = \sum_\beta (U_{\alpha\beta} C_\beta^\dagger + V_{\alpha\beta} C_\beta) \qquad (II.5)$$

Here U and V are NxN complex matrices in a basis spanned by N single-particle states. The 2Nx2N linear transformation

$$\begin{pmatrix} q^\dagger \\ q \end{pmatrix} = \begin{pmatrix} U & V \\ V^* & U^* \end{pmatrix} \begin{pmatrix} C^\dagger \\ C \end{pmatrix} \qquad (II.6)$$

is unitary. Writing

$$M = \begin{bmatrix} U & V \\ V^* & U^* \end{bmatrix} \tag{II.7}$$

the unitarity conditions $MM^\dagger = M^\dagger M = I$ lead to the relations

$$UU^\dagger + VV^\dagger = U^\dagger U + \tilde{V} V^* = I; \quad U \tilde{V} + V\tilde{U} = U^\dagger V + \tilde{V} U^* = 0, \tag{II.8}$$

where $U^\dagger, \tilde{U}$ and $U^*$ denote, respectively, the adjoint, transpose and the complex conjugate of the operator $U$. Since $M^{-1} = M^\dagger$, we can invert the relations (II.5):

$$C_\alpha^\dagger = \sum_\beta (U_{\beta\alpha}^* q_\beta^\dagger + V_{\beta\alpha} q_\beta) \tag{II.9}$$

The quasiparticle vacuum is defined through the condition

$$q_\alpha \mid \Phi_0 > = 0 \quad (\text{all } \alpha) \tag{II.10}$$

Thus a solution to above equation is

$$\mid \Phi_0 > = (\text{normalization}) \cdot \prod_\alpha q_\alpha \mid 0 > \tag{II.11}$$

where $\mid 0 >$ is the particle vacuum.

## Derivation of the HFB equations by the "equations-of-motion" method[23]

The density matrix $\rho$ and the pairing tensor $t$ are defined in terms of the expectation values of the operators $C_\beta^\dagger C_\alpha$ and $C_\beta C_\alpha$ respectively, with respect to the quasiparticle vacuum given by equation (II.10):

$$\rho_{\alpha\beta} = <\Phi_0 \mid C_\beta^\dagger C_\alpha \mid \Phi_0>; \quad t_{\alpha\beta} = <\Phi_0 \mid C_\beta C_\alpha \mid \Phi_0> \quad \text{(II.12)}$$

From the anticommutation relations for $C_\alpha$'s, it follows that $\rho$ is Hermitian and $t$ is antisymmetric. One can easily evaluate $\rho$ and $t$ by using $M^{-1}$ to convert $C$'s into $q$'s, in conjunction with the condition (II.10). Thus we have

$$\rho_{\alpha\beta} = <\Phi_0 \mid C_\beta^\dagger C_\alpha \mid \Phi_0>$$

$$= <\Phi_0 \mid (\sum_\gamma U_{\gamma\beta}^* q_\gamma^\dagger + V_{\gamma\beta} q_\gamma)(\sum_\delta V_{\delta\alpha}^* q_\delta^\dagger + U_{\delta\alpha} q_\delta) \mid \Phi_0>$$

$$= \sum_\gamma \sum_\delta V_{\gamma\beta} V_{\delta\alpha}^* \delta_{\gamma\delta} = \sum_\delta V_{\delta\beta} V_{\delta\alpha}^* = (V^\dagger V)_{\alpha\beta} \quad \text{(II.13)}$$

Here we have used the anticommutation relations
$$[q_\alpha^\dagger, q_\beta] = \delta_{\alpha\beta}, [q_\alpha^\dagger, q_\beta^\dagger] = [q_\alpha, q_\beta] = 0.$$
In a similar manner we can show that

$$t = V^\dagger U \quad \text{(II.14)}$$

As a next step, we apply Wick's theorem to replace the products of operators appearing in $H'$ by the sum of normal products containing all possible contractions. (A normal product $: C_1^\dagger C_2^\dagger \ldots C_N^\dagger :$ of particle operators is obtained by first writing these operators in terms of $q^\dagger$'s and $q$'s, and then ordering them so that the creation operators are to the left of the annihilation operators. A sign $(-1)^p$ is included where $p$ is the number of permutations to go from the original to normal ordering sequence). We then obtain

$$H' = H_0' + H_2' + H_4' \qquad \text{(II.15)}$$

where $H_n'$ involves n uncontracted operators:

$$H_0' = \text{tr}[(\varepsilon - \lambda_\pi N_\pi - \lambda_\nu N_\nu + \tfrac{1}{2}\Gamma)\rho + \tfrac{1}{2}\Delta t^\dagger] \qquad \text{(II.16)}$$

$$H_2' = \sum_{\alpha\beta} (h - \lambda_\pi N_\pi - \lambda_\nu N_\nu)_{\alpha\beta} : C_\alpha^\dagger C_\beta :$$

$$+ \tfrac{1}{2} \sum_{\alpha\beta} \Delta_{\alpha\beta} : C_\alpha^\dagger C_\beta^\dagger : + \tfrac{1}{2} \sum_{\alpha\beta} \Delta_{\alpha\beta}^\dagger : C_\alpha C_\beta :$$

$$\text{(II.17)}$$

$$H_4' = (1/4) \sum_{\alpha\beta\gamma\delta} \langle \alpha\beta | V_A | \gamma\delta \rangle \ : C_\alpha^\dagger C_\beta^\dagger C_\delta C_\gamma : \qquad \text{(II.18)}$$

Here the HF Hamiltonian h, the HF potential $\Gamma$, and the pair potential $\Delta$ are given as

$$h = \varepsilon + \Gamma, \quad \Gamma_{\alpha\beta} = \sum_{\gamma\delta} \langle \alpha\gamma | V_A | \beta\delta \rangle \rho_{\delta\gamma} \qquad \text{(II.19)}$$

$$\Delta_{\alpha\beta} = \tfrac{1}{2} \sum_{\gamma\delta} \langle \alpha\beta | V_A | \gamma\delta \rangle t_{\gamma\delta} \qquad \text{(II.20)}$$

From the Hermiticity of $\rho$ and the antisymmetric nature of t, one can immediately deduce that $\Gamma$ is Hermitian and $\Delta$ is antisymmetric by invoking the properties of $\langle |V_A| \rangle$:

$$\langle \alpha\beta | V_A | \gamma\delta \rangle = - \langle \beta\alpha | V_A | \gamma\delta \rangle \ ; \ \langle \alpha\gamma | V_A | \beta\delta \rangle = \langle \beta\delta | V_A | \alpha\gamma \rangle$$

The expectation values $\langle \Phi | : C_1^\dagger C_2^\dagger \dots C_N^\dagger : | \Phi \rangle$ vanish by construction. Thus

$$\langle \Phi_0 | H | \Phi_0 \rangle = \text{tr}[(\varepsilon - \lambda_\pi N_\pi - \lambda_\nu N_\nu + \tfrac{1}{2}\Gamma)\rho + \tfrac{1}{2}\Delta t^\dagger] \text{(II.21)}$$

Now assuming an "independent quasiparticle" form for the part $H_2'$ we can write

$$H_2' = \sum_\alpha E_\alpha q_\alpha^\dagger q_\alpha \qquad \text{(II.22)}$$

Equation (II.22) leads to the commutator

$$[H_2^{'}, q_\alpha^\dagger] = E_\alpha \, q_\alpha^\dagger = E_\alpha \sum_\beta (U_{\alpha\beta} C_\beta^\dagger + V_{\alpha\beta} C_\beta) \qquad (II.23)$$

On the other hand the use of the equation (II.17) results in the expression:

$$[H_2^{'}, q_\alpha^\dagger] = \sum_{\beta,\gamma} [h_{\beta\gamma}^{'} U_{\alpha\gamma} + \Delta_{\beta\gamma} V_{\alpha\gamma}] C_\beta^\dagger + \sum_{\beta,\gamma} [-\Delta_{\beta\gamma}^* U_{\alpha\gamma} - h_{\beta\gamma}^{'*} V_{\alpha\gamma}] C_\beta$$

$$(II.24)$$

Equating the coefficients of $C_\beta^\dagger$ and $C_\beta$ we obtain the general HFB equations:

$$\begin{pmatrix} h^{'} & \Delta \\ -\Delta^* & -h^{'*} \end{pmatrix} \begin{pmatrix} \vec{U}_i \\ \vec{V}_i \end{pmatrix} = E_i \begin{pmatrix} \vec{U}_i \\ \vec{V}_i \end{pmatrix}, \quad h^{'} = h - \lambda_\pi N_\pi - \lambda_\nu N_\nu$$

$$(II.25)$$

where $\vec{U}_i \equiv (U_{i1}, U_{i2}, \ldots\ldots U_{iN})$.

## Time-reversal Symmetry

In our calculations we have divided all the basis states in the configuration space spanned by the orbits $1f_{5/2}$, $2p_{3/2}$, $2p_{1/2}$ and $1g_{9/2}$ into two sets. The first set contains the states $|k\rangle$, which are restricted to have $(m - 1/2)$ equal to an even integer. The second set contains the time-reversed states $|\bar{k}\rangle = T|k\rangle$, which have $(m - \frac{1}{2})$ = odd integer. The phase convention is $T|nljm\rangle = (-1)^{l+j-m} |nl \; j-m\rangle$. The first set is

$$[\ (1g_{9/2,9/2}),\ (1g_{9/2,5/2},\ 1f_{5/2,5/2}),(1g_{9/2,1/2},\ 1f_{5/2,1/2},$$
$$2p_{3/2,1/2},\ 2p_{1/2,1/2}),$$
$$(1g_{9/2,-3/2},\ 1f_{5/2,-3/2},\ 2p_{3/2,-3/2})\ \text{and}\ 1g_{9/2,-7/2}\ ]$$

For quasiparticle operators

$$q_\alpha^\dagger\ =\ \sum_\beta\ \ (U_{\alpha\beta}\ c_\beta^\dagger\ +\ V_{\alpha\beta} c_{\overline{\beta}}) \qquad (II.26)$$

$$q_{\overline{\alpha}}^\dagger\ =\ \sum_\beta\ \ (\overline{U}_{\alpha\beta} c_{\overline{\beta}}^\dagger\ +\ \overline{V}_{\alpha\beta}\ c_\beta) \qquad (II.27)$$

we notice that $\rho$ can not connect $|k>$ and $|\overline{k}>$. Further the only nonzero elements of $t$ connect the states $|k>$ to the states $|\overline{k}>$. Since the interaction $V$ conserves the magnetic projections, the potentials $(\Gamma,\Delta)$ are partitioned in the same manner as the densities $(\rho,\ t)$. Thus,

$$\rho\ =\ \begin{bmatrix} \rho_1 & 0 \\ 0 & \rho_2 \end{bmatrix},\ t\ =\ \begin{bmatrix} 0 & t_1 \\ t_2 & 0 \end{bmatrix},\ h\ =\ \begin{bmatrix} h_1 & 0 \\ 0 & h_2 \end{bmatrix},\ \Delta\ =\ \begin{bmatrix} 0 & \Delta_1 \\ \Delta_2 & 0 \end{bmatrix}$$

$$(II.28)$$

where $\rho$ and $h$ are Hermitian. Since $t$ and $\Delta$ are by definition antisymmetric, $t_2 = -\tilde{t}_1$ and $\Delta_2 = -\tilde{\Delta}_1$.

Substitution of (II.28) into (II.25) reveals that the energy matrix is also partitioned into two blocks and that the forms (II.26), (II.27) of the wave-functions is retained. We have imposed time-reversal symmetry by requiring that

$$q_{\overline{\alpha}}^\dagger\ =\ T\ q_\alpha^\dagger\ T^{-1} \qquad (II.29)$$

so that $\overline{U}_{\alpha\beta} = U^*_{\alpha\beta}$ , $\overline{V}_{\alpha\beta} = -V^*_{\alpha\beta}$ . $\qquad$ (II.30)

The quasiparticle vacuum is now time-reversal invariant and

$$\rho_2 = \rho^*_1 \ , \ h_2 = h^*_1 \ , \ t^\dagger_1 = t_1, \ \Delta^\dagger_1 = \Delta_1 \qquad (II.31)$$

Therefore only the block of the energy matrix that is related to (II.26) is diagonalized.

## Canonical representation for time-reversally symmetric HFB wave-functions (Block-Messiah Theorem)

We next consider the question of simultaneous diagonalization of $\rho$ and $t$. We have just seen that these are Hermitian. Therefore we have to check their commutator.

Consider

$$A^\dagger = \begin{pmatrix} q^\dagger_\alpha \\ q_\alpha \end{pmatrix} \ , \quad B^\dagger = \begin{pmatrix} c^\dagger_\alpha \\ c_\alpha \end{pmatrix} \qquad (II.32)$$

Then

$$A^\dagger = M B^\dagger \qquad (II.33)$$

We can now define the generalized quasiparticle density matrix Q:

$$Q_{\alpha\beta} = < \Phi_0 \mid A^\dagger_\beta A_\alpha \mid \Phi_0 > \qquad (II.34)$$

Since $<q^\dagger_\alpha q_\beta> = <q^\dagger_\alpha q^\dagger_\beta> = <q_\alpha q_\beta> = 0, <q_\alpha q^\dagger_\beta> = \delta_{\alpha\beta}$, we have

$$Q = \begin{pmatrix} 0 & 0 \\ 0 & 1 \end{pmatrix} \qquad (II.35)$$

The generalized particle density matrix is defined as

$$R_{\alpha\beta} = \langle \Phi_0 \mid B_\beta^\dagger B_\alpha \mid \Phi_0 \rangle \qquad (II.36)$$

Using the definitions (II.12) we get

$$R = \begin{pmatrix} \rho & t \\ t^\dagger & 1-\tilde{\rho} \end{pmatrix} \qquad (II.37)$$

Inverting relation (II.33) we find that R and Q are related by a unitary transformation:

$$R = M^\dagger Q M$$

Since $Q^2 = Q$, we have $R^2 = R$. The latter relation yields

$$\rho - \rho^2 = t\, t^\dagger \qquad (II.38)$$

$$\rho t = t\,\tilde{\rho} \qquad (II.39)$$

Thus $\rho_1 t_1 = t_1 \rho_1$, and this ensures that $\rho_1$ and $t_1$ can be diagonalized simultaneously. One can therefore have a basis spanned by $[\ \mid k_1\rangle,\ \mid k_2\rangle \ldots\ldots;\ \mid \bar{k}_1\rangle,\ \mid \bar{k}_2\rangle \ldots\ldots]$ such that $\rho$ and $t$ have the canonical forms shown below:

$$\rho = \begin{pmatrix} \rho_1 & 0 & & & \\ 0 & \rho_1 & & & 0 \\ & & \rho_2 & 0 & \\ & & 0 & \rho_{\bar{2}} & \\ & 0 & & & \end{pmatrix} \qquad t = \begin{pmatrix} 0 & t_{1\bar{1}} & & & \\ -t_{1\bar{1}} & 0 & & & 0 \\ & & 0 & t_{2\bar{2}} & \\ & & -t_{2\bar{2}} & 0 & \\ & 0 & & & \end{pmatrix} \qquad (II.40)$$

Here $\mid k \rangle = a_k^\dagger \mid 0 \rangle$ and

$$a_k^\dagger = \sum_\alpha D_{k,\alpha}\, C_\alpha^\dagger\ ;\quad a_{\bar{k}}^\dagger = \sum_\alpha D_{k,\alpha}^*\, C_{\bar{\alpha}}^\dagger \qquad (II.41)$$

Denoting the (real) eigenvalues of Hermitian $\rho_1$ and $t_1$ by $\rho_k$ and $t_{k\bar{k}}$ respectively, we obtain from the relation (II.37)

$$| t_{k\bar{k}} | = [ \rho_k (1 - \rho_k) ]^{1/2} \qquad (II.42)$$

Setting $\rho_k = V_k^2$ $(U_k^2 + V_k^2 = 1)$ we get $t_{k\bar{k}} = U_k V_k \qquad (II.43)$

Recalling the definitions (II.12) we see that the quasiparticle vacuum can be expressed as

$$| \Phi_0 > = \prod_k (U_k + V_k a_k^\dagger a_{\bar{k}}^\dagger) |0> \qquad (II.44)$$

Approximations employed in the present calculations

Inverting the special quasiparticle transformation

$$q_k^\dagger = U_k^* a_k^\dagger - V_k^* a_{\bar{k}} \; ; \quad q_{\bar{k}}^\dagger = U_k^* a_{\bar{k}}^\dagger + V_k^* a_k \qquad (II.45)$$

and substituting in (II.17) we get

$$H_2' = H_{11}' + H_{20}' ; \quad H_{11}' = \sum_{kk'} (H_{11}')_{kk'} q_k^\dagger q_{k'}$$

$$H_{20}' = \sum_{kk'} [(H_{20}')_{kk'} q_k^\dagger q_{k'}^\dagger + (H_{20}')_{kk'}^* q_{k'} q_k] \qquad (II.46)$$

As pointed out earlier, $H_{20}'$ acquires the form (II.22) when $H_{20}' = 0$ and $H_{11}'$ is diagonal. Whereas the conduction $(H_{20}')_{k\bar{k}} = 0$ leads to the BCS equations, the requirements $(H_{20}')_{k\bar{k}} = 0$, $(H_{11}')_{kk'} = 0$ $(k \neq k')$ lead to "HF-like" equations provided $h_{kk'} = 0$ and $\Delta_{k\bar{k}'} = 0$ $(k \neq k')$. We have made the latter

approximation, viz. $\Delta_{k\bar{k}'} = 0$. The expansion coefficients appearing in (II.41) have been obtained by diagonalizing in the spherical basis the HF-like potential h' which includes the appropriate density $\rho_k = V_k^2$:

$$h'_{\alpha\beta} = <\alpha| \ \varepsilon - \lambda_\pi N_\pi - \lambda_\nu N_\nu |\beta> + \sum_k \ <\alpha k |V_A| \beta k> V_k^2 \tag{II.47}$$

The occupation probabilities $V_k^2$ are obtained by solving the BCS equations:

$$\Delta_{k\bar{k}} \ = \ \sum_{k'} \ <k\bar{k}|V_A| \ k' \ \bar{k}'> \ U_{k'} \ V_{k'} \tag{II.48}$$

The calculation involves iteration between equations (II.47) and (II.48) until a reasonable convergence is achieved in terms of both the expansion coefficients $D_{k,\alpha}$ as well as the occupation probabilities $V_k^2$. Denoting by $\theta_k$ the eigenvalues of (II.47), it turns out that the condition $(H'_{20})_{k\bar{k}} = 0$ yields

$$2\theta_k \ U_k \ V_k \ - \ \Delta_{k\bar{k}} \ (U_k^2 - V_k^2) = 0 \tag{II.49}$$

The above equation leads to the following non-trivial implicit solutions of (II.47) and (II.48) (here $U_k^2 + V_k^2 = 1$)

$$U_k^2 = \frac{1}{2} \left[ 1 + \frac{\theta_k}{\sqrt{(\theta_k^2 + \Delta_{k\bar{k}}^2)}} \right], \ V_k^2 = \frac{1}{2} \left[ 1 - \frac{\theta_k}{\sqrt{(\theta_k^2 + \Delta_{k\bar{k}}^2)}} \right]$$

$$\tag{II.50}$$

Using (II.50) in (II.48) one gets

$$\Delta_{k\bar{k}} = \frac{1}{2} \sum_{k'} <k\bar{k} \mid V_A \mid k' \ \bar{k}'> \frac{\Delta_{k'\bar{k}'}}{\sqrt{(\Theta_{k'}^2 + \Delta_{k'\bar{k}'}^2)}} \qquad (II.51)$$

The condition $2\sum_{k} V_{k,\pi/\nu}^2 = N_{\pi/\nu}$ yields

$$\sum_{k} {}_{\pi/\nu}[1 - \frac{\Theta_k}{\sqrt{(\Theta_k^2 + \Delta_{k\bar{k}}^2)}}] = N_{\pi,\nu} \qquad (II.52)$$

## II.2.2 Projection of states of good angular momentum from the HFB intrinsic states

Restricting ourselves to axially symmetric intrinsic states $\mid \Phi_0>$, we can label the states $\mid k>$ by the expectation values of the operator $\hat{j}_z$. The state $\mid \Phi_0>$ given by equation (II.44) can thus be rewritten as

$$\mid \Phi_0 > = \prod_{im} (U_{im} + V_{im} \ a_{im}^\dagger \ a_{i\bar{m}}^\dagger) \mid 0> \qquad (II.53)$$

Here 'i' labels the different orbitals with the same $<\hat{j}_z>= m$.

The creation operators $a_{im}^\dagger$ can be rewritten as

$$a_{im}^\dagger = \sum_{\alpha} D_{im,\alpha} \ C_{\alpha m}^\dagger \ ; \ a_{i\bar{m}}^\dagger = \sum_{\alpha} (-1)^{l+j-m} D_{im,\alpha} \ C_{\alpha,-m}^\dagger$$

$$(II.54)$$

Here $\alpha$ labels the spherical single-particle orbits $2p_{3/2}$, $2p_{1/2}$, $1f_{5/2}$ and $1g_{9/2}$.

The wavefunction (II.53) can be recast into the form

$$\mid \Phi_0> = N \exp (\frac{1}{2} \sum_{\alpha\beta} f_{\alpha\beta} C_{\alpha}^\dagger C_{\beta}^\dagger) \mid 0 > \qquad (II.55)$$

with

$$f_{\alpha\beta} = \sum_i D_{im_\alpha, j_\alpha} \, D_{im_\beta, j_\beta} (V_{im_\alpha}/ U_{im_\alpha}) \, \delta_{m_\alpha, -m_\beta} \qquad (II.56)$$

Here N is a normalization constant.

Employing the shell model Hamiltonian (II.1) with $\langle\alpha|\varepsilon|\alpha\rangle = \varepsilon_\alpha$ we can write the energy of a state with angular momentum J as

$$E_J = \langle\Phi_0|H\,P_{00}^J|\Phi_0\rangle/\langle\Phi_0|P_{00}^J|\Phi_0\rangle$$

$$= \left(\int_0^\pi h(\theta)\, d_{00}^J(\theta)\, Sin\theta d\theta\right)/\left(\int_0^\pi n(\theta)\, d_{00}^J(\theta) Sin\theta d\theta\right)$$

$$(II.57)$$

The intensities of the various angular momenta contained in the intrinsic wavefunction are given by

$$a_J^2 = \frac{1}{2}(2J+1)\int_0^\pi n(\theta)\, d_{00}^J(\theta)\, Sin\,\theta\, d\theta \qquad (II.58)$$

The overlap integrals $h(\theta)$ and $n(\theta)$ are given by

$$h(\theta) = n(\theta)\left[\sum_\alpha \varepsilon_\alpha(M/(1+M))_{\alpha\alpha}+ (1/4) \sum_{\alpha\beta\gamma\delta} \langle\alpha\beta| V_A |\gamma\delta\rangle\cdot\right.$$

$$\left.\{2(M/(1+M))_{\gamma\alpha}(M/(1+M))_{\delta\beta}+ \sum_{\nu\rho}(1/1+M)_{\gamma\rho}F_{\rho\delta}(1/(1+M))_{\nu\alpha}\, f_{\nu\beta}^*\}\right] (II.59)$$

$$n(\theta) = [det(1 + M(\theta))]^{1/2} \qquad (II.60)$$

Here,

$$F_{\alpha\beta}(\theta) = \sum_{m'_\alpha, m'_\beta} d_{m_\alpha m'_\alpha}^{j_\alpha}(\theta)\, d_{m_\beta m'_\beta}^{j_\beta}(\theta)\, f_{j_\alpha m'_\alpha, j_\beta m'_\beta} \qquad (II.61)$$

$$M = F\, f^\dagger \qquad (II.62)$$

Employing the angular momentum projected wavefunctions $|\Psi_K^J\rangle = P_K^J \, |\Phi_0\rangle$ one can write

$$\langle \Psi_K^{J'} | Q_0^2 | \Psi_K^J \rangle = [n^J \, n^{J'}]^{-1/2} \int_0^\pi \sum_\mu \begin{bmatrix} J & 2 & J' \\ -\mu & \mu & o \end{bmatrix} d_{\mu o}^J(\theta) \, n(\theta)$$

$$\times \, b^2 \left( \sum_{\tau_3 \alpha \beta} e_{\tau_3} \langle \alpha | Q_\mu^2 | \beta \rangle \rho_{\alpha\beta}^{\tau_3}(\theta) \right) Sin\theta \, d\theta \qquad (\text{II.63})$$

The static quadrupole moments as well as the E2 transition matrix elements, $B(E2, J_i^+ \to J_f^+)$, can easily be obtained by using the above relation. Here b is the oscillator length parameter and $Q_\mu^2 = (16\pi/5)^{1/2} (r^2/b^2) \, Y_\mu^2(\Omega)$. The matrix $\rho$ appearing in equation (II.63) is defined as

$$\rho \;=\; M/(1+M) \qquad (\text{II.64})$$

Further, the normalization $n^J$ are given as

$$n^J \;=\; \int_0^\pi n(\theta) \, d_{oo}^J(\theta) \, Sin\theta \, d\theta \qquad (\text{II.65})$$

The method of performing the projection calculation is as follows. Employing, the HFB wavefunctions we first set up the f matrix. Then F, M and $1/(1+M)$ are evaluated for twenty values of the Gaussian quadrature points between the range $(0,\pi/2)$. (The axial symmetry of the intrinsic state permits us to change the integration limits from $(0,\pi)$ to $(0,\pi/2)$). The projected energies are calculated using the equations (II.58)-(II.62).

## II.2.3 The "Variation-after-angular momentum projection" (VAP) Prescription for the High-spin Yrast Spectra

The VAP calculations have been carried out by employing the following procedure. We first generate self-consistent HFB solutions, $\Phi(\beta)$, by carrying out HFB calculations with the Hamiltonian $(H - \beta Q_0^2)$. The optimum intrinsic state for each yrast level, $\Phi_{opt}(\beta_J)$, is then selected by finding out the <u>minimum</u> of the projected energy $E_J(\beta)$ . $(= <\Phi(\beta)| H\ P_{oo}^J | \Phi(\beta)> / <\Phi(\beta)| P_{oo}^J | \Phi(\beta)>)$ as a function of $\beta$. Stated differently, the intrinsic state for each J satisfies the following condition.

$$\delta\left[<\Phi(\beta)| H\ P_{oo}^J | \Phi(\beta)> / < \Phi(\beta) |P_{oo}^J | \Phi(\beta) >\right]\ = 0 \qquad (II.66)$$

## <u>Electric quadrupole transition matrix element for the yrast states</u>

The matrix elements of the quadrupole operator between the yrast states belonging to <u>different</u> intrinsic states can be given as

$$<\Psi_K^{J'}(\beta')| Q_0^2 | \Psi_K^J(\beta)> = [n^J(\beta)\ n^{J'}(\beta')]^{-1/2} \int_o^{\pi/2} \sum_{\mu} \begin{bmatrix} J & 2 & J' \\ -\mu & \mu & 0 \end{bmatrix} d_{\mu o}^J(\theta)$$

$$\times\ n(\beta,\beta',\theta)b^2 \left[ \sum_{\tau_3 \alpha\beta} e_{\tau_3} <\alpha| Q_\mu^2 |\beta> \rho_{\alpha\beta}^{\tau_3}(\beta,\beta',\theta) \right] \text{Sin}\theta\ d\theta$$

$$(II.67)$$

where

$$n^J(\beta) = \int_o^{\pi}[\det\ (1 + F(\beta,\theta)\ f^\dagger(\beta,\theta))]^{1/2}\ d_{oo}^J(\theta)\ \text{Sin}\theta\ d\theta$$

$$(II.68)$$

$$n(\beta,\beta',\theta) = [\det (1 + F(\beta, \theta) f^\dagger(\beta',\theta))]^{1/2} \qquad (\text{II.69})$$

and

$$\rho^{\tau_3}_{\alpha\beta}(\beta,\beta', \theta) = (M(\beta,\beta',\theta)/(1+M(\beta, \beta',\theta)))^{\tau_3}_{\alpha\beta} \qquad (\text{II.70})$$

with

$$M(\beta, \beta',\theta) = F(\beta, \theta) f^\dagger(\beta',\theta) \qquad (\text{II.71})$$

## Subshell occupation numbers in the yrast states

The sub-shell occupation numbers $(\eta_j)$ in a given yrast state $J$ are simply the expectation values of the operator $(\sum_{m=-j,+j} c^\dagger_{jm} c_{jm})$ with respect to the angular momentum projected wavefunctions. We have

$$\eta_j \ (j=1/2,3/2,5/2,9/2) = \langle\Phi_0| (\sum_{m=-j,+j} c^\dagger_{jm} c_{jm}) P^J_{00} |\Phi_0\rangle /$$

$$\langle\Phi_0| P^J_{00} |\Phi_0\rangle$$

$$= (\int_0^\pi p(\theta)d^J_{00}(\theta)\sin\theta d\theta)/$$

$$(\int_0^\pi n(\theta) d^J_{00}(\theta) \sin\theta d\theta$$

$$(\text{II.72})$$

where

$$p(\theta) = n(\theta) [ \sum_{m=-j,+j} (M/(1+M))_{jm,jm} ] \qquad (\text{II.73})$$

## II.2.4  The input parameters of the calculation

In the calculations presented here we have employed the valence space spanned by the $2p_{3/2}$, $2p_{1/2}$, $1f_{5/2}$ and $1g_{9/2}$ orbits. The doubly closed nucleus $^{56}$Ni is treated as an inert core. The relevant effective two-body interaction that we have employed is a renormalized G matrix due to Kuo[25] which is the sum of $G_{bare}$, $G_{3p-1h}$ and $G_{2p-2h}$ in the $^{56}$Ni core (see Appendix A). The single-particle energies we have taken are (in MeV) : $\varepsilon(2p_{3/2}) = 0.0$, $\varepsilon(1f_{5/2}) = 0.78$, $\varepsilon(2p_{1/2}) = 1.08$ and $\varepsilon(1g_{9/2}) = 3.50$ for the Ge isotopes. In our calculations for the Se isotopes we have taken $\varepsilon(1g_{9/2}) = 3.25$.

The effective interaction employed here has recently[26] provided a satisfactory explanation of the observed anomalous high spin sequence in $^{60}$Ni in the framework of exact shell model calculations. This interaction has also been employed in the recent theoretical studies of electromagnetic properties of the yrast and yrare states in Zn, Ge, Se and Kr isotopes by Ahalpara and Bhatt[27].

## II.3  Results and Discussion
## II.3.1  Intrinsic states

In Table II.1 we present the quadrupole moments of the optimum intrinsic states associated with the yrast states in the nuclei $^{68,70,72,74}$Ge and $^{72,74,76,78}$Se. The results have also been displayed graphically in Figure II.1.

## TABLE II.1

Quadrupole deformations,$< \Phi_{opt} (\beta_J) | Q_o^2 | \Phi_{opt}(\beta_J) >$, of the optimum intrinsic states associated with the yrast levels in the nuclei $^{68,70,72,74}Ge$ and $^{72,74,76,78}Se$. Here $< Q_o^2 >_{max}$ gives the maximum possible value of the intrinsic quadrupole moment for each isotope

| Nucleus | $< \Phi_{opt} (\beta_J) \ | Q_o^2 | \ \Phi_{opt} (\beta_J) >$ | | | | | | | | $< Q_o^2 >_{max}$ |
|---|---|---|---|---|---|---|---|---|---|
| | $J^\pi_{yrast} = $ $0^+$ | $2^+$ | $4^+$ | $6^+$ | $8^+$ | $10^+$ | $12^+$ | $14^+$ | |
| $^{68}Ge$ | 24.7 | 28.4 | 28.4 | 30.6 | 31.7 | 32.0 | 32.6 | 32.6 | 37.7 |
| $^{70}Ge$ | 32.1 | 32.1 | 32.1 | 35.6 | 37.2 | 37.5 | 37.5 | 37.5 | 39.9 |
| $^{72}Ge$ | 31.0 | 31.0 | 33.2 | 33.2 | 33.2 | 33.2 | 33.2 | 33.2 | 41.2 |
| $^{74}Ge$ | 30.1 | 30.1 | 28.0 | 26.9 | 26.9 | 26.9 | 26.9 | 26.9 | 38.6 |
| $^{72}Se$ | 35.9 | 35.9 | 39.4 | 39.4 | 40.8 | 40.8 | 40.8 | 40.8 | 43.9 |
| $^{74}Se$ | 36.4 | 36.4 | 38.6 | 40.5 | 41.6 | 41.6 | 41.7 | 41.7 | 45.2 |
| $^{76}Se$ | 35.5 | 35.5 | 35.5 | 36.3 | 37.3 | 37.7 | 38.1 | 37.8 | 42.6 |
| $^{78}Se$ | 30.7 | 32.2 | 32.2 | 32.2 | 33.3 | 33.3 | 33.3 | 33.3 | 37.8 |
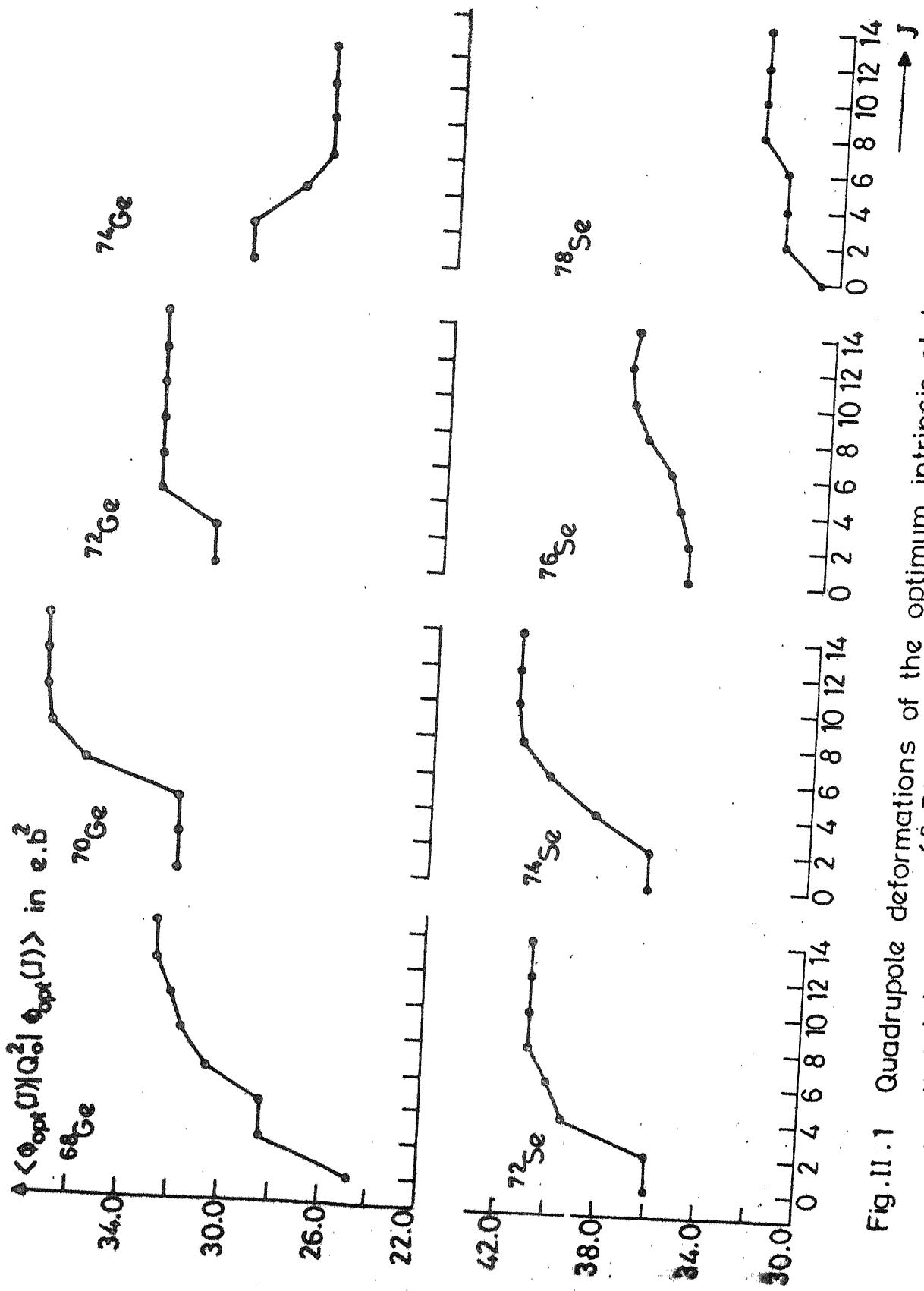
Fig. II.1 Quadrupole deformations of the optimum intrinsic states associated with the yrast levels in $^{68-74}Ge$ and $^{72-78}Se$.

We first discuss the results for the $Q_o^2$ moments of the intrinsic states associated with the ground states. It is seen that, with the nucleus $^{68}$Ge as the sole exception, the $<Q_o^2>$ values in the remaining nuclei are nearly 80 percent of their maximum possible values for the $(2p_{3/2}, 2p_{1/2}, 1f_{5/2}, 1g_{9/2})$ configuration space. For the nucleus $^{68}$Ge, however, the calculated intrinsic deformation for the ground state is only about 65 percent. As expected, the intrinsic deformations first register an increase with the mass number. The decrease in the $<Q_o^2>$ values for the ground states in heavy nuclei is just a signature of the approaching shell closure at N=50.

We next discuss the variation of the quadrupole moments of the optimum intrinsic states along the yrast sequence in various isotopes. We find that the intrinsic deformations for the levels with $J^\pi \geq 6^+$ are considerably larger than the values associated with the states with $J^\pi = 0^+, 2^+, 4^+$ in the nuclei $^{68,70}$Ge and $^{72,74}$Se. In the nucleus $^{68}$Ge, for example, the intrinsic deformation changes by as much as 32 percent between $J^\pi = 0^+$ and $14^+$. As mentioned in the Introduction, a number of observed features in the Ge and Se isotopes suggest strong deviations from the predictions based on the rotational model. The results obtained here, which indicate rather large variation of the intrinsic deformations along the yrast cascade, provide a qualitative understanding of the observed features.

## II.3.2 Yrast levels

In Figure II.2 we have presented the observed[1-5] as well as the theoretical yrast spectra resulting from the VAP prescription. The yrast spectra obtained by carrying out angular momentum projection on the minimum-energy HFB intrinsic states have also been presented in the column labelled PHFB.

In the calculated yrast spectra, the $J=2$ states have been aligned with their observed position in all cases to facilitate a comparison of the results with the observed one. An interesting feature of the computed spectra that we notice here is the following. Whereas the present calculational framework predicts the observed positions of the yrast levels with $2 < J < 10$ reasonably accurately relative to those of the states with $J=2$, one finds discrepancies in the position of the calculated $J=0$ level. This discrepancy is seen to be maximum in the case of the nucleus $^{70}Ge$. The inadequacy of the present method to reproduce the position of the $J=0$ relative to the remaining part of the yrast spectra may be either due to the noninclusion of the $1f_{7/2}$-excited, $J=0$ configurations, or due to a mixing of the $J=0$ state projected from deformed HFB state with additional $J=0$ states arising within $(2p_{3/2}, 2p_{1/2}, 1f_{5/2}, 1g_{9/2})^n$ configuration space.

We find that the VAP prescription leads to dramatic improvements over the PHFB results in the nuclei $^{68,70}Ge$; the results are particularly striking in the latter nucleus.
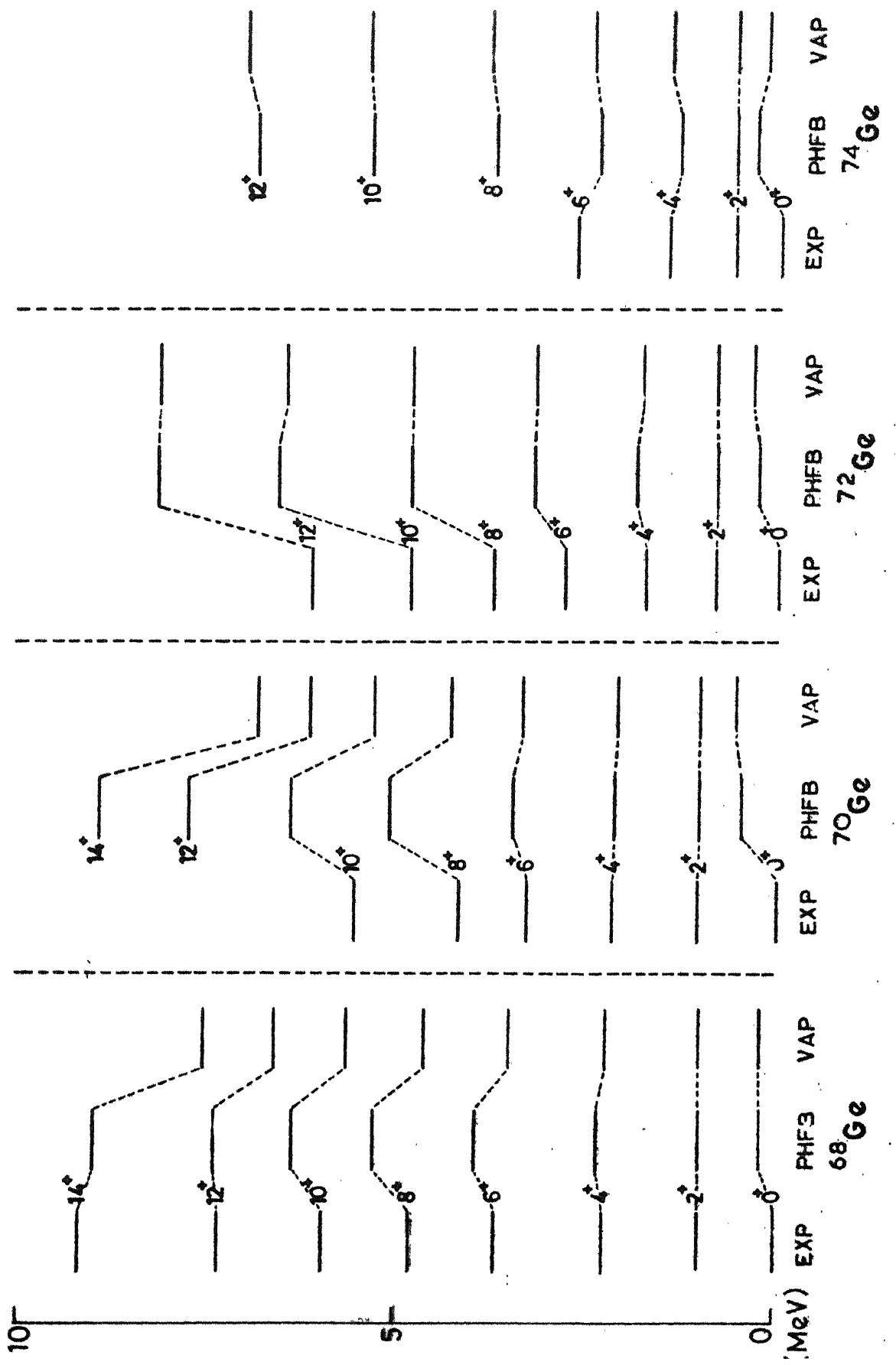
Fig. II.2 Calculated and experimental yrast levels in $^{68,70,72,74}$Ge.

The VAP prescription, however, underestimates the energies of the levels with J=12,14 in $^{68}$Ge by about 0.75 MeV and 1.5 MeV respectively.  In the nuclei $^{72,74}$Ge we find that the yrast energies obtained via the PHFB prescription are practically unchanged when we invoke the VAP degree of freedom.  This is not particularly surprising since the results presented in the preceding section have indicated relatively small variation of the quadrupole deformation of the optimum intrinsic states associated with the yrast levels in these isotopes.

The results for the calculated PHFB as well as VAP yrast spectra in the nuclei $^{72,74,76,78}$Se are presented in Figure II.3 together with the observed[6-9] ones.  An alignment of the calculated J=2 states with their experimentally observed positions again reveals a systematically decreasing discrepancy so far as the position of the calculated J≠0 states are concerned.  Hamilton et al.[28] have sometime ago pointed out that the anomalous $2^+$-$0^+$ separation in the nucleus $^{72}$Se can be satisfactorily reconciled with the quasirotational nature of the observed high-spin yrast spectrum in terms of the coexistence of deformed and nearly-spherical J=0 states. In view of the results obtained here, it appears that this feature of coexistence of two J=0 states, one with a deformed and the other with a spherical parentage, may be a general characteristic of the low-lying energy levels in the A=70-80 mass region.
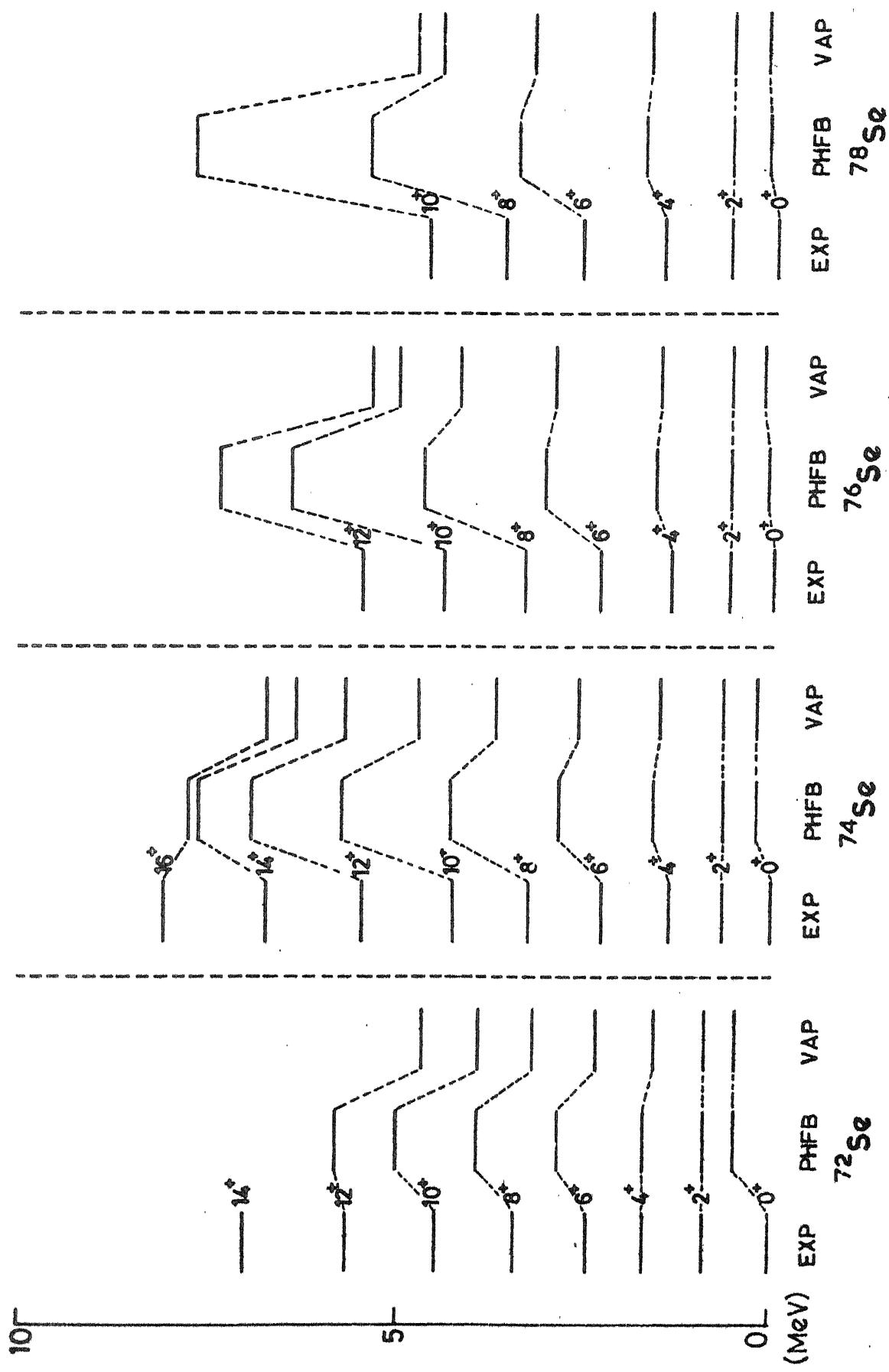
Fig. II.3  Calculated and experimental yrast levels in $^{72,74,76,78}$Se.

We find that the VAP prescription leads to a dramatic improvement over the PHFB energies in <u>all</u> the Se isotopes considered here; unlike the PHFB yrast spectra, the VAP spectra display good qualitative agreement with the experiments. The success of the VAP method in explaining the observed yrast energies in the nuclei $^{72,74}$Se is particularly striking.

The present calculation precludes the onset of non-axial deformations. Therefore, our results indicate that the observed deviations of the yrast energies from the $J(J+1)$-law arise largely from the softness of these nuclei towards an <u>increase</u> in the <u>axial</u> deformations along the yrast sequence.

## II.3.3  Electromagnetic Properties

We now move on to a discussion of the electro-magnetic properties of the yrast levels in the nuclei $^{68,70,72,74}$Ge and $^{72,74,76,78}$Se. In Tables II.2-II.9 we have presented the results for the reduced transition probabilities for the intercascade E2 transitions. We have also calculated here the static quadrupole moments for the yrast states.

The experimental $B(E2, J_i \rightarrow J_f)$ values have been extracted from the measured half-lives using the relation:

## TABLE II.2

The reduced transition probabilities for the E2 transitions as well as the static quadrupole moments for the yrast levels in the nucleus $^{68}$Ge. Here $e_p(e_n)$ denotes the effective charge for protons (neutrons). The entries presented in the second column correspond to the reduced matrix elements resulting from equation (II.63). The reduced matrix elements as well as the static moments have been expressed in a form that brings out their explicit dependence on the effective charges.

| Transition $(J_i^+ \rightarrow J_f^+)$ | $[B(E2; J_i^+ \rightarrow J_f^+)]^{1/2}_{th}$ | $[Q(J_i^+)]_{th}$ | $B(E2, J_i^+ \rightarrow J_f^+)$ $e_p=1.3, e_n=0.3$ | expt[a] | $Q(J_i^+)$ $e_p=1.3, e_n=0.3$ | expt |
|---|---|---|---|---|---|---|
| $2^+ \rightarrow 0^+$ | $0.75e_p+0.91e_n$ | $-16.70e_p-20.16e_n$ | 1.55 | $2.51^{+1.26}_{-0.63}$ | -27.75 | - |
| $4^+ \rightarrow 2^+$ | $0.99e_p+1.35e_n$ | $-21.66e_p-27.53e_n$ | 2.89 | $1.77^{+0.64}_{-0.37}$ | -36.41 | - |
| $6^+ \rightarrow 4^+$ | $0.93e_p+1.37e_n$ | $-23.50e_p-31.52e_n$ | 2.63 | $1.97^{+0.78}_{-0.44}$ | -39.99 | - |
| $8^+ \rightarrow 6^+$ | $0.97e_p+1.53e_n$ | $-24.72e_p-35.16e_n$ | 2.96 | $2.81^{+0.70}_{-0.47}$ | -42.68 | - |
| $10^+ \rightarrow 8^+$ | $0.99e_p+1.63e_n$ | $-25.37e_p-37.45e_n$ | 3.17 | $4.12^{+0.91}_{-0.88}$ | -44.20 | - |
| $12^+ \rightarrow 10^+$ | $0.99e_p+1.75e_n$ | $-25.92e_p-40.02e_n$ | 3.28 | - | -45.69 | - |
| $14^+ \rightarrow 12^+$ | $1.03e_p+1.56e_n$ | $-26.56e_p-43.14e_n$ | 2.86 | - | -47.47 | - |

The BE2 values are in units of $10^{-50}$ $e^2$ cm$^4$ and the static quadrupole moments have been given in units of e.fm$^2$.

[a] ref.2.

## TABLE II.3

The results for the nucleus $^{70}$Ge

| Transition $(J_i^+ \to J_f^+)$ | $[B(E2, J_i^+ \to J_f^+)]^{\frac{1}{2}}_{th}$ | $[Q(J_i^+)]_{th}$ | $B(E2, J_i^+ \to J_f^+)$ $e_p=1.5, e_n=0.5$ | expt | $Q(J_f^+)$ $e_p=1.5, e_n=0.5$ | expt |
|---|---|---|---|---|---|---|
| $2^+ \to 0^+$ | $0.87e_p+1.33e_n$ | $-17.58e_p-26.43e_n$ | 3.87 | $3.58\pm0.6$ [a] | -39.59 | $3\pm6$ [b] |
| $4^+ \to 2^+$ | $1.01e_p+1.60e_n$ | $-22.02e_p-32.88e_n$ | 5.39 | $5.33\pm3.0$ [a] | -49.47 | — |
| $6^+ \to 4^+$ | $0.85e_p+1.44e_n$ | $-23.74e_p-40.01e_n$ | 3.96 | | -55.61 | — |
| $8^+ \to 6^+$ | $0.88e_p+1.62e_n$ | $-25.11e_p-46.59e_n$ | 4.53 | | -60.96 | — |
| $10^+ \to 8^+$ | $1.09e_p+1.97e_n$ | $-26.22e_p-47.48e_n$ | 6.82 | | -63.06 | — |
| $12^+ \to 10^+$ | $1.11e_p+1.93e_n$ | $-26.88e_p-47.09e_n$ | 6.92 | | -63.84 | — |
| $14^+ \to 12^+$ | $1.11e_p+1.87e_n$ | $-27.44e_p-46.06e_n$ | 6.77 | | -64.19 | — |

[a] ref.20.
[b] ref.31.

## TABLE II.4

The results for the nucleus $^{72}$Ge

| transition $(J_i^+ \to J_f^+)$ | $[B(E2, J_i^+ \to J_f^+)]^{\frac{1}{2}}_{th}$ | $[Q(J_i^+)]_{th}$ | $B(E2, J_i^+ \to J_f^+)$ $e_p=1.6, e_n=0.6$ | expt | $Q(J_f^+)$ $e_p=1.6, e_n=0.6$ | expt |
|---|---|---|---|---|---|---|
| $2^+ \to 0^+$ | $0.87e_p+1.27e_n$ | $-17.57e_p-25.01e_n$ | 4.62 | $5.46\pm0.10$ [a] | $-43.12$ | $-13\pm6$ [b] |
| $4^+ \to 2^+$ | $0.95e_p+1.49e_n$ | $-21.94e_p-32.99e_n$ | 5.79 | – | $-54.90$ | – |
| $6^+ \to 4^+$ | $1.04e_p+1.78e_n$ | $-23.92e_p-37.16e_n$ | 7.44 | – | $-60.56$ | – |
| $8^+ \to 6^+$ | $1.02e_p+1.82e_n$ | $-24.68e_p-37.72e_n$ | 7.41 | – | $-62.11$ | – |
| $10^+ \to 8^+$ | $0.98e_p+1.82e_n$ | $-24.96e_p-37.58e_n$ | 7.12 | – | $-62.48$ | – |
| $12^+ \to 10^+$ | $0.94e_p+1.79e_n$ | $-25.00e_p-36.84e_n$ | 6.67 | – | $-62.10$ | – |
| $14^+ \to 12^+$ | $0.87e_p+1.77e_n$ | $-24.22e_p-31.51e_n$ | 6.16 | – | $-57.65$ | – |

[a] ref.20.

[b] ref.31.

## TABLE II.5

The results for the nucleus $^{74}$Ge

| Transition $(J_i^+ \to J_f^+)$ | $[B(E2;J_i^+\to J_f^+)]^{\frac{1}{2}}_{th}$ | $[Q(J_i^+)]_{th}$ | $B(E2;J_i^+\to J_f^+)$ $e_p=1.7,e_n=0.7$ | expt | $Q(J_i^+)$ $e_p=1.7,e_n=0.7$ | expt |
|---|---|---|---|---|---|---|
| $2^+\to 0^+$ | $0.86e_p+1.22e_n$ | $-17.48e_p-23.96e_n$ | 5.37 | $6.3\pm0.5$ [a] | $-46.48$ | $-25\pm6$ [b] |
| $4^+\to 2^+$ | $1.04e_p+1.50e_n$ | $-21.92e_p-27.27e_n$ | 7.94 | – | $-56.35$ | – |
| $6^+\to 4^+$ | $1.03e_p+1.56e_n$ | $-22.94e_p-25.07e_n$ | 8.13 | – | $-56.62$ | – |
| $8^+\to 6^+$ | $0.96e_p+1.56e_n$ | $-23.35e_p-23.48e_n$ | 7.40 | – | $-56.13$ | – |
| $10^+\to 8^+$ | $0.91e_p+1.62e_n$ | $-23.46e_p-21.96e_n$ | 7.16 | – | $-55.25$ | – |
| $12^+\to 10^+$ | $0.66e_p+1.33e_n$ | $-10.68e_p-7.70e_n$ | 4.21 | – | $-23.56$ | – |
| $14^+\to 12^+$ | $0.40e_p+0.78e_n$ | $-21.18e_p-19.03e_n$ | 1.50 | – | $-49.32$ | – |

[a] ref.20.

[b] ref.31.

$$B(E2, J_f \to J_i)(e^2 fm^4) = \frac{816}{E^5(\gamma) \ (MeV)\tau(J_f)(p \ sec)} \qquad (II.74)$$

where $E(\gamma)$ represents the transition energy, $\tau(J_f)$ is the meanlife and $J_f = J_i + 2$. The calculated as well as the observed[2,6,29,8] values in the nuclei $^{68}Ge$, $^{72,74,76}Se$ have been presented graphically in Figures II.4-II.7. We have also shown in the Figures the "rigid rotor" values for the transition probabilities; these values have been calculated with the relations:

$$\left[B(E2, J_f \to J_i)\right]_{rigid \ rotor} = (5/16\pi) \begin{bmatrix} J_f & 2 & J_i \\ 0 & 0 & 0 \end{bmatrix}^2 (<Q_o^2>_{HFB})^2$$

$$(II.75)$$

We first discuss the results for the nuclei $^{68,70,72,74}Ge$. From the results presented in Figure II.4 it becomes obvious that the experimental data suggest a deviation from the rigid rotor values in the direction predicted by our VAP calculations. The calculated $B(E2, \ 2^+ \to 0^+)$ values in the nuclei $^{70,72,74}Ge$ are seen to lie within 15 percent of the experimental values[30,4,20] provided one chooses $(e_p, e_n) = (1.5, \ 0.5)$, $(1.6, \ 0.6)$ and $(1.7, \ 0.7)$ respectively. The slight enhancement in the values of effective charges, as one approaches $^{74}Ge$, is not entirely unexpected. The involvement of the $^{56}Ni$ core, an effect which is mocked up by choosing effective charges, is expected to increase in heavier – and more deformed – isotopes.

We next discuss the $B(E2, \ J_i^+ \to J_f^+)$ values in the nuclei $^{72,74,76,78}Se$. A large number of experimental groups have, in
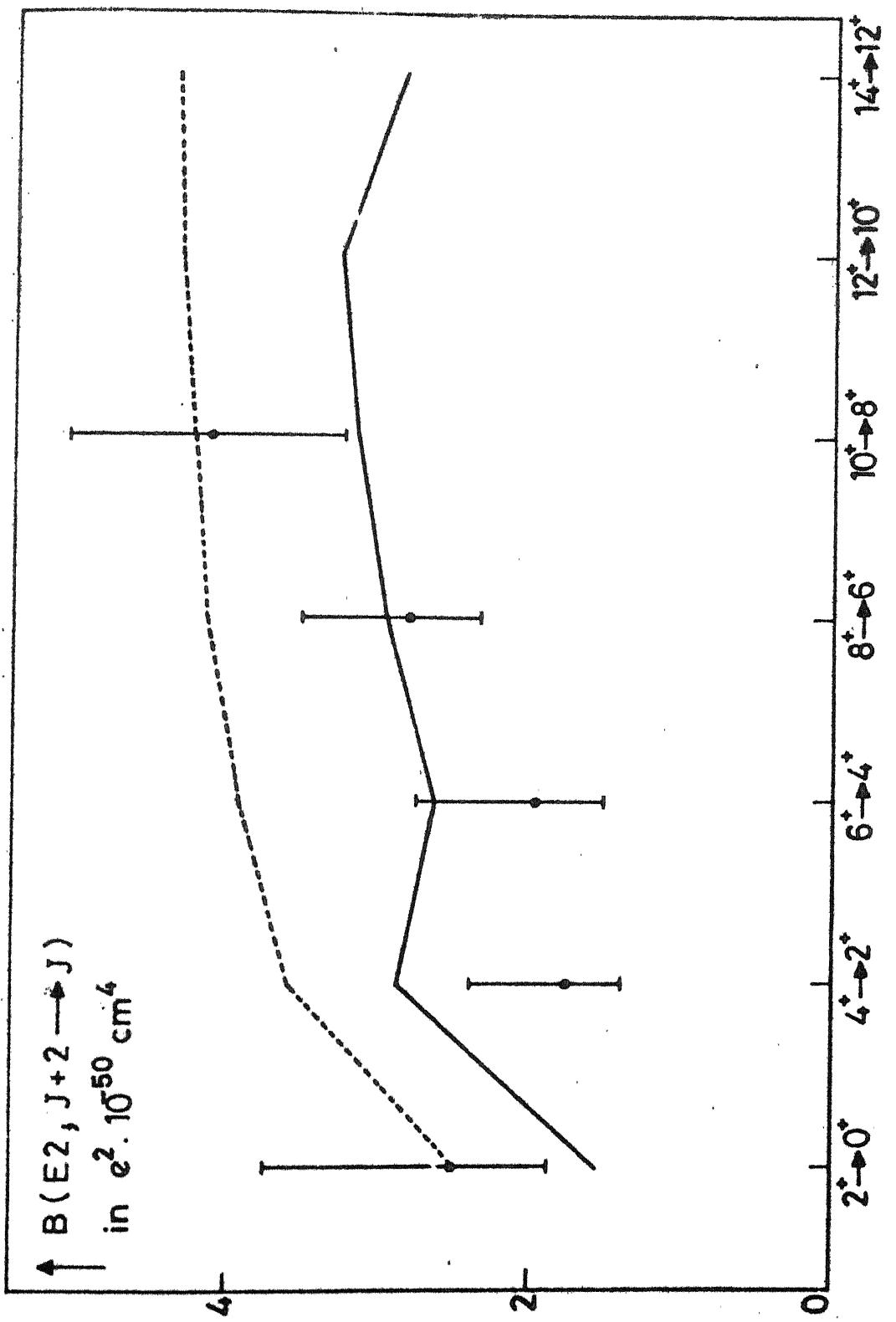
Fig. II.4  Comparison of the observed B(E2) values in $^{68}$Ge with the predictions of the VAP model (solid line) and the rigid rotor values (dashed line).

## TABLE II.6

B(E2; $J_i^+ \rightarrow J_f^+$) and Q($J_i^+$) values in the nucleus $^{72}$Se

| Transition ($J_i^+ \rightarrow J_f^+$) | $[B(E2;J_i^+ \rightarrow J_f^+)]^{\frac{1}{2}}_{th}$ | $[Q(J_i^+)]_{th}$ | B(E2;$J_i^+ \rightarrow J_f^+$) $e_p=1.6, e_n=0.6$ | RDM | DSAM | $Q(J_i^+)$ $e_p=1.6, e_n=0.6$ ex. |
|---|---|---|---|---|---|---|
| $2^+ \rightarrow 0^+$ | $1.04e_p+1.40e_n$ | $-21.00e_p-28.16e_n$ | 6.24 | (a) $3.24\pm0.38$<br>(b) $4.90\pm0.82$<br>(c) $3.16\pm0.68$<br>(d) $3.42\pm0.42$ | –<br>–<br>–<br>– | $-50.49$ |
| $4^+ \rightarrow 2^+$ | $1.02e_p+1.47e_n$ | $-26.68e_p-38.53e_n$ | 6.34 | (a) $11.0\pm1.22$<br>(b) $16.17\pm6.55$<br>(c) $6.67\pm1.78$<br>(d) $6.61\pm0.61$ | $<24.50$<br>–<br>$<11.78$<br>– | $-65.81$ |
| $6^+ \rightarrow 4^+$ | $1.29e_p+1.91e_n$ | $-27.79e_p-44.40e_n$ | 10.29 | (a) $9.55\pm0.9$<br>(b) $>29.56$<br>(c) $4.08+1.66$<br>(d) – | $<14.82$<br>$8.03\pm0.62$<br>$25.89\pm8.65$ | $-74.29$ |
| $8^+ \rightarrow 6^+$ | $1.29e_p+1.88e_n$ | $-31.57e_p-47.07e_n$ | 10.19 | (a) –<br>(c) –<br>(d) – | $12.16+3.36$<br>$13.69+1.68$<br>$7.04\pm2.22$ | $-78.76$ |
| $10^+ \rightarrow 8^+$ | $1.42e_p+1.99e_n$ | $-32.73e_p-47.89e_n$ | 12.00 | (a) –<br>(c) –<br>(d) – | $15.30+4.61$<br>$16.51\pm3.32$<br>$>55.3$ | $-81.10$ |
| $12^+ \rightarrow 10^+$ | $1.43e_p+1.96e_n$ | $-33.42e_p-47.82e_n$ | 12.01 | (a) –<br>(c) –<br>(d) – | $21.42$<br>$13.19+2.1$<br>$>32.09$ | $-82.15$ |
| $14^+ \rightarrow 12^+$ | $1.44e_p+1.91e_n$ | $-34.20e_p-47.28e_n$ | 11.96 | (a) – | $28.71\pm10.78$ | $-83.07$ |

The values (a), (b), (c) and (d) correspond to the experimental results of the groups at BNL/Köln, München, ORNL/Vanderbilt and Leningrad respectively. (ref.6).

## TABLE II.7

$B(E2; J_i^+ \rightarrow J_f^+)$ and $Q(J_f^+)$ values in the nucleus $^{74}\text{Se}$

| Transition $(J_i^+ \rightarrow J_f^+)$ | $[B(E2; J_i^+ \rightarrow J_f^+)]^{\frac{1}{2}}_{th}$ | $[Q(J_i^+)]_{th}$ | $B(E2; J_i^+ \rightarrow J_f^+)$ $e_p=1.7, e_n=0.7$ | $B(E2; J_i^+ \rightarrow J_f^+)$ expt[a] | $Q(J_i^+)$ $e_p=1.7, e_n=0.7$ | $Q(J_i^+)$ expt |
|---|---|---|---|---|---|---|
| $2^+ \rightarrow 0^+$ | $1.05e_p+1.44e_n$ | $-21.22e_p-28.80e_n$ | 7.80 | $7.48\pm0.28$ | -56.23 | $-36\pm7$[b] |
| $4^+ \rightarrow 2^+$ | $1.15e_p+1.66e_n$ | $-26.89e_p-37.97e_n$ | 9.72 | $14.94\pm0.56$ | -71.29 | — |
| $6^+ \rightarrow 4^+$ | $1.17e_p+1.79e_n$ | $-29.64e_p-45.04e_n$ | 10.56 | $7.20\pm0.90$ | -81.92 | — |
| $8^+ \rightarrow 6^+$ | $1.20e_p+1.89e_n$ | $-31.25e_p-49.03e_n$ | 11.31 | $12.85\pm0.99$ | -87.45 | — |
| $10^+ \rightarrow 8^+$ | $1.36e_p+2.08e_n$ | $-32.98e_p-48.36e_n$ | 14.20 | $12.22\pm2.43$ | -89.92 | — |
| $12^+ \rightarrow 10^+$ | $1.36e_p+2.01e_n$ | $-32.98e_p-48.68e_n$ | 13.23 | $15.54\pm7.81$ | -90.14 | — |
| $14^+ \rightarrow 12^+$ | $1.38e_p+1.94e_n$ | $-33.73e_p-47.51e_n$ | 13.72 | — | -97.40 | — |

[a] ref.29.

[b] ref.32.

## TABLE II.8

$B(E2, J_i^+ \rightarrow J_f^+)$ and $Q(J_f^+)$ in the nucleus $^{76}Se$

| Transition $(J_i^+ \rightarrow J_f^+)$ | $[B(E2; J_i^+ \rightarrow J_f^+)]^{\frac{1}{2}}_{th}$ | $[Q(J_f^+)]_{th}$ | $B(E2; J_i^+ \rightarrow J_f^+)$ $e_p=1.7, e_n=0.7$ | expt[a] | $Q(J_i^+)$ $e_p=1.7, e_n=0.7$ | expt[b] |
|---|---|---|---|---|---|---|
| $2^+ \rightarrow 0^+$ | $1.05e_p+1.37e_n$ | $-21.34e_p-27.42e_n$ | 7.52 | $7.40\pm0.30$ | $-55.47$ | $-34\pm7$ |
| $4^+ \rightarrow 2^+$ | $1.23e_p+1.64e_n$ | $-27.12e_p-34.05e_n$ | 10.55 | $13.61\pm4.0$ | $-69.94$ | $-$ |
| $6^+ \rightarrow 4^+$ | $1.23e_p+1.68e_n$ | $-29.78e_p-36.94e_n$ | 10.68 | $11.70^{+47.0}_{-4.7}$ | $-76.48$ | $-$ |
| $8^+ \rightarrow 6^+$ | $1.22e_p+1.68e_n$ | $-31.51e_p-38.81e_n$ | 10.54 | $19.81^{+1.98}_{-6.58}$ | $-80.73$ | $-$ |
| $10^+ \rightarrow 8^+$ | $1.33e_p+1.77e_n$ | $-32.76e_p-39.46e_n$ | 12.28 | $8.90^{+8.90}_{-3.00}$ | $-83.31$ | $-$ |
| $12^+ \rightarrow 10^+$ | $1.39e_p+1.76e_n$ | $-34.13e_p-39.66e_n$ | 12.87 | $-$ | $-85.78$ | $-$ |
| $14^+ \rightarrow 12^+$ | $1.45e_p+1.78e_n$ | $-36.14e_p-38.53e_n$ | 13.76 | $-$ | $-88.40$ | $-$ |

[a] ref.8.

[b] ref.33.

## TABLE II.9

$B(E2; J_i^+ \to J_f^+)$ and $Q(J_f^+)$ values in the nucleus $^{78}$Se

| Transition $(J_i^+ \to J_f^+)$ | $[B(E2;J_i^+ \to J_f^+)]^{\frac{1}{2}}_{th}$ | $[Q(J_i^+)]_{th}$ | $B(E2;J_i^+ \to J_f^+)$ $e_p=1.7, e_n=0.7$ | expt | $Q(J_i^+)$ $e_p=1.7, e_n=.7$ | expt |
|---|---|---|---|---|---|---|
| $2^+ \to 0^+$ | $0.98e_p+1.04e_n$ | $-21.28e_p-22.16e_n$ | 5.77 | $8.4\pm0.3$ [a] | -51.69 | $-26\pm09$ [b] |
| $4^+ \to 2^+$ | $1.25e_p+1.38e_n$ | $-27.59e_p-28.05e_n$ | 9.54 | | -66.53 | — |
| $6^+ \to 4^+$ | $1.26e_p+1.47e_n$ | $-30.26e_p-29.04e_n$ | 10.07 | | -71.76 | — |
| $8^+ \to 6^+$ | $1.15e_p+1.38e_n$ | $-31.69e_p-29.19e_n$ | 8.55 | | -74.31 | — |
| $10^+ \to 8^+$ | $1.30e_p+1.52e_n$ | $-32.91e_p-28.09e_n$ | 10.71 | | -75.60 | — |
| $12^+ \to 10^+$ | $1.30e_p+1.50e_n$ | $-34.21e_p-26.68e_n$ | 10.63 | | -76.82 | — |

[a] ref.27.

[b] ref.33.

the recent years, carried out measurements of the mean-lives
of the yrast levels using the recoil-distance (RD) and/or
the Doppler-shift attenuation (DSA) techniques. As shown in
Figure II.5, the experimental estimates for the reduced transi-
tion probabilities in the nucleus $^{72}$Se display considerable
scatter around their average values. However, it is seen
that, in contrast with the results obtained in earlier projected
HF calculation[27], the VAP estimates for higher yrast, states
are <u>not</u> inconsistent with the available data. Due to large
error bars (see Figures II.6 and II.7) associated with the
available reduced transition probabilities in the nuclei $^{74,76}$Se,
and the non-availability of the results in the nucleus $^{78}$Se,
it is difficult to assess the VAP results in these nuclei.

The static quadrupole moments for the $2^+$ states have
been measured[31-33] only in the nuclei $^{70,72,74}$Ge and $^{74,76,78}$Se.
The signatures of the measured static moments provide a confir-
mation of the prolate character of the variational intrinsic
states for the $2^+$ levels obtained in the present work.
However, the magnitudes of the observed static moments are
considerably smaller compared to the theoretical estimates;
the descrepancies are particularly striking in the nuclei
$^{70,72}$Ge where the calculation predicts the values $-39.6$ efm$^2$
and $-43.12$ efm$^2$ to be compared with the observed values
$Q_{2^+} = 3\pm6$ efm$^2$ and $Q_{2^+} = -13\pm6$ efm$^2$, respectively. The
theoretical estimates are likely to decrease upon the inclusion
of the effects due to nonaxial deformations; an increase in the

Fig. II.5: $B(E2)$-values in $^{72}...$
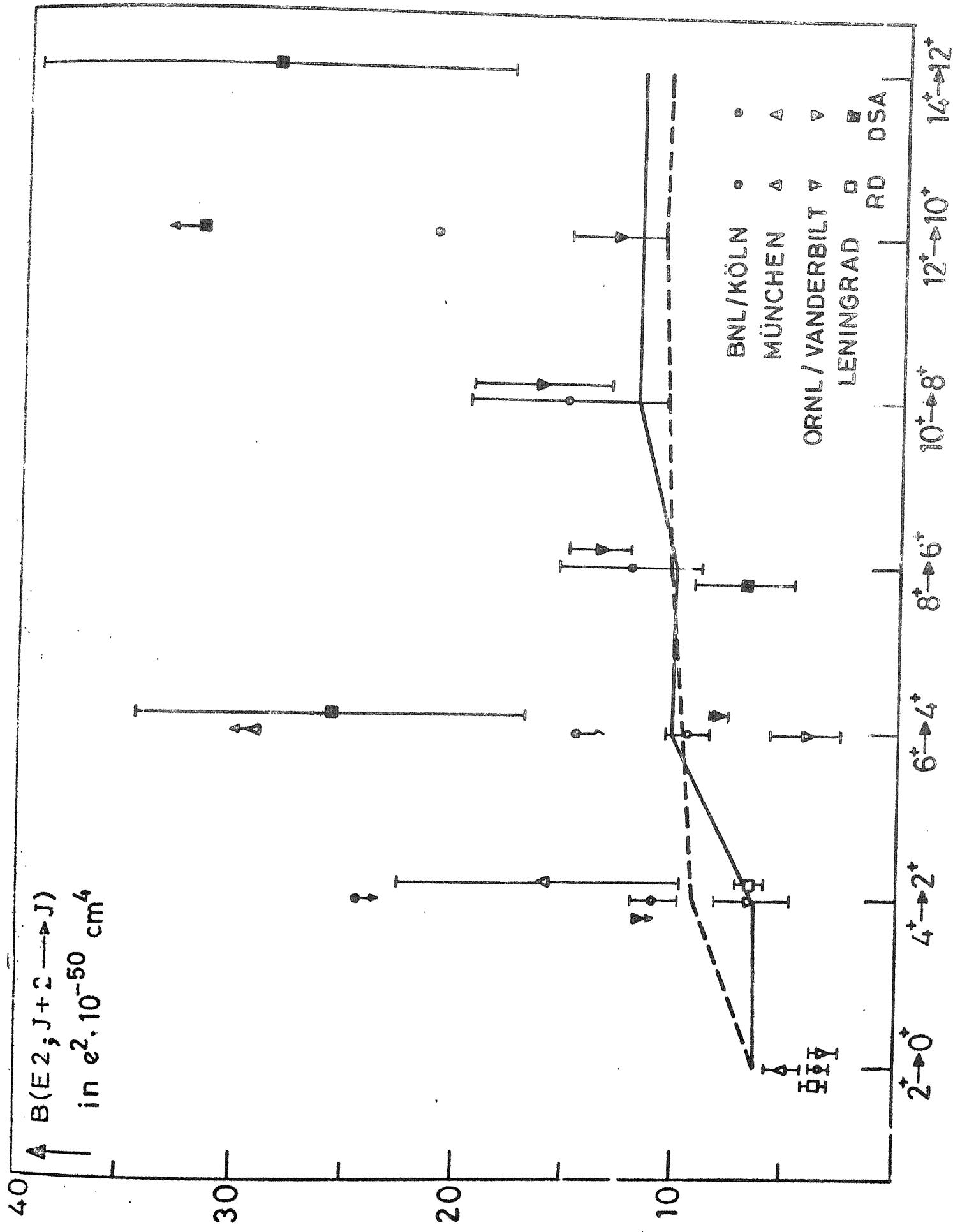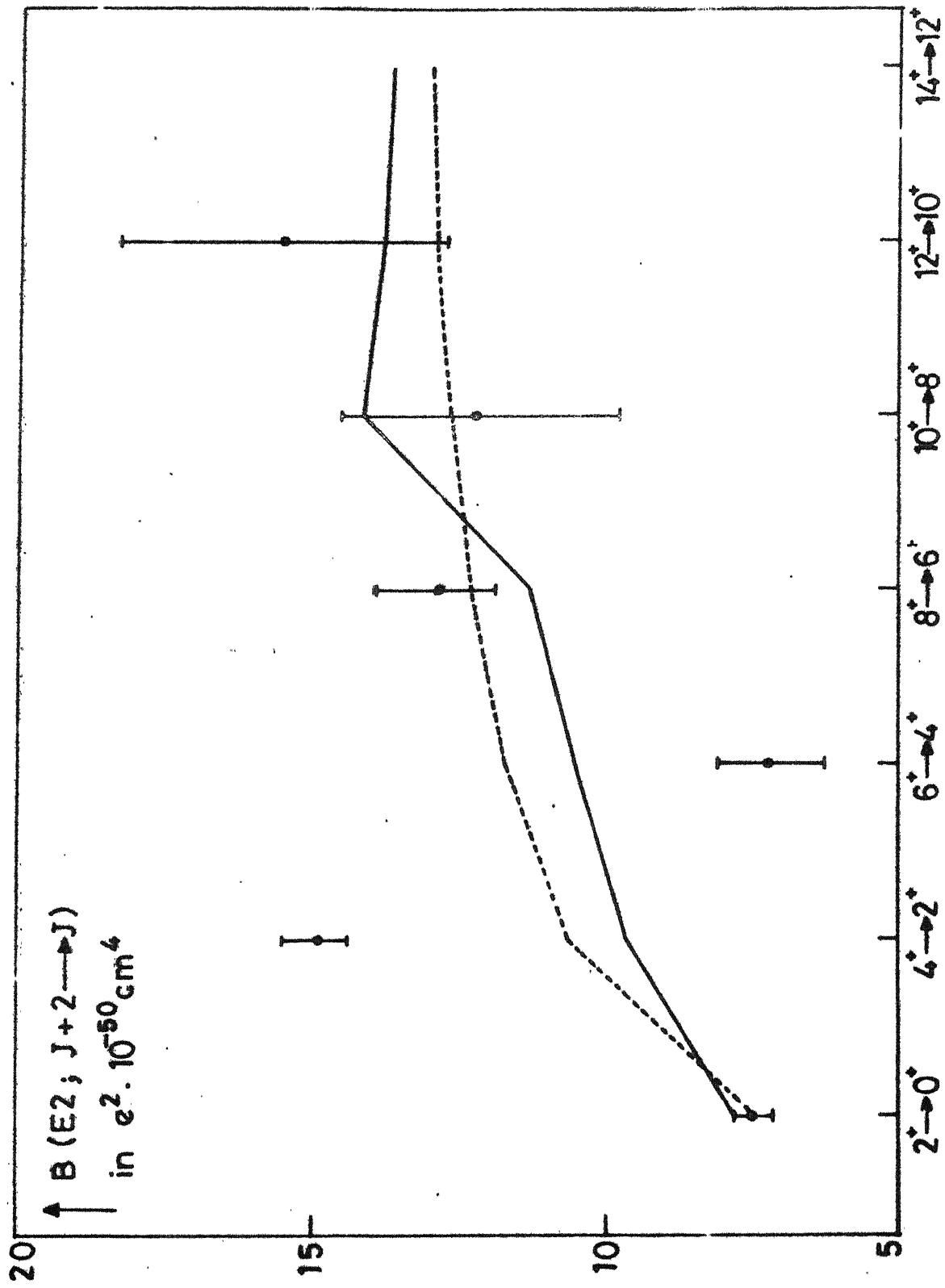
Fig. II.6   B(E2) values in $^{74}$Se.
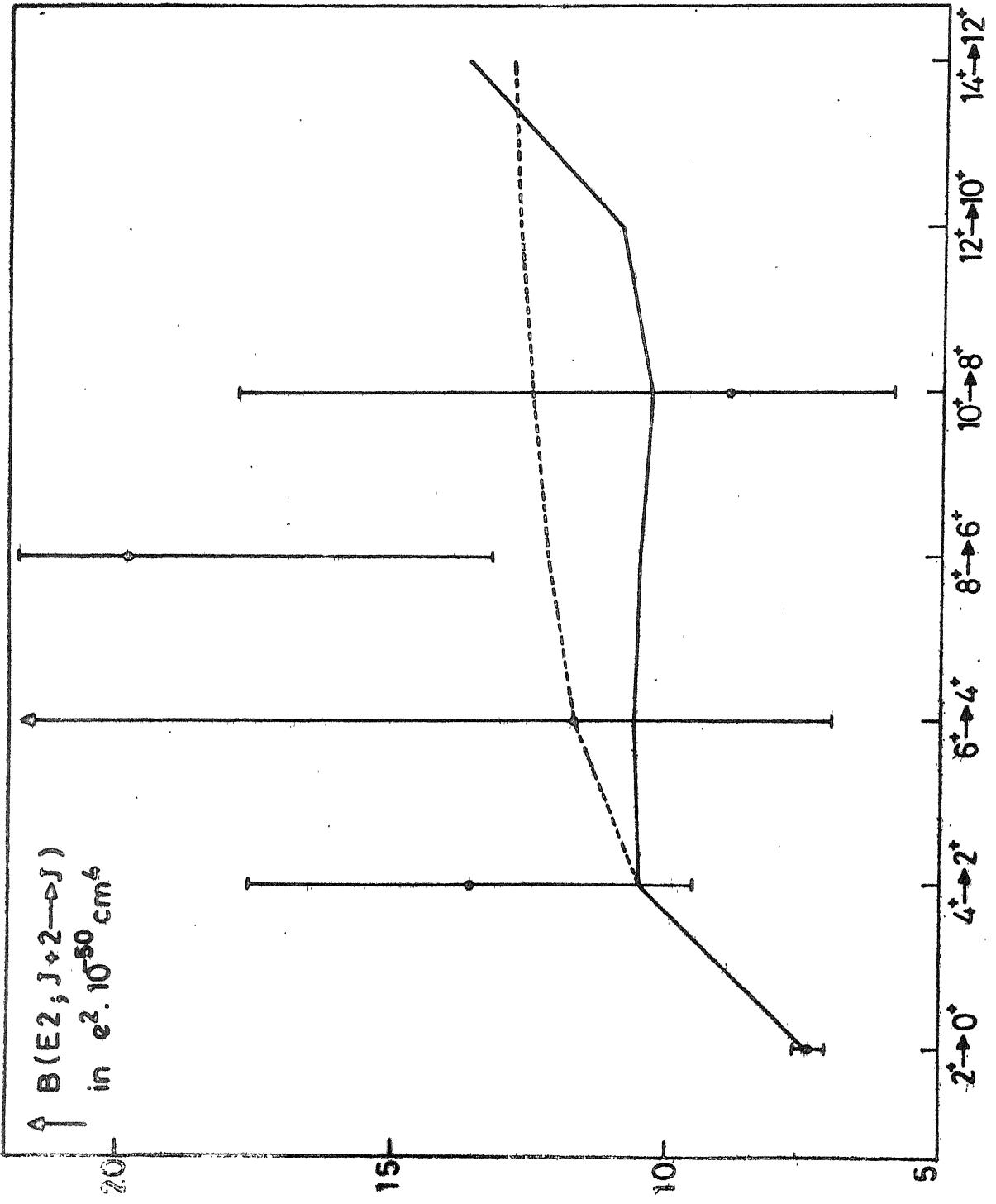
Fig. II.7   B(E2)   values   in   $^{76}$Se.

$< Q_\mu^2 >$ $(\mu \neq 0)$ values is usually associated with a decrease in the $< Q_0^2 >$ values. The experimental values presently involve large error bars which arise due to the uncertainties associated with the effects of higher excited states in the Coulomb excitation processes. More precise measurements of the static moments in near future will provide a better test of the wavefunctions involved.

## II.3.4  Occupation Numbers for Shell-model Orbits

In Tables II.10 and II.11 we have given the results for the occupation numbers of the $2p_{3/2}$, $1f_{5/2}$, $2p_{1/2}$ and $1g_{9/2}$ orbits in the ground states of the nuclei $^{68,70,72,74,76}$Ge and $^{72,74,76,78,80}$Se. Here one finds (see Figure II.8) that the occupation numbers for the $(1g_{9/2})$ orbit increase monotonically upon the addition of neutrons. The neutron occupation numbers for the $1f_{5/2}$ orbit also exhibit small but noticeable increase as a function of neutron number. The occupation numbers for the $2p_{3/2}$ - and $2p_{1/2}$ neutron orbits, however, remain nearly constant along the isotopic sequences.

We have also given in Table II.10 and II.11 the experimental results of Rotbard et al[24,34], as well as the theoretical estimates obtained by Kota, Pandya and Potbhare[35] using spectral distribution methods, in conjunction with the same set of input parameters - the spherical single-particle energies for the $2p_{3/2}$, $2p_{1/2}$, $1f_{5/2}$ and $1g_{9/2}$ orbits as well

Fig. II.8 Subshell occupation numbers in some Ge and Se isotopes.
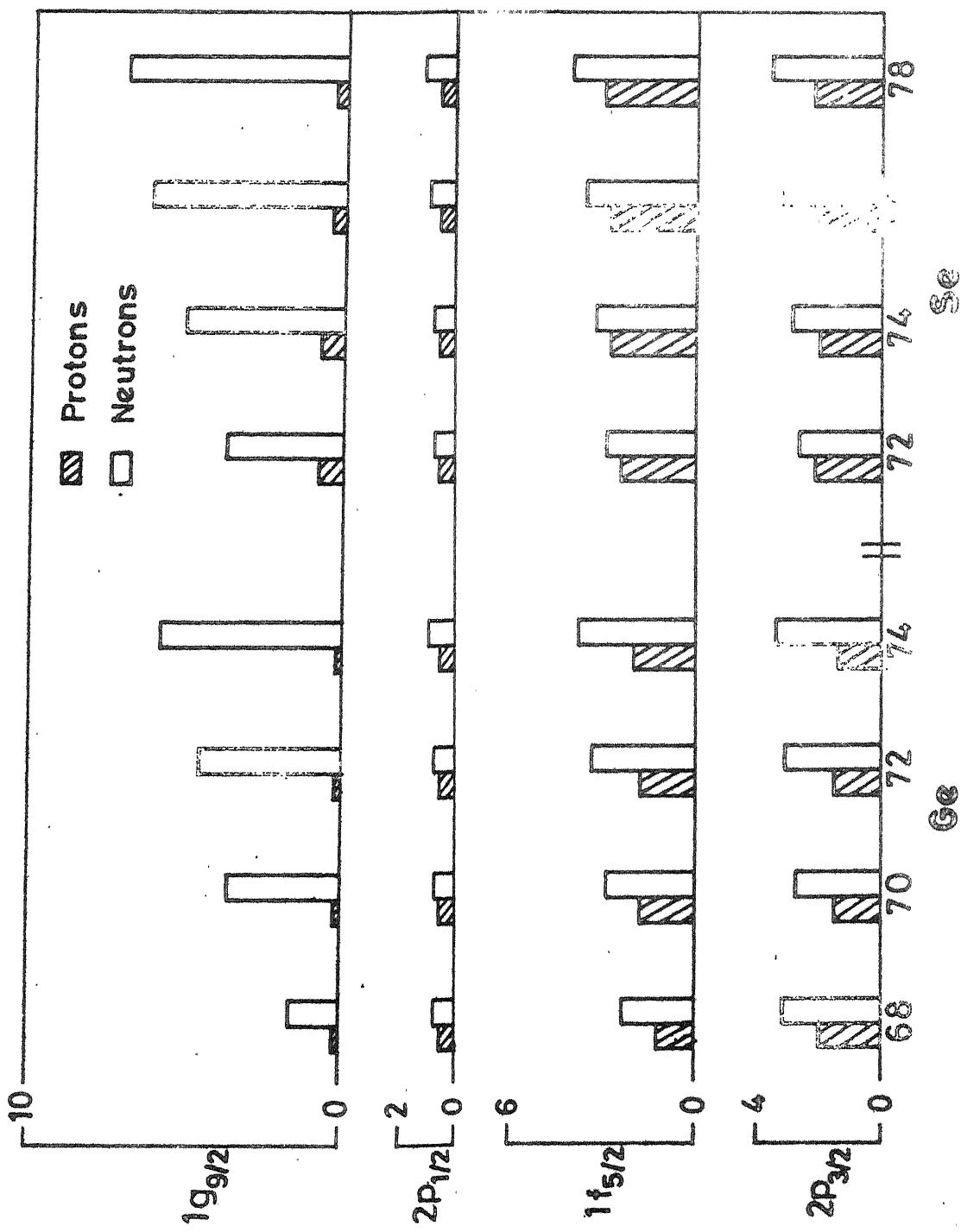
## TABLE II.10

The calculated values of the occupation numbers for various sub-shells in the ground states of some Ge isotopes. The theoretical estimates obtained by Kota, Pandya and Potbhare in the framework of the spectral distribution methods have been given in round brackets. The available experimental values of Rotbard et al.[24] have been given in square brackets.

| Nucleus | Protons | | | | Neutrons | | | |
|---|---|---|---|---|---|---|---|---|
| | $2p_{1/2}$ | $2p_{3/2}$ | $1f_{5/2}$ | $1g_{9/2}$ | $2p_{1/2}$ | $2p_{3/2}$ | $1f_{5/2}$ | $1g_{9/2}$ |
| $^{68}$Ge | 0.67 | 2.02 | 1.13 | 0.18 | 0.88 | 3.34 | 2.26 | 1.48 |
| | (0.93) | (2.97) | (0.10) | (0.00) | | | | |
| $^{70}$Ge | 0.58 | 1.52 | 1.71 | 0.19 | 0.66 | 2.93 | 2.92 | 3.49 |
| | (0.90) | (2.95) | (0.15) | (0.00) | | | | |
| | [0.59] | [2.36] | [1.24] | [0.25] | | | | |
| $^{72}$Ge | 0.54 | 1.47 | 1.79 | 0.20 | 0.84 | 3.26 | 3.43 | 4.47 |
| | (0.87) | (2.79) | (0.30) | (0.04) | | | | |
| | [0.43] | [2.35] | [1.34] | [0.24] | | | | |
| $^{74}$Ge | 0.51 | 1.34 | 1.94 | 0.21 | 1.02 | 3.48 | 3.91 | 5.59 |
| | (0.78) | (2.40) | (0.82 | (0.00) | | | | |
| | [0.43] | [1.44] | [2.20] | [0.37] | | | | |
| $^{76}$Ge | 0.44 | 1.31 | 1.99 | 0.12 | 1.36 | 3.69 | 4.51 | 6.68 |
| | (0.51) | (1.45) | (2.04) | (0.00) | | | | |
| | [0.40] | [1.25] | [2.44] | [0.25] | | | | |

as the effective two-body interaction - as the ones employed
in the present work. The present calculation is seen to
explain satisfactorily the observed proton subshell occupation
numbers in the ground states of the nuclei $^{74,76}$Ge and $^{76,78,80}$Se.
In the nuclei $^{70,72}$Ge and $^{74}$Se the VAP estimates suggest signi-
ficantly increased occupation of the $1f_{5/2}$-proton orbit at
the expense of the $2p_{1/2}$ and $2p_{3/2}$ orbits. Overall, the cal-
culations reported here do reproduce the qualitative feature of
the observed data - a transfer of the protons from the 2p orbits
to the $1f_{5/2}$ orbit in going from $^{70}$Ge to $^{76}$Ge. In keen
contrast with the results obtained in the present work, the
proton occupation numbers for the $1f_{5/2}$ orbit resulting from
the spectral distribution methods show significant discrepancies.
in the cases of nuclei $^{70,72,74}$Ge and $^{74,76}$Se.

Recently Kar and Ray[36] have examined various mechanisms
of unblocking the blocked allowed electron-capture during
gravitational collapse in type II supernovae. In the framework
of the zeroth-order shell-model, the allowed electron-capture
rates get blocked as the neutron number approaches 40, because
the protons from the f or p orbits then can not go to the f
or p neutron orbits. The results presented in Tables II.10
and II.11 show that the neutron occupation numbers for
$N \geq 40$ as substantially different from the zeroth-order shell
model estimates. Using the proton and neutron occupation
numbers in the ground states of N=40,42 nuclei obtained in
the present work, Kar and Ray have shown that the recognition of

the deformed nature of the nuclei in the Ge region leads to a
higher value of A - around A=84 instead of A ~74 - at which
the blocking is expected to set in.

## II.4  Conclusions

We have discussed here the results for the calculation
of high-spin yrast spectra, static quadrupole moments as well
as the reduced transition probabilities for E2 transitions
involving the yrast states, and the subshell occupation numbers
for proton and neutrons in some doubly even Ge and Se isotopes.
We have considered here the VAP prescription with the HFB
ansatz for the trial wavefunctions, employing the realistic
effective interactions operating in the valence space spanned
by the $2p_{3/2}$, $2p_{1/2}$, $1f_{5/2}$ and $1g_{9/2}$ orbits.  It turns out that
the VAP method permits a reasonably successful qualitative
as well as quantitative interpretation of the observed high-
spin yrast spectra in a parameter-free, microscopic manner.  In
particular, the method employed here reproduces to a large
extent the observed significant deviations of the yrast energies
from the $J(J+1)$-law; in this context we obtain considerably
improvement over the results obtained in an earlier calcu-
lation[37] involving eigenstates of $\hat{J}^2$ projected from single
HFB states for each isotope.

Present calculations have revealed significant
discrepancies between the observed and the calculated $(E_{2^+} - E_{0^+})$

energies. In the discussion of the yrast states presented here we have avoided introduction of the usual competing and coexisting degrees of freedom such as oblate, triaxial, $\gamma$-soft and hexadecapole shapes. However, it is expected that a consistent attempe to calculate the mixing of two $J=0$ states, one projected from the deformed HFB state and the other with a near-spherical origin, may improve considerably the position of the calculated $2^+$ states relative to the ground states.

<u>REFERENCES</u>

1.  A.P. de Lima et al., Phys. Lett. 83B (1979) 43.

2.  A.P. de Lima et al., Phys. Rev. C23 (1981) 213.

3.  C. Morand et al., Phys. Rev. C13 (1976) 2182.

4.  C. Morand et al., Nucl. Phys. A313 (1979) 45.

5.  C. Lebrum et al., Phys. Rev. C19 (1979) 1294.

6.  K.P. Lieb and J.J. Kolata, Phys. Rev. C15 (1977) 939.

7.  R.B. Piercey et al., Phys. Rev. C19 (1979) 1344.

8.  J.C. Wells, Jr., et al., Phys. Rev. C22 (1980) 1126.

9.  T. Matsuzaki and H. Taketani, Nucl. Phys. A390 (1982) 413.

10. M. Sakakura, Y. Shikata, A. Arima and T. Sebe, Z.Phys. A289 (1979) 163.

11. D. Ardouin et al., Phys. Rev. C11 (1975) 1649; Phys. Rev. C12 (1975) 1745.

12. M. Girod and B. Grammaticos, in Proceedings of the Conference on the Structure of Medium-heavy Nuclei, Rhodes, 1979, edited by the 'Demokritos' Tandem Accelerator Group, Athens (Institute of Physics, Bristol, 1980), p.225.

13. K. Kumar, J. Phys. G4 (1978) 849.

14. T. Matsuzaki and H. Taketani, Nucl. Phys. A390 (1982) 413.

15. H.F. de Vries and P.J. Brussaard, Z. Phys. A286 (1978) 1.

16. J. Haderman and A.C. Rester, Nucl. Phys. A231 (1974) 120.

17. F. Sakata, S. Iwasaki, T. Marumori and K. Takada, Z. Phys. A286 (1978) 195.

18. M. Vergnes, in Proceedings of the Conference on the Structure of Medium-heavy Nuclei, Rhodes, 1979, edited by the 'Demokritos' Tandem Accelerator Group, Athens (Institute of Physics, Bristol, 1980), p.25.

19. M.N. Vergnes et al., Phys. Lett. 72B (1978) 447.

20. R. Lecomte et al., Phys. Rev. C22 (1980) 2420.

21. R. Lecomte et al., Phys. Rev. C25 (1982) 2812.

22. M.L. Halbert et al., Nucl. Phys. A256 (1976) 496.

23. A.L. Goodman, in Advances in Nuclear Physics, eds. J.W. Negele and E. Vogt (Plenum Press, New York-London 1979), Vol. 11.

24. G. Rotbard et al., Phys. Rev. C18 (1978) 86.

25. T.T.S. Kuo, private communication to Professor K.H. Bhatt.

26. V. Potbhare, S.K. Sharma and S.P. Pandya, Phys. Rev. C24 (1981) 2355.

27. D.P. Ahalpara and K.H. Bhatt, Phys. Rev. C25 (1982) 2072.

28. J.H. Hamilton et al., Phys. Rev. Letters 32 (1974) 239.

29. R.B. Piercey et al., Phys. Rev. Letters 37 (1976) 497.

30. J.H. Hamilton, R.L. Robinson and A.V. Ramayya in Proceedings of the International Conference on Nuclear Interactions, Canberra, 1976, edited by B.A. Robson (Springer, New York, 1978), p.253.

31. R. Lecomte et al., Phys. Rev. C22 (1980) 1530.

32. R. Lecomte, S. Landsberger, P. Paradis, and S. Monaro, Phys. Rev. C18 (1978) 2801.

33. R. Lecomte et al., Nucl. Phys. A284 (1977) 123.

34. G. Rotbard et al., Nucl. Phys. A401 (1983) 41.

35. V.K.B. Kota, S.P. Pandya and V. Potbhare, Phys. Rev. C25 (1982) 1667.

36. K. Kar and A. Ray, Phys. Lett. 96A (1983) 322.

37. S.K. Sharma, Phys. Rev. C22 (1980) 2612.

# CHAPTER III

## HIGH-SPIN YRAST SPECTRA IN DOUBLY EVEN
## KRYPTON AND STRONTIUM ISOTOPES

## III.1  Introduction

In this Chapter we report on the calculations of the high-spin yrast spectra of the doubly even nuclei $^{74,76,78,80,82}$Kr and $^{80,82,84}$Sr.  Apart from the energy spectra we shall also discuss here the results of the calculations of static quadrupole moments and the reduced transition probabilities for E2 transitions for the yrast states, as well as the subshell occupation numbers for the $2p_{1/2}$, $2p_{3/2}$, $1f_{5/2}$ and $1g_{9/2}$ orbits in the ground states of these nuclei.

Recent years have witnessed a rapid increase in the experimental activity of measuring the properties of the yrast levels (with $J^{\pi} = 16^{+}$) in Kr and Sr isotopes.  In Tables III.1 and III.2 we give references[1-18] to papers that have recently provided experimental information concerning the energies as well as the reduced E2 transition probabilities for the yrast levels in the nuclei $^{74,76,78,80,82}$Kr and $^{80,82,84}$Sr.

The available experimental information in the nuclei $^{74,76,78}$Kr and $^{80}$Sr suggests existence of sizable quadrupole deformation – and the associated rotational collectivity – in the ground states.  The $(E_{2^{+}} - E_{0^{+}})$ energies in these isotopes range between 0.385 MeV to 0.455 MeV and

## TABLE III.1

### Summary of the available experimental information
### for the yrast levels in Kr isotopes

| Nucleus | Yrast levels | Half-lives |
|---|---|---|
| $^{74}$Kr | J.Rath et al.[1] $(0^{\pm}20^+)$ | - |
| | J.H.Hamilton et al.[2] $(0^{\pm}20^+)$ | - |
| $^{76}$Kr | R.B.Piercey et al.[3,4] $(0^{\pm}12^+)$ | R.B.Piercey et al.[3,4] $(0^{\pm}12^+)$ |
| | J.H.Hamilton et al.[2] $(0^{\pm}12^+)$ | - |
| | S.Matsuki et al.[5] $(0^{\pm}8^+)$ | - |
| $^{78}$Kr | H.P.Hellmeister et al.[6-8] $(0^{\pm}16^+)$ | H.P.Hellmeister et al.[6-8] $(0^{\pm}1$ |
| | R.L.Robinson et al.[9] $(0^{\pm}12^+)$ | R.L.Robinson et al.[9] $(0^{\pm}10^+)$ |
| | D.G.McCauley and J.E.Draper[10] $(0^{\pm}10^+)$ | - |
| $^{80}$Kr | L.Funke et al.[11] $(0^{\pm}14^+)$ | L.Funke et al.[11] $(0^{\pm}14^+)$ |
| | D.G.McCauley and J.E.Draper[10] $(0^+-8^+)$ | H.G.Friederichs et al.[12] $(0^{\pm}8^+)$ |
| | D.L.Sastry et al.[13] $(0^{\pm}12^+)$ | - |
| $^{82}$Kr | D.G.McCauley and J.E.Draper[10] $(0^{\pm}6^+)$ | C.M.Cartwright et al.[14] $(0^{\pm}2^+)$ |

## TABLE III.2

### Summary of the available experimental information
### for the yrast levels in Sr isotopes

| Nucleus | Yrast levels | Half lives |
|---------|--------------|------------|
| $^{80}$Sr | C.J.Lister et al.[15] $(0^{\pm}16^{+})$ | C.J.Lister et al.[15] $(0^{\pm}4^{+})$ |
|  | C.A.Fields et al.[16] $(0^{\pm}6^{+})$ | – |
|  | T.Higo et al.[17] $(0^{\pm}10^{+})$ | – |
| $^{82}$Sr | C.A.Fields et al.[16] $(0^{\pm}10^{+})$ | – |
|  | T.Higo et al.[17] $(0^{\pm}1C^{+})$ | – |
| $^{84}$Sr | A.Dewald et al.[18] $(0^{+}14^{+})$ | A.Dewald et al.[18] $(0^{\pm}12^{+})$ |
|  | C.A.Fields et al.[17] $(0^{\pm}10^{+})$ | – |

the B(E2, $2^+ \to 0^+$) values are more than 52 W.u. The available information in the nuclei $^{80,82}$Kr and $^{82,84}$Sr, on the other hand, implies a significant reduction of rotational collectivity; the $(E_{2^+} - E_{0^+})$ values lie in the range 0.576-0.777 MeV and the observed B(E2, $2^+ \to 0^+$) estimates are smaller than 25 W.u. The reduced rotational collectivity in nuclei with A > 80 is just an empirical manifestation of the shell closure at N=50.

A large number of recent calculations have attempted a description of the high-spin yrast levels in Kr and Sr isotopes in the framework of phenomenological models. Kaup and Gelberg[19,20], Ramayya[21], Bucurescu et al.[22] and Dewald et al.[18] have carried out calculations in the framework of the Interacting Boson Model. Sastry et al.[13], Funke et al.[11] and Soundranayagam et al.[23] have performed two-quasiparticle plus rotor model calculations for $^{80}$Kr.

In this Chapter we study the high-spin levels in the Kr and Sr isotopes in the framework of the VAP technique discussed in the preceding Chapter. The calculations presented here employ the same configuration space as well as the effective interaction as the one employed in our calculations in the Ge and Se isotopes. The single-particle energies we have taken are (in MeV) : $\varepsilon(2p_{3/2}) = 0.0$, $\varepsilon(1f_{5/2}) = 0.78$, $\varepsilon(2p_{1/2}) = 1.08$ and $\varepsilon(1g_{9/2}) = 3.25$ for the Kr isotopes. In our calculations for the Sr isotopes we have taken $\varepsilon(1g_{9/2}) = 3.0$ MeV.

In Section III.2 we present a comparison of the calculated yrast spectra, static quadrupole moments as well as the reduced transition probabilities for E2 transitions with the available[1-18] experimental results. Section III.3 contains some concluding remarks.

## III.2 Results and Discussion
### III.2.1 Intrinsic States

The calculated quadrupole moments of the optimum intrinsic states associated with the yrast levels in the nuclei $^{74,76,78,80,82}$Kr and $^{80,82,84}$Sr have been presented in Table III.3

Discussing first the results for the $Q_o^2$ moments of the optimum intrinsic states associated with the ground states, we notice that the $<Q_o^2>$ values in the nuclei $^{74,76,78}$Kr and $^{80,82}$Sr are nearly 90 percent of their maximum possible values for the given valence space. This ties in nicely with the observed enhanced rotational collectivity in these isotopes. As mentioned earlier, the reduction in the intrinsic quadrupole deformation of the ground states in the nuclei $^{80,82}$Kr and $^{84}$Sr is due to the approaching shell closure at N=50.

We next discuss the variation of the quadrupole moments of the optimum intrinsic states along the yrast cascade. In keen contrast with the results obtained earlier in the case

# TABLE III.3

Quadrupole deformations, $<\tilde{\Phi}_{opt} | Q_o^2 | \tilde{\Phi}_{opt}(\beta_J)>$ , of the optimum intrinsic states associated with the yrast levels in the nuclei $^{74,76,78,80,82}Kr$ and $^{80,82,84}Sr$. Here $<Q_o^2>_{max.}$ gives the maximum possible value of the intrinsic quadrupole moment for each isotope

| Nucleus | $<\tilde{\Phi}_{opt}(\beta_J) | Q_o^2 | \tilde{\Phi}_{opt}(\beta_J)>$ | | | | | | | | $<Q_o^2>_{max.}$ |
|---------|---------|------|------|------|------|------|------|------|------|
| $J^{\pi}_{yrast}=$ | $0^+$ | $2^+$ | $4^+$ | $6^+$ | $8^+$ | $10^+$ | $12^+$ | $14^+$ | |
| $^{74}Kr$ | 44.2 | 44.2 | 44.6 | 44.6 | 44.6 | 44.6 | 44.6 | 44.6 | 46.7 |
| $^{76}Kr$ | 43.4 | 43.4 | 45.6 | 45.6 | 45.6 | 45.6 | 45.6 | 45.6 | 48.0 |
| $^{78}Kr$ | 39.5 | 39.5 | 39.5 | 39.5 | 39.5 | 39.5 | 39.5 | 39.5 | 45.4 |
| $^{80}Kr$ | 34.3 | 34.3 | 35.1 | 36.3 | 36.3 | 36.3 | 36.3 | 36.3 | 40.6 |
| $^{82}Kr$ | 27.0 | 28.4 | 29.6 | 29.6 | 29.6 | 29.6 | 29.6 | 29.6 | 35.5 |
| $^{80}Sr$ | 44.6 | 45.6 | 45.6 | 45.6 | 45.6 | 45.6 | 45.6 | 45.6 | 47.5 |
| $^{82}Sr$ | 41.0 | 41.0 | 41.5 | 41.5 | 41.5 | 41.7 | 41.7 | 41.7 | 42.8 |
| $^{84}Sr$ | 29.7 | 32.7 | 34.9 | 37.2 | 37.2 | 37.2 | 37.2 | 37.2 | 37.6 |

of Ge and Se isotopes, it turns out that the variations in the quadrupole deformations of the optimum intrinsic states associated with various yrast levels in most of the isotopes is quite small. This feature of the calculated results is partly related to the non-occurence of crossings of Nilsson levels in the neighbourhood of the relevant Fermi surfaces for various isotopes.

### III.2.2 Yrast Levels

We first discuss here the nuclei $^{74,76,78,80,82}$Kr. In Figures III.1 and III.2 we have presented the observed[1-11,13] as well as the theoretical yrast spectra resulting from the VAP method. We have also given here the yrast spectra obtained by carrying out angular momentum projection on the minimum-energy HFB intrinsic states for various nuclei. Keeping in view the possibility of a change in the position of the calculated $0^+$ states because of its mixing with the coexisting $0^+$ states of spherical origin, we have focussed only on a comparison of the calculated and observed yrast spectra for $J \geq 2$. We have, therefore, aligned the calculated $2^+$ states with the observed ones.

It is seen that the VAP yrast spectra in the nuclei $^{74,76}$Kr are in reasonably good agreement with the experiments. The VAP prescription is seen to yield small but significant improvements over the PHFB yrast energies in these nuclei.
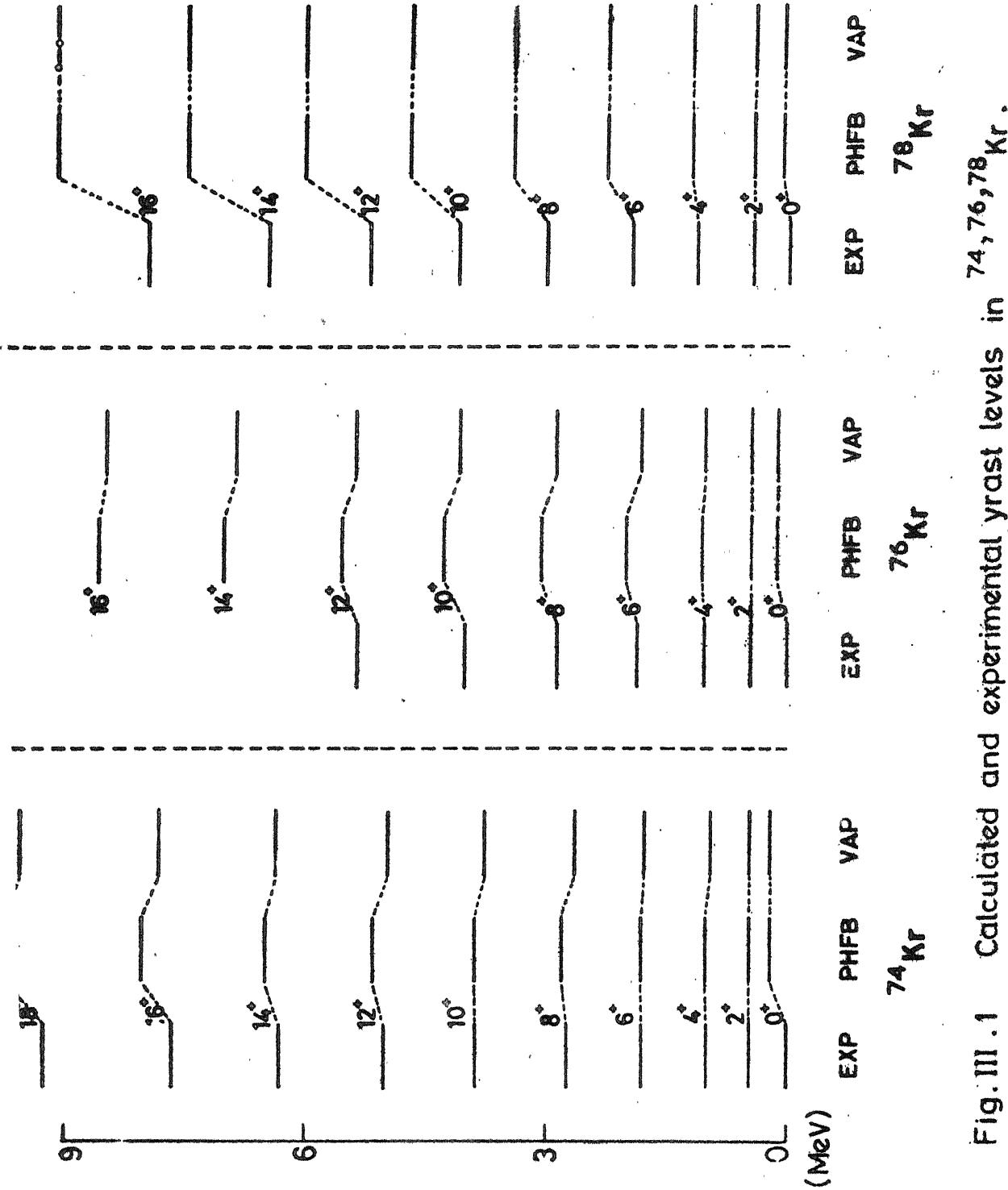
Fig. III.1   Calculated and experimental yrast levels in $^{74,76,78}Kr$.
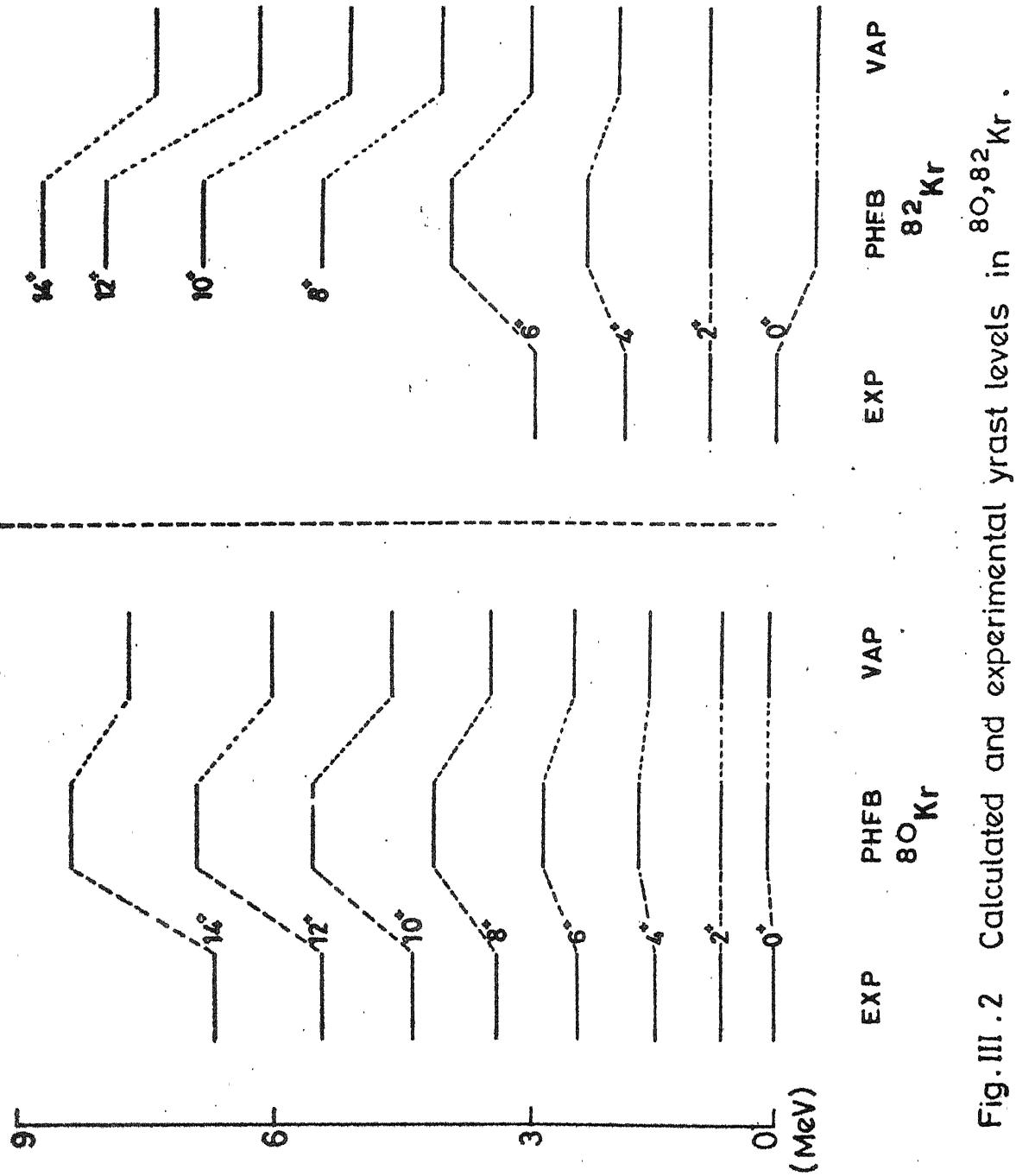
Fig. III.2 Calculated and experimental yrast levels in $^{80,82}$Kr.

In the case of the nucleus $^{78}$Kr, the VAP results — and these are almost identical with the PHFB ones - display significant discrepancies for the levels with $J > 8$.

The observed spectra in the nuclei $^{80,82}$Kr display significant departure from the rotational pattern. Whereas the spectra in the nuclei $^{74,76,78}$Kr can be described by the relation $E_J = A\,J(J+1) + B\,J^2(J+1)^2$ with the parameters $[A(keV), B(keV)] = [86.60, -1.80]$, $[78.80, -1.35]$ and $[84.35, -1.42]$ respectively, the yrast spectra in $^{80,82}$Kr require the values $[116.11, -2.21]$ and $[145.98, -2.75]$ respectively. We find (see Figure III.2) that the VAP energies for the yrast levels with $2^+ < J^\pi < 12^+$ in the nucleus $^{80}$Kr are in very good agreement with the observed ones; the maximum discrepancy between the calculated and observed levels is just 260 keV.

The present calculation yields rather poor agreement with the experiments in the case of the nucleus $^{82}$Kr. This may be reflecting the inadequacy of the present valence space for this isotope.

The results for the calculated PHFB as well as VAP yrast energies in the nuclei $^{80,82,84}$Sr have been presented in Figure III.3 together with the observed yrast energies. Although the VAP energies represent considerable improvement over the PHFB results, some significant discrepancies still occur for $J > 8$ in the nuclei $^{80,82}$Sr. It will be interesting
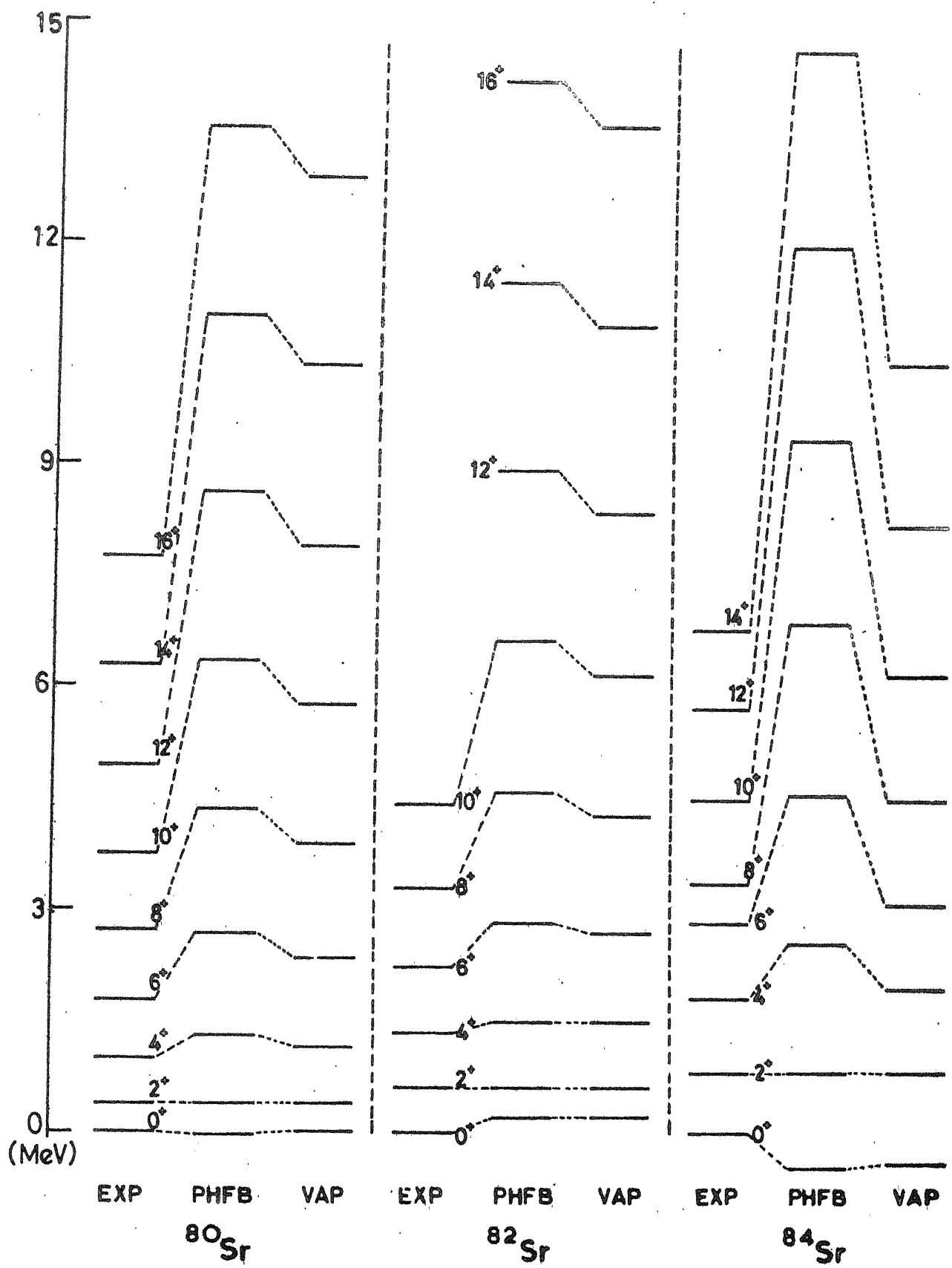
Fig. III .3   Calculated  and  experimental  yrast  levels  in  $^{80,82,84}$Sr .

to examine the effect of inclusion of non-axial deformations vis-à-vis the observed spectra by invoking the cranked HFB prescription.

The observed spectra in the nucleus $^{84}$Sr is characterized by anomalously small $8^+ \to 6^+$ separation. This suggests large structural changes in this nucleus at $J^\pi = 6^+$. The present calculation does not reproduce this feature; the calculated positions of the levels with J=8,10 and 12 are about 1.5 MeV too high compared to the experiment.

## III.2.3 Electromagnetic Properties

We now discuss the electromagnetic properties of the yrast levels in the nuclei $^{74,76,78,80,82}$Kr and $^{80,82,84}$Sr. The results for the reduced transition probabilities for the E2 transitions involving the yrast levels have been presented in Tables III.4-III.11. We have also given here the VAP results for the static quadrupole moments for the yrast states. The electromagnetic properties discussed here have been computed with a single set of effective charges: $e_p = 1.7$ and $e_n = 0.7$.

We first discuss the results for the yrast states in Kr isotopes. The calculated as well as the observed[3,4,6-8], values in the nuclei $^{76,78,80}$Kr have been plotted in Figures III.4-III.6. The rigid rotor values for various transitions calculated from the relation (II.75) have also been

## TABLE III.4

The reduced transition probabilities for the E2 transitions as well as the static quadrupole moments for the yrast levels in the nucleus $^{74}$Kr. Here $e_p(e_n)$ denotes the effective charge for protons (neutrons). The entries presented in the second column correspond to the reduced matrix elements resulting from equation (II.62). The reduced matrix elements as well as the static moments have been expressed in a form that brings out their explicit dependence on the effective charges

| Transition | $[B(E2; J_i^+ \to J_f^+)]^{1/2}_{th}$ | $[Q(J_i^+)]_{th}$ | $B(E2, J_i^+ \to J_f^+)$ | | $Q(J_i^+)$ | |
|---|---|---|---|---|---|---|
| | | | $e_p=1.7, e_n=0.7$ | expt. | $e_p=1.7, e_n=0.7$ | expt. |
| $2^+ \to 0^+$ | $1.38e_p+1.69e_n$ | $-27.89e_p-34.09e_n$ | 12.43 | – | -71.27 | – |
| $4^+ \to 2^+$ | $1.64e_p+1.99e_n$ | $-35.45e_p-43.18e_n$ | 17.38 | – | -90.50 | – |
| $6^+ \to 4^+$ | $1.74e_p+2.09e_n$ | $-38.86e_p-47.19e_n$ | 19.59 | – | -99.10 | – |
| $8^+ \to 6^+$ | $1.78e_p+2.11e_n$ | $-40.51e_p-49.08e_n$ | 20.23 | – | -103.23 | – |
| $10^+ \to 8^+$ | $1.80e_p+2.10e_n$ | $-41.45e_p-49.94e_n$ | 20.42 | – | -105.42 | – |
| $12^+ \to 10^+$ | $1.82e_p+2.08e_n$ | $-41.91e_p-49.94e_n$ | 20.62 | – | -106.20 | – |
| $14^+ \to 12^+$ | $1.78e_p+2.02e_n$ | $-42.33e_p-49.57e_n$ | 19.69 | – | -106.66 | – |

The B(E2) values are in units of $10^{-50}$ e$^2$cm$^4$ and the static quadrupole moments have been given in units of efm$^2$.

## TABLE III.5

The results for the nucleus $^{76}$Kr

| Transition $(J_i^+ \to J_f^+)$ | $[B(E2; J_i^+ \to J_f^+)]^{1/2}_{th}$ | $[Q(J_i^+)]_{th}$ | $B(E2, J_i^+ \to J_f^+)$ $e_p=1.7, e_n=0.7$ | expt. | $Q(J_i^+)$ $e_p=1.7, e_n=0.7$ | expt |
|---|---|---|---|---|---|---|
| $2^+ \to 0^+$ | $1.37e_p+1.66e_n$ | $-27.71e_p-33.57e_n$ | 12.21 | $11.28\pm1.34$ | $-70.60$ | – |
| $4^+ \to 2^+$ | $1.35e_p+1.71e_n$ | $-25.10e_p-44.85e_n$ | 12.15 | $14.72^{+4.40}_{-2.68}$ | $-91.07$ | – |
| $6^+ \to 4^+$ | $1.73e_p+2.21e_n$ | $-38.56e_p-49.80e_n$ | 20.08 | $17.01\pm1.53$ | $-100.42$ | – |
| $8^+ \to 6^+$ | $1.76ep+2.22e_n$ | $-40.20e_p-51.48e_n$ | 20.69 | $23.51\pm2.49$ | $-104.28$ | – |
| $10^+ \to 8^+$ | $1.78e_p+2.20e_n$ | $-41.10e_p-51.99e_n$ | 20.80 | $24.66\pm3.63$ | $-106.26$ | – |
| $12^+ \to 10^+$ | $1.78e_p+2.15e_n$ | $-41.67e_p-51.78e_n$ | 20.61 | $9.91\pm2.10$ | $-107.09$ | – |
| $14^+ \to 12^+$ | $1.78e_p+2.10e_n$ | $-42.21e_p-55.80e_n$ | 20.17 | – | $-110.82$ | – |

TABLE III.6

The results for the nucleus $^{78}$Kr

| Transition $(J_i^+ \rightarrow J_f^+)$ | $[B(E2, J_i^+ \rightarrow J_f^+)]^{1/2}_{th}$ | $[Q(J_i^+)]_{th}$ | $B(E2, J_i^+ \rightarrow J_f^+)$ $e_p=1.7, e_n=0.7$ | expt. | $Q(J_i^+)$ $e_p=1.7, e_n=0.7$ | expt. |
|---|---|---|---|---|---|---|
| $2^+ \rightarrow 0^+$ | $1.35e_p+1.42e_n$ | $-27.29e_p-28.46e_n$ | $10.81$ | $13.09^{+0.87}_{-0.77}$ | $-56.31$ | – |
| $4^+ \rightarrow 2^+$ | $1.61e_p+1.70e_n$ | $-34.42e_p-35.52e_n$ | $15.39$ | $17.49^{+2.14}_{-2.45}$ | $-33.38$ | – |
| $6^+ \rightarrow 4^+$ | $1.68e_p+1.79e_n$ | $-37.41e_p-37.99e_n$ | $16.85$ | $19.50^{+3.90}_{-2.80}$ | $-90.19$ | – |
| $8^+ \rightarrow 6^+$ | $1.71e_p+1.83e_n$ | $-37.87e_p-38.62e_n$ | $16.76$ | $16.90^{+2.50}_{-2.00}$ | $-93.12$ | – |
| $10^+ \rightarrow 8^+$ | $1.72e_p+1.83e_n$ | $-39.69e_p-38.30e_n$ | $17.08$ | $> 9.60$ | $-94.27$ | – |
| $12^+ \rightarrow 10^+$ | $1.72e_p+1.84e_n$ | $-40.28e_p-37.36e_n$ | $17.11$ | – | $-94.63$ | – |
| $14^+ \rightarrow 12^+$ | $1.71e_p+1.82e_n$ | $-40.86e_p-35.95e_n$ | $17.55$ | $11.55^{+6.60}_{-3.07}$ | $-94.63$ | – |

## TABLE III.7

The results for the nucleus $^{80}\text{Kr}$

| Transition $(J_i^+ \to J_f^+)$ | $[B(E2, J_i^+ \to J_f^+)]_{th}^{1/2}$ | $[Q(J_i^+)]_{th}$ | $B(E2, J_i^+ \to J_f^+)$ | | $Q(J_i^+)$ | |
|---|---|---|---|---|---|---|
| | | | $e_p=1.7, e_n=0.7$ | expt. | $e_p=1.7, e_n=0.7$ | expt. |
| $2^+ \to 0^+$ | $1.28e_p + 1.14e_n$ | $-25.79e_p - 22.70e_n$ | 8.86 | $7.60 \pm 0.60$ | $-59.73$ | — |
| $4^+ \to 2^+$ | $1.52e_p + 1.36e_n$ | $-32.97e_p - 28.08e_n$ | 12.46 | $9.20^{+2.28}_{-1.45}$ | $-75.70$ | — |
| $6^+ \to 4^+$ | $1.58e_p + 1.42e_n$ | $-37.23e_p - 30.33e_n$ | 13.51 | $10.20^{+6.42}_{-2.69}$ | $-84.52$ | — |
| $8^+ \to 6^+$ | $1.73e_p + 1.54e_n$ | $-39.28e_p - 30.58e_n$ | 16.09 | $18.40^{+16.56}_{-8.28}$ | $-88.18$ | — |
| $10^+ \to 8^+$ | $1.74e_p + 1.57e_n$ | $-40.11e_p - 29.77e_n$ | 16.38 | $9.60^{+5.99}_{-3.52}$ | $-89.02$ | — |
| $12^+ \to 10^+$ | $1.73e_p + 1.58e_n$ | $-40.90e_p - 28.53e_n$ | 16.13 | $17.40^{+18.63}_{-6.21}$ | $-89.51$ | — |
| $\to 12^+$ | $1.71e_p + 1.58e_n$ | $-41.84e_p - 26.89e_n$ | 16.10 | $> 3$ | $-89.96$ | — |

TABLE III.8

The results for the nucleus $^{82}$Kr

| Transition $(J_i^+ \to J_f^+)$ | $[B(E2,J_i^+ \to J_f^+)]^{1/2}_{th}$ | $[Q(J_i^+)]_{th}$ | $B(E2,J_i^+ \to J_f^+)$ | | $Q(J_i^+)$ | |
|---|---|---|---|---|---|---|
| | | | $e_p=1.7,e_n=0.7$ | expt. | $e_p=1.7,e_n=0.7$ | expt. |
| $2^+ \to 0^+$ | $1.11e_p+0.83e_n$ | $-22.46e_p-16.70e_n$ | 5.92 | $4.86\pm0.21$ | -49.89 | - |
| $4^+ \to 2^+$ | $1.39e_p+1.03e_n$ | $-30.24e_p-20.40e_n$ | 9.51 | - | -65.73 | - |
| $6^+ \to 4^+$ | $1.65e_p+1.14e_n$ | $-33.72e_p-20.60e_n$ | 11.83 | - | -71.74 | - |
| $8^+ \to 6^+$ | $1.58e_p+1.19e_n$ | $-34.88e_p-19.13e_n$ | 12.37 | - | -72.69 | - |
| $10^+ \to 8^+$ | $1.59e_p+1.23e_n$ | $-35.56e_p-16.59e_n$ | 12.64 | - | -72.33 | - |
| $12^+ \to 10^+$ | $1.59e_p+1.24e_n$ | $-36.23e_p-14.57e_n$ | 12.71 | - | -71.80 | - |
| $14^+ \to 12^+$ | $1.57e_p+1.25e_n$ | $-36.29e_p-11.62e_n$ | 12.55 | - | -69.83 | - |

## TABLE III.9

### The results for the nucleus $^{80}$Sr

| Transition ($J_i^+ \to J_f^+$) | $[B(E2, J_i^+ \to J_f^+)]^{1/2}_{th}$ | $[Q(J_i^+)]_{th}$ | $B(E2, J_i^+ \to J_f^+)$ $e_p=1.7, e_n=0.7$ | expt. | $Q(J_i^+)$ $e_p=1.7, e_n=0.7$ | expt. |
|---|---|---|---|---|---|---|
| $2^+ \to 0^+$ | $1.54e_p + 1.32e_n$ | $-34.22e_p - 29.25e_n$ | $12.54$ | $17.97^{+1.59}_{-1.34}$ | $-78.65$ | — |
| $4^+ \to 2^+$ | $2.03e_p + 1.75e_n$ | $-43.70e_p - 37.31e_n$ | $21.86$ | $22.69^{+4.05}_{-2.98}$ | $-100.41$ | — |
| $6^+ \to 4^+$ | $2.11e_p + 1.83e_n$ | $-47.59e_p - 40.59e_n$ | $23.70$ | — | $-109.32$ | — |
| $8^+ \to 6^+$ | $2.12e_p + 1.87e_n$ | $-49.46e_p - 42.10e_n$ | $24.14$ | — | $-113.55$ | — |
| $10^+ \to 8^+$ | $2.11e_p + 1.89e_n$ | $-50.26e_p - 42.65e_n$ | $24.11$ | — | $-115.30$ | — |
| $12^+ \to 10^+$ | $2.08e_p + 1.90e_n$ | $-50.36e_p - 42.59e_n$ | $23.86$ | — | $-115.43$ | — |
| $14^+ \to 12^+$ | $2.04e_p + 1.90e_n$ | $-49.59e_p - 42.07e_n$ | $23.02$ | — | $-113.75$ | — |

## TABLE III.10

The results for the nucleus $^{82}$Sr

| Transition $(J_i^+ \rightarrow J_f^+)$ | $[B(E2, J_i^+ \rightarrow J_f^+)]^{1/2}_{th}$ | $[Q(J_i^+)]_{th}$ | $B(E2, J_i^+ \rightarrow J_f^+)$ $e_p=1.7, e_n=0.7$ | expt. | $Q(J_i^+)$ $e_p=1.7, e_n=0.7$ | expt. |
|---|---|---|---|---|---|---|
| $2^+ \rightarrow 0^+$ | $1.69e_p+1.18e_n$ | $-34.11e_p-23.75e_n$ | 13.68 | – | -74.61 | – |
| $4^+ \rightarrow 2^+$ | $1.94e_p+1.36e_n$ | $-43.42e_p-29.89e_n$ | 18.06 | – | -94.76 | – |
| $6^+ \rightarrow 4^+$ | $2.11e_p+1.50e_n$ | $-47.54e_p-32.38e_n$ | 21.50 | – | -103.48 | – |
| $8^+ \rightarrow 6^+$ | $2.12e_p+1.53e_n$ | $-49.29e_p-33.21e_n$ | 21.86 | – | -107.04 | – |
| $10^+ \rightarrow 8^+$ | $2.06e_p+1.54e_n$ | $-50.12e_p-33.46e_n$ | 20.98 | – | -108.63 | – |
| $12^+ \rightarrow 10^+$ | $2.06e_p+1.58e_n$ | $-50.01e_p-32.96e_n$ | 21.23 | – | -108.09 | – |
| $14^+ \rightarrow 12^+$ | $2.01e_p+1.60e_n$ | $-49.28e_p-31.92e_n$ | 20.58 | – | -106.12 | – |

## TABLE III.11

### The results for the nucleus $^{84}$Sr

| Transition $(J_i^+ \to J_f^+)$ | $[B(E2;J_i^+ \to J_f^+)]_{th}^{1/2}$ | $[Q(J_i^+)]_{th}$ | $B(E2,J_i^+ \to J_f^+)$ | | $Q(J_i^+)$ | |
|---|---|---|---|---|---|---|
| | | | $e_p=1.7, e_n=0.7$ | expt. | $e_p=1.7, e_n=0.7$ | expt. |
| $2^+ \to 0^+$ | $1.23e_p+0.80e_n$ | $-26.79e_p-17.09e_n$ | 7.03 | $5.68\pm0.66$ | $-57.51$ | – |
| $4^+ \to 2^+$ | $1.65e_p+0.98e_n$ | $-38.16e_p-21.40e_n$ | 12.19 | $3.72\pm0.44$ | $-79.85$ | – |
| $6^+ \to 4^+$ | $1.53e_p+0.85e_n$ | $-46.91e_p-23.54e_n$ | 10.21 | $4.59\pm0.87$ | $-96.23$ | – |
| $8^+ \to 6^+$ | $2.12e_p+0.15e_n$ | $-49.39e_p-23.93e_n$ | 19.44 | $0.92\pm0.44$ | $-100.71$ | – |
| $10^+ \to 8^+$ | $2.09e_p+1.17e_n$ | $-49.88e_p-23.36e_n$ | 19.11 | $1.53\pm0.22$ | $-101.15$ | – |
| $14^+ \to 12^+$ | $1.97e_p+1.21e_n$ | $-48.41e_p-20.49e_n$ | 17.61 | – | $-117.13$ | – |
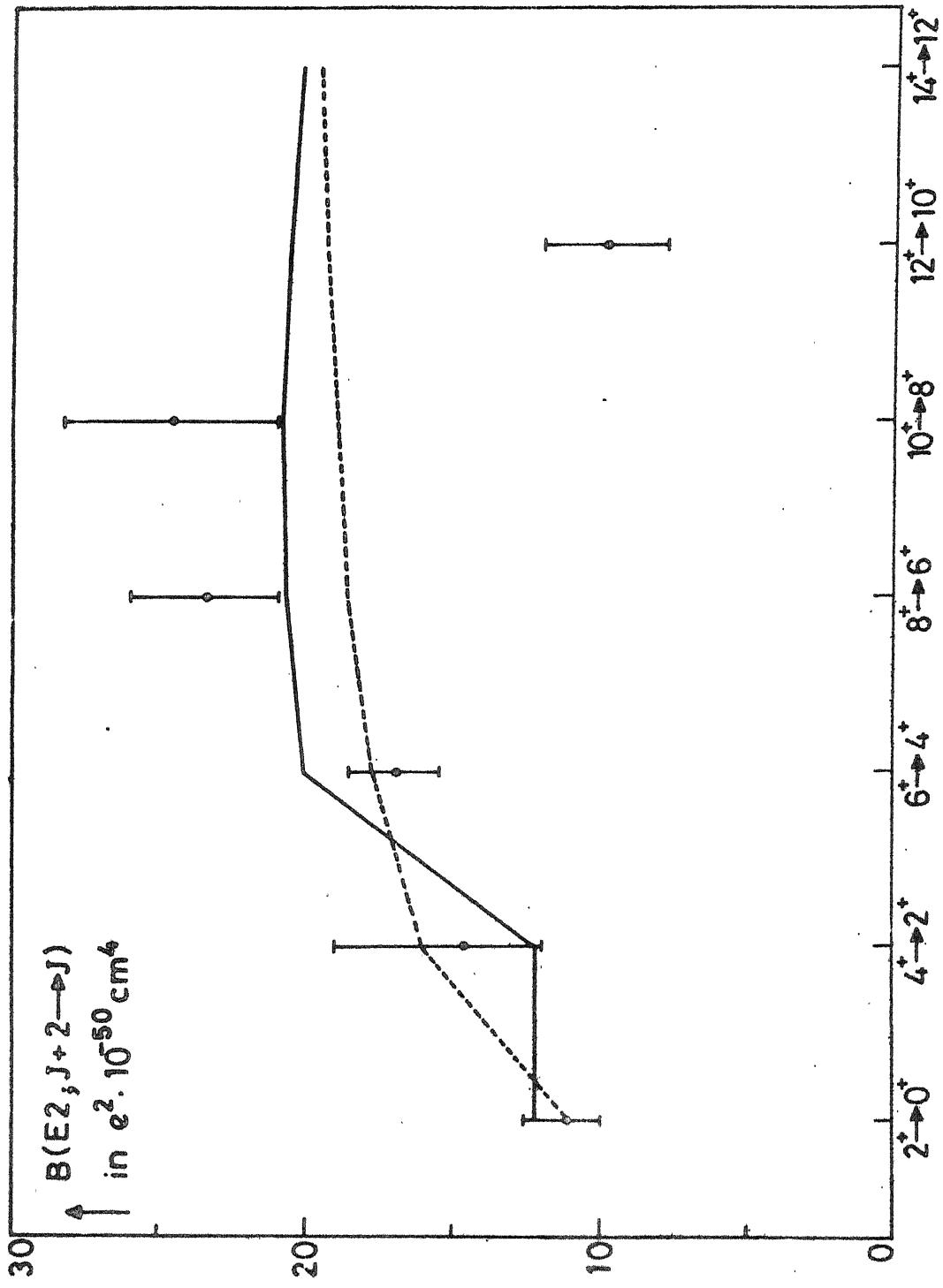
Fig. III.4   Comparison of the observed B(E2) values in $^{76}Kr$ with the predictions of the VAP model (solid line) and the rigid rotor values (dashed line).
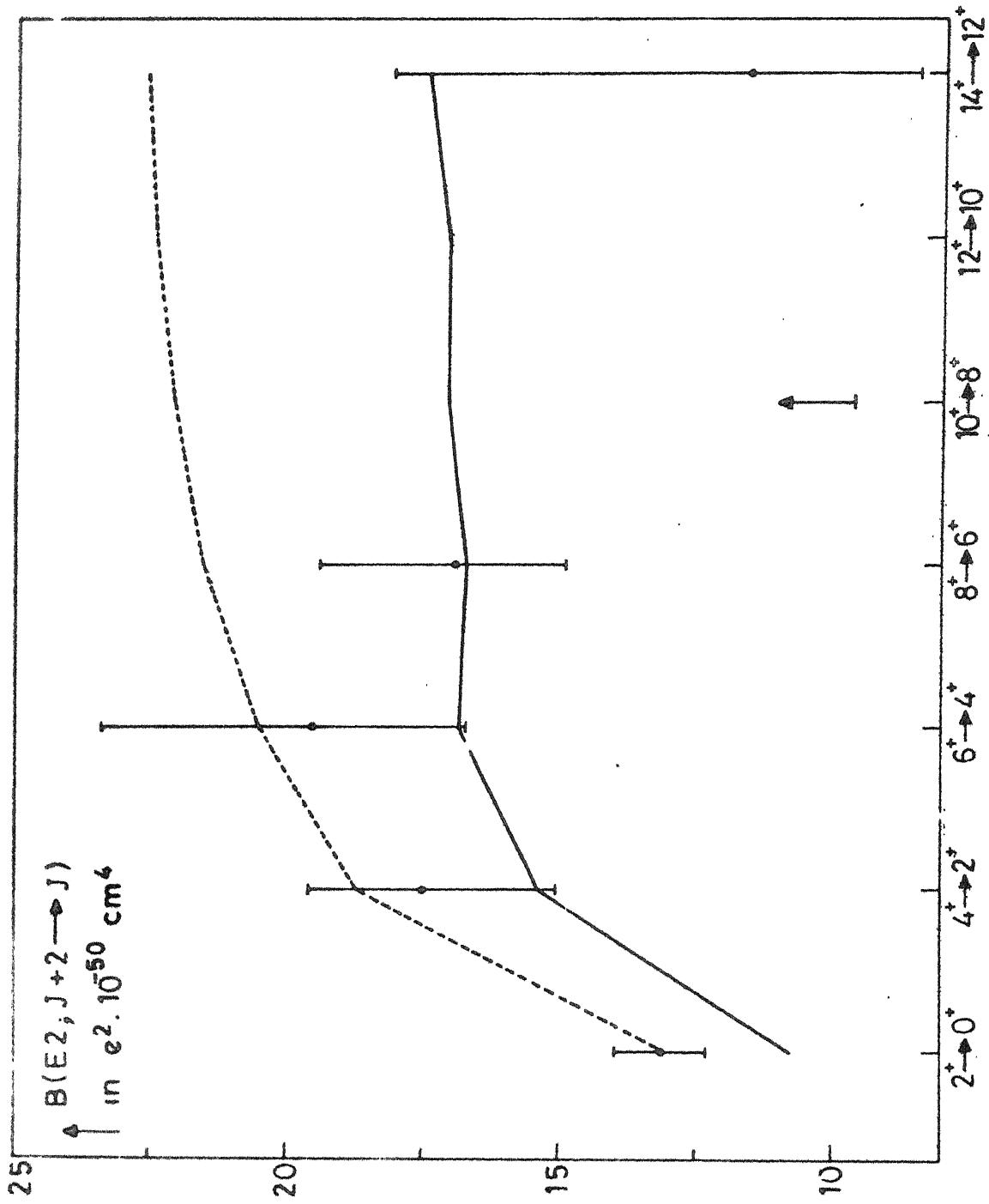
Fig. III.5   B(E2) values in $^{78}$Kr
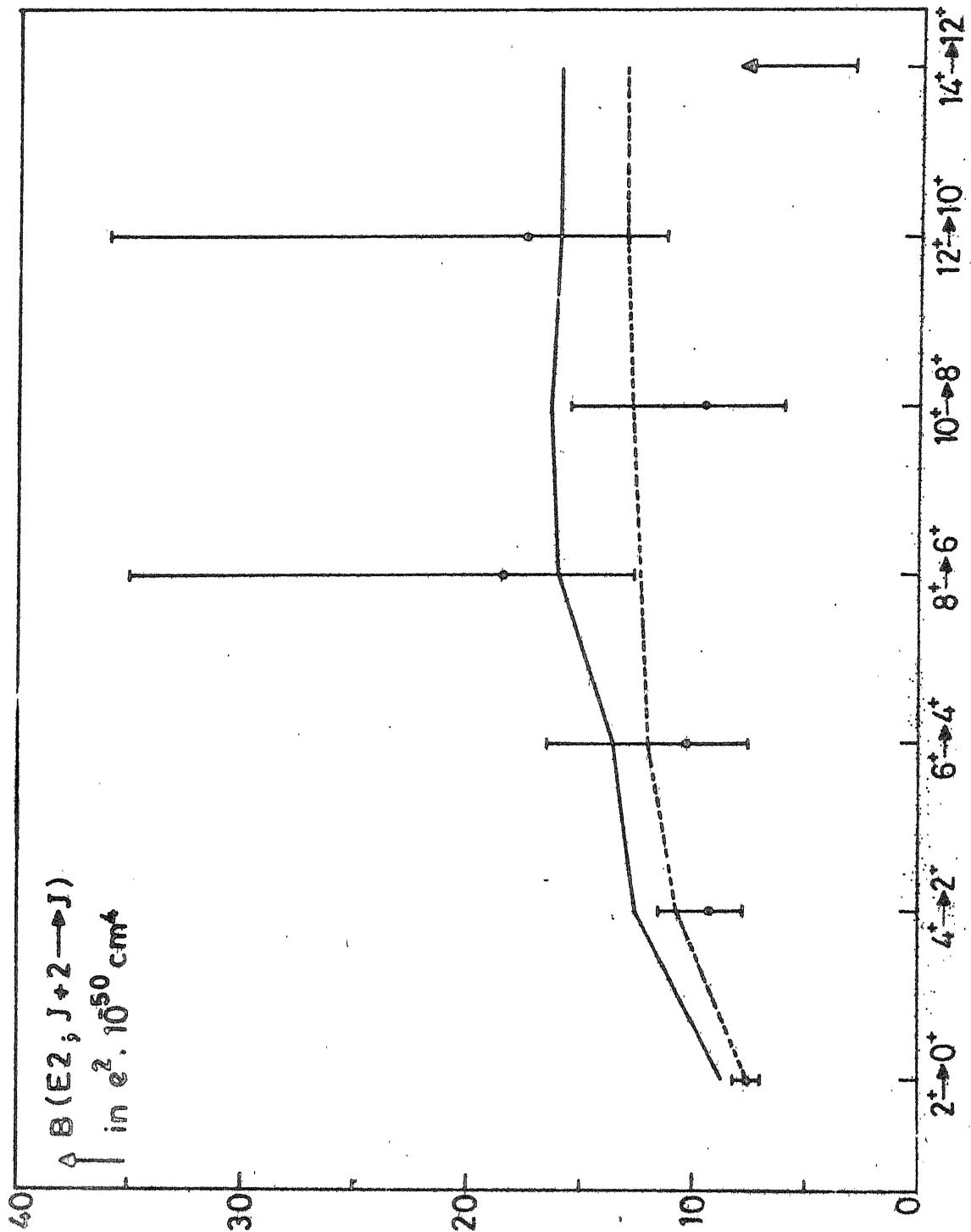
Fig. III.6 . B (E2) values in $^{80}$Kr.

shown in the Figures. From the results presented in Figure III.4 it is clear that, despite large error bars, the available data favour the VAP predictions over the rigid rotor values. Further, in the nucleus $^{78}$Kr (see Figure III.5) the deviations of the observed mean values from the rigid rotor estimates are, in most of the cases, in the directions indicated by the VAP results. Large error bars on the experimental B(E2) values in the nucleus $^{80}$Kr, however, prevent a definite conclusion; both rigid-rotor as well as VAP predictions are consistent with the available data.

The calculated VAP results for the B(E2, $J_i^+ \rightarrow J_f^+$) values in the nuclei $^{80,82,84}$Sr have been presented in Tables III.9-III.11. The observed E2 transition probabilities for the $2^+ \rightarrow 0^+$ as well as $4^+ \rightarrow 2^+$ transitions are in good agreement with the VAP estimates. The VAP prescription, however, does not provide an adequate interpretation of the observed data in the nucleus $^{84}$Sr; the computed values are quite inconsistent with the observed data for most of the transitions.

III.2.4  Occupation Numbers for Shell Model Orbits

In Tables III.12 we have given the results for the occupation numbers of the $2p_{3/2}$, $1f_{5/2}$, $2p_{1/2}$ and $1g_{9/2}$ orbits in the ground states of the nuclei $^{74,76,78,80,82}$Kr and $^{80,82,84}$Sr. Here one finds that (see Figure III.7), whereas

# TABLE III.12

The calculated values of the occupation numbers of various orbits in the ground states of some Kr and Sr isotopes. The results obtained by Kota, Pandya and Potbhare for the Kr isotopes in the framework of the spectral distribution methods have been given in round brackets

| Nucleus | Protons | | | | Neutrons | | | |
|---|---|---|---|---|---|---|---|---|
| | $2p_{1/2}$ | $2p_{3/2}$ | $1f_{5/2}$ | $1g_{9/2}$ | $2p_{1/2}$ | $2p_{3/2}$ | $1f_{5/2}$ | $1g_{9/2}$ |
| $^{74}$Kr | 0.52 | 2.09 | 3.04 | 2.28 | 0.52 | 2.27 | 3.17 | 4.03 |
| $^{76}$Kr | 0.50 (1.84) | 2.05 (3.81) | 3.21 (1.81) | 2.13 (0.54) | 0.57 | 2.47 | 3.42 | 5.56 |
| $^{78}$Kr | 0.49 (1.71) | 2.11 (3.65) | 3.24 (2.13) | 2.03 (0.51) | 0.79 | 3.17 | 3.88 | 6.30 |
| $^{80}$Kr | 0.49 (1.49) | 2.21 (3.36) | 3.31 (2.67) | 1.88 (0.48) | 1.15 | 3.57 | 4.44 | 7.07 |
| $^{82}$Kr | 0.53 (1.09) | 2.47 (3.01) | 3.45 (3.33) | 1.53 (0.57) | 1.57 | 3.81 | 5.12 | 7.79 |
| $^{80}$Sr | 0.51 | 2.02 | 3.46 | 4.03 | 0.72 | 2.88 | 3.99 | 6.54 |
| $^{82}$Sr | 0.51 | 2.00 | 3.48 | 4.04 | 0.94 | 3.33 | 4.49 | 7.39 |
| $^{84}$Sr | 0.58 | 2.47 | 3.80 | 3.14 | 1.43 | 3.75 | 5.24 | 7.85 |
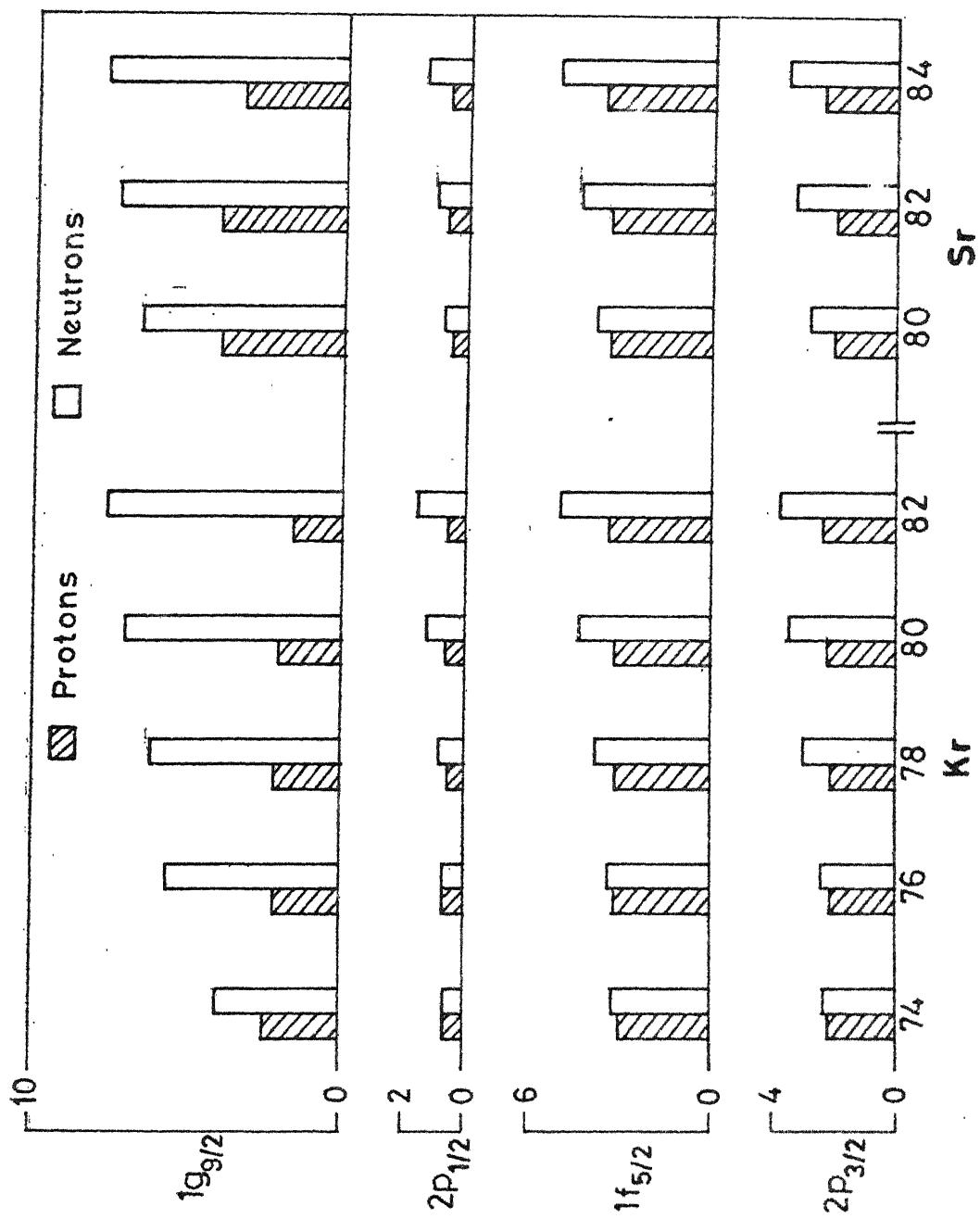
Fig. III.7    Subshell occupation numbers in some Kr and Sr isotopes.

the neutron occupation numbers for the $1f_{5/2}$ and $1g_{9/2}$ orbits display monotonic increase as a function of the neutron number, the occupation numbers for the $2p_{1/2}$ and $2p_{3/2}$ orbits remain nearly constant.

We have also given in Table III.12 the estimates obtained by Kota, Pandya and Potbhare[24] employing the spectral distribution methods. The calculations employed the same set of input parameter as the ones involved in our VAP calculations except for the slight lowering of the $1g_{9/2}$ energy by 250 keV. In contrast with the results obtained in the present work, the spectral distribution methods predict a transfer of valence protons from the 2p orbits to the $1f_{5/2}$ orbit in going from the nucleus $^{76}Kr$ to $^{82}Kr$. The estimates for the $1g_{9/2}$-proton occupation numbers resulting from the VAP method are also substantially larger than the values obtained by the spectral methods.

III.3  Conclusions

The results presented here represent an extension of the calculational framework discussed in preceding Chapter for computing the high-spin yrast spectra, static quadrupole moments, reduced transition probabilities for E2 transitions involving yrast levels, as well as the subshell occupation numbers in some Kr and Sr isotopes.

It turns out that the VAP prescription, in conjunction with the Kuo's effective interaction for the $(2p-1f-1g_{9/2})$ space, provides a fairly accurate microscopic description of the observed high-spin yrast spectra in the nuclei $^{74,76,78,80}Kr$ However, the present microscopic description appears inadequate in the nuclei $^{82}Kr$ and $^{80,82,84}Sr$; the calculated yrast spectra display significantly reduced degree of rotational collectivity in these nuclei. It may therefore be necessary to incorporate additional configurational admixtures through an explicit involvement of the $(2d_{5/2}, 3s_{1/2}, 2d_{3/2}, 1g_{7/2})$ orbits.

# REFERENCES

1.  J.Rath et al., in Proceedings of Conference of Nuclear Behaviour at High Angular Momentum (Strassbourg, France, 1980), p.25.

2.  J.H.Hamilton et al., invited talk - Fourth International Conference on Nuclei far from Stability, Helsinger, Denmark (1981) p.391.

3.  R.B.Piercey et al., Phys. Rev. Lett. 47 (1981) 1514.

4.  R.B.Piercey et al., Phys. Rev. C25 (1982) 1941.

5.  S.Matsuki et al., Nucl. Phys. A370 (1981) 1.

6.  H.P.Hellmeister et al., Nucl. Phys. A332 (1979) 241.

7.  H.P.Hellmeister et al., Phys. Lett. B85 (1979) 34.

8.  H.P.Hellmeister, Ph.D. thesis (1980), Köln University.

9.  R.L.Robinson et al., Phys. Rev. C21 (1980) 603.

10. D.G.McCauley and J.E.Draper, Phys. Rev. C4 (1971) 475.

11. L.Funke et al., Nucl. Phys. A355 (1981) 328.

12. H.G.Friederichs et al., Phys. Rev. Lett. 34 (1975) 745.

13. D.L. Sastry et al., Phys. Rev. C23 (1981) 2086.

14. C.M.Cartwright et al., J. Phys. G7 (1981) 65.

15. C.J.Lister, B.J.Varley, H.G.Price and J.W.Olness, Phys. Rev. Lett. 49 (1982) 308.

16. C.A.Fields, F.W.N.De-Boer, E.Sugarbaker and P.M.Walker, Nucl. Phys. A363 (1981) 352.

17. T.Higo, S.Matsuki and T.Yanabu, Nucl. Phys. A393 (1983) 224.

18. A.Dewald et al., Phys.Rev. C25 (1982) 226.

19. U.Kaup and A.Gelberg, Z. Phys. A293 (1979) 311.

20. A.Gelberg and U.Kaup, in _Interacting Bosons in Nuclear Physics_, edited by F.Iachello, Plenum Press, New York-London (1979) p.59.

21. A.V.Ramayya, _IEEE Transactions on Nuclear Science_ NS-28 (1981) 1273.

22. D.Bucurescu _et al._, Nucl. Phys. A401 (1983) 22.

23. R.Soundranayagam _et al._, Phys. Rev. C25 (1982) 2983.

24. V.K.B.Kota, S.P.Pandya and V.Potbhare, Phys. Rev. C25 (1982) 1667.

# CHAPTER IV

## ONSET OF LARGE DEFORMATIONS IN THE ZIRCONIUM REGION AND THE POSSIBILITY OF OCCURRENCE OF THE BACKBENDING ANOMALY IN MOLYBDENUM ISOTOPES WITH A ~ 100

## IV.1 Introduction

Cheifetz et al.[1] have some time ago discovered a new region of deformation around mass number A = 100; well-developed rotational spectra were observed in several highly neutron-rich isotopes of Zr and Mo during a study of the fission fragments of $^{252}$Cf. The observed $B(E2, 0^+ \to 2^+)$ values were as enhanced as in the rare-earth and the actinide regions.

A striking feature of the observed spectra (see Figure IV.1) in $^{90-102}$Zr is the sudden onset of deformation at N = 60; whereas one observes large energy separations (~ 0.92 MeV) between the ground and the first excited states in $^{90-98}$Zr, the yrast spectra (with $J^{\pi}_{max} = 8^+$) in the nuclei $^{100,102}$Zr are almost rotational with $(E_{2^+} - E_{0^+}) \simeq 0.21$ MeV. In the doubly-even Mo isotopes also one observes a distinct increase of rotational collectivity in going from N = 58 to N = 60.

The mass region A = 90-106 thus offers a nice example of shape transition. The region includes at one end nuclei which can be described in terms of shell model wavefunctions involving a small number of configurations[2,3]. At the other
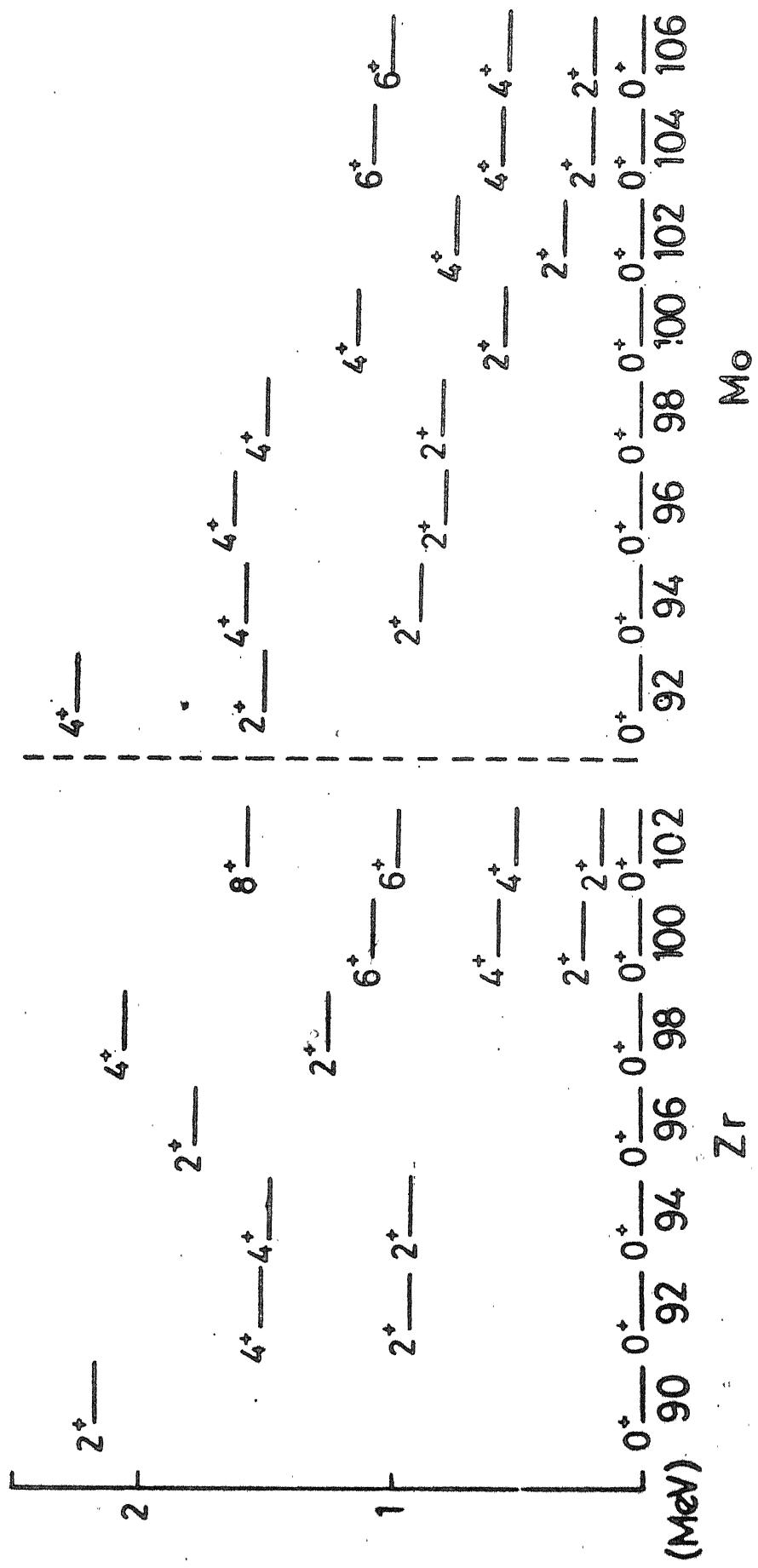
Fig. IV·1 Experimental spectra in some doubly even Zr and Mo isotopes.

$0^+$ level in $^{98}$Zr (with $E_x = 0.9$ MeV) turns out to possess a "collective" wavefunction - a wavefunction spread over many shell model configurations. It is seen that the degree of configuration mixing in the $0^+_1$ state depends very much on the relative positions of the single-particle energies of the $(1g_{9/2})_\pi$ and $(1g_{7/2})_\nu$ orbits. Having established a connection between the simultaneous occupation of the SOP orbits and the "collective" nature of the first-excited state in $^{98}$Zr, Federman et al. have suggested that the rotational states in $^{100}$Zr may also be having a structure quite similar to that of this state.

In this Chapter we examine quantitatively the dramatic onset of large deformations in the A = 90-106 mass region in the framework of the HFB method employing a valence space which is large enough to permit a systematic and unbiased study of the nuclei $^{90-102}$Zr and $^{92-106}$Mo. To this end we employ the usual pairing-plus-quadrupole-quadrupole effective interaction operating in a valence space spanned by the $2p_{1/2}$, $3s_{1/2}$, $2d_{3/2}$, $2d_{5/2}$, $1g_{7/2}$, $1g_{9/2}$ and $1h_{11/2}$ orbits for protons as well as for neutrons. The nucleus $^{76}$Sr (N = Z = 38) has been considered as an inert core. The orbit $2p_{1/2}$ has been included in the valence space in order to examine explicitly the role of the Z = 40 proton core vis-à-vis the onset of large deformations in the highly neutron-rich Zr isotopes.

The present calculation in the extended configuration space is quite successful in reproducing the observed deformation systematics in the $A = 90-106$ region, the available yrast spectra with $J^{\pi} \leq 8^+$ as well as the $B(E2, 0^+ \rightarrow 2^+)$ values in some Mo isotopes. A number of interesting features associated with the observed shape/phase transition in the Zr region are revealed. The results indicate unambiguously that the occurrence of large deformations in this region is not compatible with the earlier assumption of an inert $^{94}$Sr core[4-8]. The observed onset of quasirotational features is seen to be related to the significant deformation of the $N = 56$ core as well as to the involvement of the $1h_{11/2}$ orbit, which possesses large single-particle quadrupole moment, in the valence space. The overall n-p effective interaction is seen to play an important role through the involvement of the $Z = 40$ core protons. However, the present calculations do not substantiate the earlier conjecture[4-9] concerning the role of the n-p interactions in the SOP orbits in producing deformations; we do not observe any significant correlation between the onset of deformation and the simultaneous occupation of the $(1g_{9/2})_{\pi}$ and $(1g_{7/2})_{\nu}$ orbits[10].

Our calculations revealed the presence of the time-reversed $k = \pm 1/2$ neutron pairs from the $1h_{11/2}$ shell just below the relevant Fermi surfaces in the nuclei $^{100-104}$Mo. Since the involvement of low-k orbitals of high j parentage –

the orbitals $1i_{13/2,\pm 1/2}$, for example - has been shown to be related to the backbending effect in a number of nuclei in the rare-earth region[11], we were prompted to ask if the occurrence of the $1h_{11/2,\pm 1/2}$ orbitals near the Fermi surface could lead to dramatic structural changes in the high-spin ($J^\pi > 8^+$) yrast spectra of nuclei in the A $\sim$ 100 region. The results discussed later in this Chapter seem to answer this in affirmative.

In Section IV.2 we discuss the choices of the one- and two-body parts of the Hamiltonian that we have employed in the present work. In Section IV.3 we discuss the mechanism underlying the observed deformation trends in the Zirconium region. We next discuss, in Section IV.4, an explicit calculation of the energies as well as the electromagnetic properties of the available yrast levels (with $J^\pi \leq 8^+$) in the nuclei $^{100-106}$Mo in the framework of the VAP technique employed in the preceding Chapters in the context of the study of yrast spectra in nuclei with A = 60-80. It turns out that the VAP method in conjunction with the pairing-plus-quadrupole-quadrupole model of the effective interaction provides a reasonably good description of the low-lying yrast levels in the quasi-rotational Mo isotopes. Section IV.5 discusses the variational calculation of the high-spin (with $J^\pi \geq 8^+$) levels in Mo isotopes; the results suggest strongly the possibility of observing the backbending effect in the newly-discovered region of deformation around A = 100. Finally Section IV.6 contains some concluding remarks.

## IV.2 The One- and Two-body Parts of the Hamiltonian

The spherical single-particle energies (SPE's) that we have employed are (in MeV): $\varepsilon(2p_{1/2}) = -0.8$, $\varepsilon(1g_{9/2}) = 0.0$, $\varepsilon(2d_{5/2}) = 5.4$, $\varepsilon(3s_{1/2}) = 6.4$, $\varepsilon(2d_{3/2}) = 7.9$, $\varepsilon(1g_{7/2}) = 8.4$ and $\varepsilon(1h_{11/2}) = 8.8$. This set of the input SPE's is exactly the same as that employed in a number of successful shell model calculations for A ~90 nuclei by Vergados and Kuo[12] as well as by Federman and Pittel[5] except for the slight lowering of the $1h_{11/2}$ energy by 0.6 MeV.

The two-body effective interaction that we have employed is of "pairing + quadrupole-quadrupole (q.q)" type. The pairing part can be written as

$$V_p = - \frac{1}{4} G \sum_{\alpha \beta} S_\alpha S_\beta C_\alpha^\dagger C_{\bar{\alpha}}^\dagger C_{\bar{\beta}} C_\beta \qquad (IV.2.1)$$

where '$\alpha$' denotes the quantum numbers (nljm). The state $\bar{\alpha}$ is the same as $\alpha$ but with the sign of m reversed: $\bar{\alpha} \equiv (nlj-m)$. Here $S_\alpha$ is the phase factor $(-1)^{j-m}$. The quadrupole-quadrupole part of the two-body interaction is given by

$$V_{q.q} = - \frac{1}{2}\chi \sum_{\alpha\beta\gamma\delta} \sum_{\mu=-2}^{\mu+2} \langle\alpha| q_\mu^2 |\gamma\rangle\langle\beta| q_{-\mu}^2 |\delta\rangle (-1)^\mu C_\alpha^\dagger C_\beta^\dagger C_\delta C_\gamma \qquad (IV.2.2)$$

The operator $q_\mu^2$ is given by

$$q_\mu^2 = (16\pi/5)^{1/2} r^2 Y_\mu^2 (\theta,\phi) \qquad (IV.2.3)$$

As pointed out by Kumar and Baranger[13], the pairing + quadrupole-quadrupole interaction derives its validity from the limited size of the space; it leads to absurd consequences if it is allowed to operate in a complete set of states. The optimum size of the oscillator space is usually two major shells - a criterion which is approximately satisfied by the valence space chosen in the present work. Kumar and Baranger[13] have shown that the matrix elements of the q.q force computed for two major shells are quite similar to the ones obtained from Hamada-Johnstone potential, in terms of the G-matrix plus core polarization.

The strengths for the like-particle as well as the n-p components of the q.q interaction were taken as:
$X_{nn}$ (=$X_{pp}$) = -0.0105 MeV $b^{-4}$ and $X_{np}$ = -0.0231 MeV $b^{-4}$.
Here b (=$\sqrt{\hbar/m\omega}$) is the oscillator parameter. These values for the strengths of the q.q interactions are comparable to those suggested recently by Arima[14] on the basis of an empirical analysis of the effective interactions. The strength of the pairing interaction was fixed (through the approximate relation G = 18/A) at G = 0.18 MeV.

## IV.3  Deformation Trends in the Zirconium Region

We first discuss the nuclei $^{90,96}$Zr.  The observed spectra in these nuclei are characterized by large values ($\sim$ 2 MeV) of the $(E_{2^+} - E_{0^+})$ separations.  This can be interpreted in terms of the subshell closures for the $1g_{9/2}$ and $2d_{5/2}$ orbits.  The present calculation reproduces this feature – the minimum-energy HFB solutions that we obtain for the nuclei $^{90,96}$Zr with the present set of input parameters are indeed spherical with the structures $[(1g_{9/2})^{10}]_{J=0}$ and $[(1g_{9/2})^{10}(2d_{5/2})^{6}]_{J=0}$, respectively.  In Table IV.1 we have given the spherical SPE's for the $^{90}$Zr core-plus-one nucleon system resulting from the spherical HFB solution for $^{90}$Zr. The calculated energies compare favourably with the SPE's deduced from (d,p) as well as (p,p') reactions[15].

In Table IV.2 we present the intrinsic quadrupole moments of the HFB intrinsic states in the nuclei $^{94,98-102}$Zr and $^{92-106}$Mo.  The calculation reproduces the significant increase of the deformation that is observed in the Zr isotopes at N = 60; whereas the $<Q_0^2>_{HFB}$ value in the nucleus $^{98}$Zr is only 39.3 $b^2$ out of a maximum of 76.7 $b^2$, that for the nucleus $^{100}$Zr is about 64 per cent of the maximum possible value for this nucleus in the present valence space.  The calculated intrinsic quadrupole moments in the isotopes $^{92-106}$Mo are also consistent with the deformation systematics implied by the observed spectra.  The excitation energy of the first $2^+$ state in Mo isotopes shows large overall decrease in going from

## TABLE IV.1

Comparison of the Calculated $^{91}$Zr SPE's
with their experimental values

| Neutron orbit | Energy in (MeV) | |
| --- | --- | --- |
| | Theory | Expt. |
| $2d_{5/2}$ | 0.00 | 0.00 |
| $3s_{1/2}$ | 1.04 | 1.20 |
| $2d_{3/2}$ | 2.30 | 2.08 |
| $1g_{7/2}$ | 2.90 | 2.12 |

## TABLE IV.2

The intrinsic quadrupole moments of the HFB states in some doubly even Zr and Mo isotopes. Here $<Q_0^2>_\pi$ ( $<Q_0^2>_\nu$ ) gives the contribution of the protons (neutrons) to the total intrinsic quadrupole moment. $<Q_0^2>_{max}$ gives the maximum value of the intrinsic quadrupole moment for each isotope. The quadrupole moments have been computed in units of $b^2$

| Nucleus | $<Q_0^2>_{HFB}$ | $<Q_0^2>_\pi$ | $<Q_0^2>_\nu$ | $<Q_0^2>_{max}$ |
|---|---|---|---|---|
| $^{94}Zr$ | 24.8 | 7.5 | 17.3 | 73.5 |
| $^{98}Zr$ | 39.3 | 10.8 | 28.5 | 76.7 |
| $^{100}Zr$ | 48.4 | 12.8 | 35.6 | 75.4 |
| $^{102}Zr$ | 44.8 | 11.5 | 33.3 | 73.8 |
| $^{92}Mo$ | 13.9 | 8.6 | 5.3 | 77.9 |
| $^{94}Mo$ | 34.8 | 16.1 | 18.7 | 80.6 |
| $^{96}Mo$ | 42.3 | 17.7 | 24.6 | 84.8 |
| $^{98}Mo$ | 49.4 | 18.9 | 30.5 | 88.9 |
| $^{100}Mo$ | 54.0 | 19.5 | 34.5 | 87.9 |
| $^{102}Mo$ | 60.7 | 20.6 | 40.1 | 86.9 |
| $^{104}Mo$ | 63.6 | 21.0 | 42.6 | 86.2 |
| $^{106}Mo$ | 64.6 | 21.1 | 42.5 | 84.5 |

$^{92}$Mo to $^{106}$Mo (See Figure IV.1). Whereas the $E_{2^+}$ value in $^{92}$Mo is 1.51 MeV, it decreases to just 0.18 MeV in the nuclei $^{104,106}$Mo. We obtain here a near-spherical shape (with $<Q_0^2>_{HFB}/ <Q_0^2>_{max} = 0.18$) for $^{92}$Mo and highly deformed prolate shapes for the nucleus $^{106}$Mo - the computed $<Q_0^2>_{HFB}$ value for the latter isotope are about 76.4 per cent of the relevant $<Q_0^2>_{max}$ value. An interesting feature of the $2^+$ level is the rather abrupt drop in its position at $^{100}$Mo ($E_{2^+} = 0.54$ MeV), after remaining virtually constant at around 0.8 MeV in the nuclei $^{96,98}$Mo. This correlates well with the calculated $<Q_0^2>_{HFB}$ values; whereas the quadrupole moments for $^{96,98}$Mo are only 42.3 b$^2$ and 49.3 b$^2$, respectively, the $<Q_0^2>_{HFB}$ for the nucleus $^{100}$Mo is 54.0 b$^2$.

In Figure IV.2 we display the subshell occupation numbers for protons and neutrons calculated from the HFB intrinsic states. The onset of large deformations in the Zr and Mo isotopes is seen to be marked by a significant depletion of the $(2d_{5/2})_\nu$ orbit and a simultaneous increase of the $1h_{11/2}$ occupation numbers for the neutrons.

The results thus indicate significant polarization of the N = 56 core in the quasirotational nuclei $^{98,100,102}$Zr; the subshell closure at N = 50 is still valid for these nuclei. Our results for the deformed Mo isotopes (with A $\geq$ 100) also imply an eradication of the N = 56 subshell. A consideration
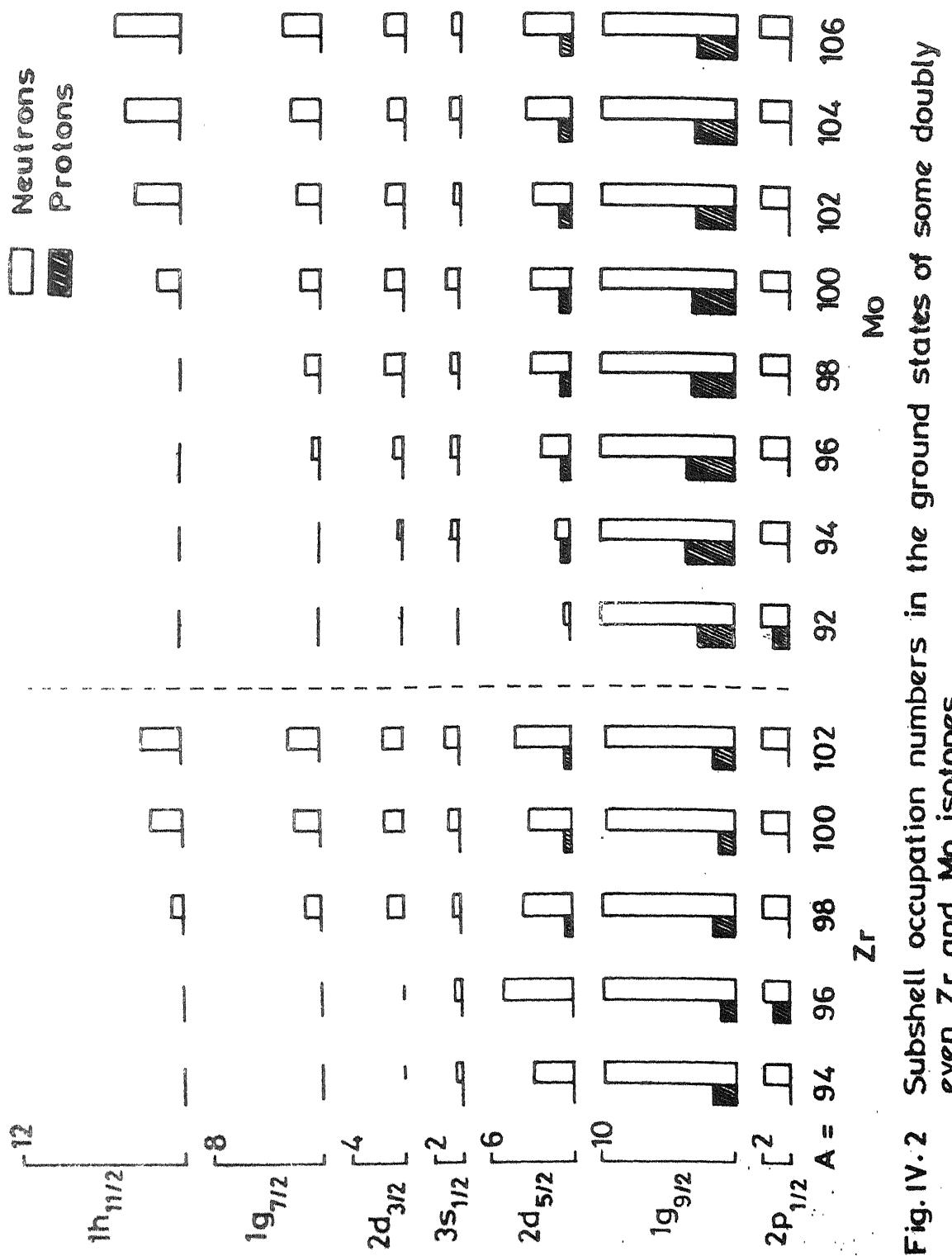
Fig. IV.2  Subshell occupation numbers in the ground states of some doubly even Zr and Mo isotopes.

of the occupation numbers for protons shows that the orbit $2p_{1/2}$ is completely empty in almost all the nuclei considered here except the nuclei $^{96}$Zr and $^{92}$Mo. This is consistent with the results obtained in some earlier shell model calculations[6] in the light (A < 98) Zr and Mo isotopes. In the nuclei $^{100-106}$Mo, the valence protons are distributed between the $1g_{9/2}$ and $2d_{5/2}$ orbits. As seen from the results presented in Table IV.2 about 30 per cent of the total $Q_0^2$ moment in these nuclei arises from protons alone. A study of the $(1g_{9/2})_\pi$ and $(1g_{7/2})_\nu$ occupation numbers in the Zr and Mo isotopes does not reveal any significant simultaneous increase in their values at A = 100. Although the $(1g_{7/2})_\nu$ occupancy is seen to increase slightly in going from A = 98 to A = 100, the $(1g_{9/2})_\pi$ occupation numbers display a small but appreciable decrease. The results obtained here, therefore, cast serious doubts on the earlier suggestion concerning the role of the n-p interaction between the valence nucleons in the SOP orbits[4-9]. The enhanced effectiveness of the $[(1g_{9/2})_\pi - (1g_{7/2})_\nu]$ interactions in producing deformations that was noticed in the earlier works[5-7] may be related to the highly restrictive nature of the valence space employed there.

IV.4  Structure of the Low-lying Yrast Levels (with $J^\pi < 8^+$) in the Isotopes $^{100-106}$Mo in the Framework of the VAP Method

As mentioned earlier, we would like to examine the consequences of the presence of the orbitals $1h_{11/2,\pm1/2}$ near the Fermi surfaces in some Mo isotopes vis-à-vis the structure of the high-spin (with $J^\pi \geq 8^+$) yrast states. However, for the calculation of these levels to be of some reliability, it is important to see whether one gets acceptable detailed agreement for the energies as well as the electromagnetic properties of the available, low-lying yrast states in the isotopes $^{100,102,104,106}$Mo.

We have computed the yrast spectra by following the procedure discussed earlier in Chapter II. We have first generated the self-consistent, axially symmetric HFB solutions $\emptyset_{K=0}(\beta)$ resulting from the Hamiltonian $(H - \beta Q_0^2)$. The optimum intrinsic state for each J, $\emptyset_{opt}(\beta_J)$, has then been selected by determining the minimum of the projected energy

$$E_J(\beta) = [<\emptyset(\beta) |HP^J| \emptyset(\beta)> / < \emptyset(\beta) |P^J| \emptyset(\beta)>] \quad (IV.4.1)$$

as a function of $\beta$. In other words, the intrinsic state for each J satisfies the following condition

$$\delta[<\emptyset(\beta) |HP^J| \emptyset(\beta)> / <\emptyset(\beta)|P^J| \emptyset(\beta)>] = 0 \quad (IV.4.2)$$

Here the operator $P^J$ projects out the eigenstates of $\hat{J}^2$ from the intrinsic states $\varnothing$ $(\beta)$. Our assumption concerning the axial symmetry of the intrinsic states is consistent with the microscopic calculation of potential energy surfaces in $^{102}Zr$ by Kumar et al.[16]; it is found that the minimum of potential energy, $V(\beta,\gamma)$, for the ground-state band occurs at $\beta = 0.4$, $\gamma = 10^\circ$ and, therefore, the effects due to non-axiality are expected to be small at least for the yrast levels in Zr and Mo isotopes with A ~100.

It may be mentioned that variational methods quite similar to the one employed here have earlier been used by Faessler et al.[17] as well as Nair and Ansari[18] in connection with the study of the back-bending effect in $^{158}Er$. The present calculation, however, employs exact angular momentum projection, in contrast with the technique used by Nair and Ansari[18] which involved an approximation suggested by Das Gupta and Van Ginneken[19].

In Figure IV.3 we present a comparison of the calculated low-lying yrast spectra in the isotopes $^{100,102,104,106}Mo$ with the experimental ones. From the figure (the portion inside the rectangles) one observes that the present calculation yields a satisfactory overall agreement with the experiments, particularly in view of the fact that we have not used any parameter to mock up the contributions of the N=Z=38 core towards the moment of inertia.
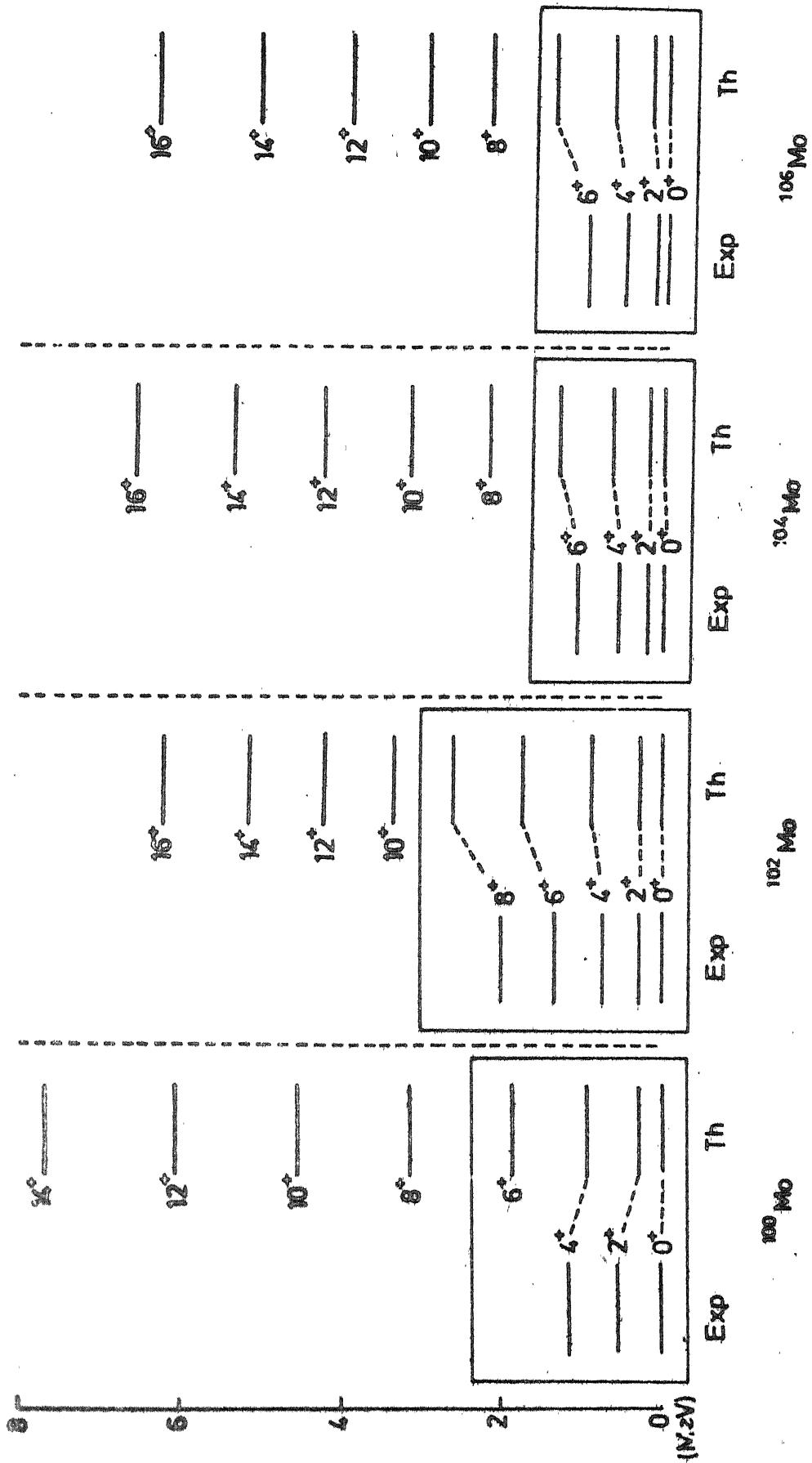
Fig. IV.3 Comparison of the observed as well as the calculated yrast spectra in the nuclei $^{100,102,104,106}$Mo.

The calculation is seen to reproduce the observed levels with $J^\pi \leq 6^+$ within an accuracy of about 400 KeV. The $J^\pi = 8^+$ level in $^{102}$Mo — and it happens to be the highest spin observed so far in the A ~100 region — shows a discrepancy of about 600 KeV.

We next consider the reduced transition probabilities for E2 transitions, B(E2, $0^+ \rightarrow 2^+$), in the Mo isotopes. In Table IV.3 we present a comparison of the observed[20] B(E2, $0^+ \rightarrow 2^+$) values with the ones computed in terms of the J=0 and J=2 states projected from the variational intrinsic states. The states with good angular momenta J projected from the axially symmetric intrinsic state $| \phi_{K=0} >$ can be written as

$$| \Psi_K^J > = P_{KK}^J | \phi_K > = \left(\frac{2J+1}{8\pi^2}\right)^{1/2} \int D_{KK}^J (\Omega) R(\Omega) |\phi_K> d\Omega \qquad (IV.4.3)$$

where $R(\Omega)$ and $D_{KK}^J(\Omega)$ are the rotation operator and the rotation matrix respectively. Using the projected wave functions one obtains

$$B(E2, 0^+ \rightarrow 2^+) = \left(\frac{1}{16\pi}\right) |< \Psi^2 || Q^2 || \Psi^2 > |^2 \qquad (IV.4.4)$$

where $Q_\mu^2 = (16\pi/5)^{1/2} (r^2/b^2) Y_\mu^2 (\Omega)$.

It is seen that the present microscopic description permits an adequate interpretation of the available electromagnetic data in terms of a reasonable variation of the isoscalar effective charges; the computed B(E2) estimates are in remarkably good agreement with the experiments provided one

## TABLE IV.3

Comparison of the calculated and the observed[20] $B(E2, 0^+ \rightarrow 2^+)$ values in some quasirotational Mo isotopes. The effective charges have been used such that for protons the effective charge is $e_p = 1 + e_{eff}$ and for neutrons it is $e_n = e_{eff}$. The values of the oscillator parameter have been calculated from the relation $b = 1.01 \ A^{1/6}$ fm.

| Nucleus | $B(E2, \ 0^+ \rightarrow 2^+) \times 10^{-50} \ e^2 \ cm^4$ | | | |
|---------|--------------------|----------|----------|------|
| | Calculated | | | Expt. |
| | $e_{eff}=0.35$ | $= 0.50$ | $= 0.65$ | |
| $^{94}$Mo | 18.2 | 26.6 | 36.7 | $19.8 \pm 0.3$ |
| $^{96}$Mo | 24.4 | 36.1 | 50.0 | $27.1 \pm 0.4$ |
| $^{98}$Mo | 28.3 | 42.3 | 59.1 | $26.7 \pm 0.5$ |
| $^{100}$Mo | 37.4 | 54.4 | 74.5 | $51.2 \pm 0.9$ |
| $^{102}$Mo | 47.9 | 70.8 | 98.2 | $108.1^{+13.9}_{-11.1}$ |

chooses $e_{eff} = 0.35$ for $^{94,96,98}Mo$, $e_{eff} = 0.50$ for $^{100}Mo$
and $e_{eff} = 0.65$ for $^{102}Mo$. It may be mentioned here that a
small, systematic increase in the effective charges in going
from A=94 to A=102 is not totally unanticipated in the present
calculational framework since the explicit involvement of the
N=Z=38 core is expected to increase during the onset of
deformation at A=100.

## IV.5 Backbending Phenomenon in the Nuclei $^{100,102,104,106}Mo$

We have extended the calculation of the yrast spectra
to $J^{\pi} = 16^{+}$. In Figure IV.4 we present the usual I-versus-$\omega^2$
curves for the nuclei $^{100-106}Mo$. The following expressions
have been used to compute the moment of inertia (I) and the
squared angular frequency ($\omega^2$) in terms of the yrast energies:

$$2I/\hbar^2 = (4J-2)/(E_J-E_{J-2}); \quad (\hbar\omega)^2 = (J^2-J+1)(E_J-E_{J-2})^2/(2J-1)^2$$

$$(IV.5.1)$$

The results presented in Figure IV.4 again indicate
that we do have good overall qualitative agreement between the
calculated and the observed variation of I as a function of $\omega^2$
for the available levels with $J^{\pi} \leq 8^{+}$. The present calcu-
lation is seen to reveal distinct backbending effect at
$J^{\pi} = 8^{+}$ in the nucleus $^{102}Mo$. From the results presented in
Table IV.4 we see that the sudden decrease of $(E_J-E_{J-2})$ at
J = 8 owes its origin to a dramatic increase in the quadrupole
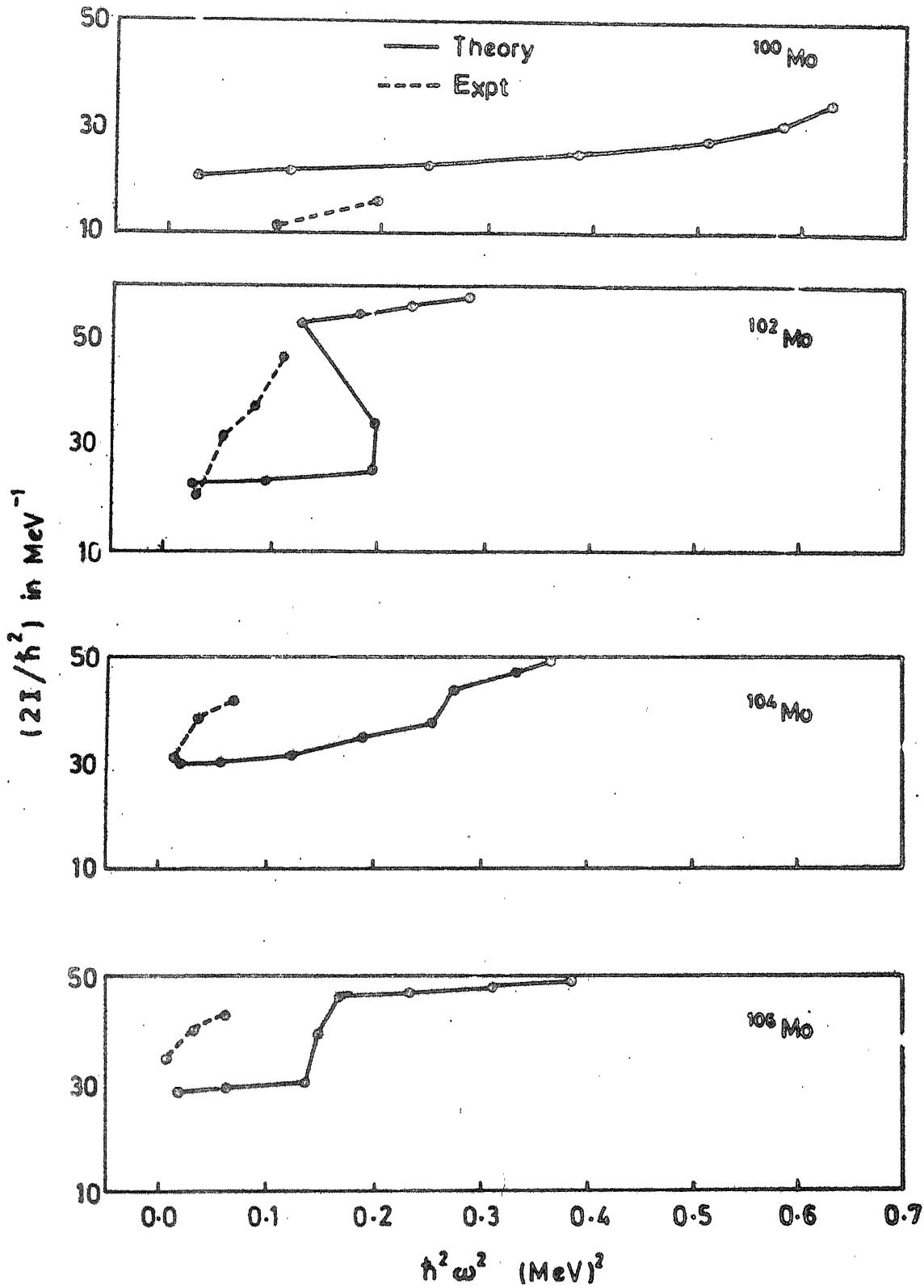
Fig. IV.4 I-versus-$\omega^2$ curves for the high-spin yrast levels in the nuclei $^{100, 102, 104, 106}$Mo.

## TABLE IV.4

Quadrupole moments as well as the subshell occupation numbers associated with the optimum intrinsic states for the yrast levels in the nuclei $100, 102, 104, 106_{Mo}$

| Nucleus | $J^\pi$ | $\langle \phi(\beta_J) | Q_0^2 | \phi(\beta_J) \rangle$ | $\langle Q_0^2 \rangle_{max}$ | Subshell occupation numbers | | | | |
| --- | --- | --- | --- | --- | --- | --- | --- | --- |
| | | | | $(2d_{5/2})_\pi$ | $(1g_{9/2})_\pi$ | $(2d_{5/2})_\nu$ | $(1g_{9/2})_\nu$ | $(1h_{11/2})_\nu$ |
| $100_{Mo}$ | $0^+-6^+$ | 57.7 | 87.9 | 0.79 | 3.03 | 2.71 | 9.78 | 1.88 |
| | $8^+$ | 59.0 | | 0.84 | 2.95 | 2.69 | 9.75 | 1.95 |
| | $10^+-16^+$ | 60.1 | | 0.89 | 2.87 | 2.61 | 9.72 | 2.00 |
| $102_{Mo}$ | $0^+-4^+$ | 61.3 | 86.9 | 0.81 | 3.00 | 2.96 | 9.80 | 3.21 |
| | $6^+$ | 62.5 | | 0.85 | 2.94 | 2.86 | 9.78 | 3.36 |
| | $8^+-16^+$ | 67.7 | | 1.03 | 2.62 | 2.32 | 9.67 | 3.97 |
| $104_{Mo}$ | $0^+-4^+$ | 63.8 | 86.2 | 0.85 | 2.94 | 3.25 | 9.81 | 4.28 |
| | $6^+-10^+$ | 65.3 | | 0.90 | 2.85 | 3.16 | 9.78 | 4.40 |
| | $12^+-16^+$ | 67.3 | | 0.98 | 2.72 | 2.99 | 9.74 | 4.65 |
| $106_{Mo}$ | $0^+-6^+$ | 65.1 | 84.5 | 0.87 | 2.91 | 3.65 | 9.83 | 5.09 |
| | $8^+-16^+$ | 70.8 | | 1.05 | 2.57 | 3.25 | 9.75 | 5.98 |

deformation of the intrinsic state — from $<Q_0^2> = 62.5$ $b^2$
at $J=6$ to $<Q_0^2> = 67.7$ $b^2$ at $J=8$ — along the yrast cascade.
An examination of the subshell occupation numbers (see columns
5-9, Table IV.4) calculated from the optimum intrinsic states
associated with the yrast levels further reveals that the
increase in the intrinsic quadrupole moment is correlated with
a significant depletion of the $(1g_{9/2})_\pi$ and $(2d_{5/2}, 1g_{9/2})_\nu$
orbits and an enhanced occupation of the $(2d_{5/2})_\pi$ and the
$(1h_{11/2})_\nu$ orbits. It may be pointed out that an increase in
the occupation number for $1h_{11/2}$ orbit from 3.36 for $J^\pi = 6^+$
to 3.97 for $J^\pi = 8^+$ is quite efficacious in enhancing the
intrinsic quadrupole deformation since it implies an increased
occupation of the $1h_{11/2, \pm 1/2; \pm 3/2}$ orbitals which are
characterized by large values of the single-particle matrix
element of the quadrupole operator.

## IV.6  Conclusions

Summarizing, the observed dramatic onset of large
deformations around $A = 100$ in the Zirconium region can be
understood in a microscopic framework in terms of the two not
unrelated features, namely, the polarization of the conven-
tional ($Z = 40$, $N = 56$) core and the participation of the
$1h_{11/2}$ orbit in the valence space. It turns out that, whereas
the cumulative n-p interaction does play an important role via
the non-closure of $Z = 40$ proton core, the calculations do not

indicate any selective involvement of the SOP orbits vis-á-vis the occurrence of large deformations for $A \geq 100$.

Further, the calculations presented in this Chapter suggest strongly the possibility of observing dramatic structural changes for $J^{\pi} > 8^+$ in the yrast spectrum in $^{102}$Mo because of a sudden increase in deformation due to crossing of $1h_{11/2;\pm1/2,\pm3/2}$ levels at the Fermi surface. If discovered experimentally, this will be the first evidence concerning a backbend in the newly discovered island of deformation around $A = 100$.

# REFERENCES

1.  E.Cheifetz et al., Phys. Rev. Letters $\underline{25}$ (1970) 38.

2.  N.Auerbach and I.Talmi, Nucl. Phys. $\underline{64}$ (1965) 458.

3.  D.H.Gloeckner, Nucl. Phys. $\underline{253A}$ (1975) 301.

4.  P.Federman and S.Pittel, Phys. Letters $\underline{69B}$ (1977); 385.

5.  P.Federman and S.Pittel, Phys.Letters $\underline{77B}$ (1978) 29.

6.  P.Federman, S.Pittel and R.Campos, Phys. Letters $\underline{82B}$ (1979) 9.

7.  P.Federman Sand S.Pittel, Phys. Rev. $\underline{C20}$ (1979) 820.

8.  S.Pittel, Nucl.Phys. $\underline{A347}$ (1980) 417.

9.  R.F.Casten et.al., Phys. Rev. Letters $\underline{47}$ (1981) 1433.

10. S.K.Khosa, P.N.Tripathi and S.K.Sharma, Phys. Lett. $\underline{119B}$ (1982) 257.

11. A.L.Goodman, in Advances in Nuclear Physics, Eds. J.W.Negele and E.Vogt (Plenum Press, New York-London 1979), Vol.11.

12. J.D.Vergados and T.T.S.Kuo, Phys. Lett. $\underline{35B}$ (1971) 93.

13. M.Baranger and K.Kumar, Nucl. Phys. $\underline{A110}$ (1968) 490.

14. A.Arima, Nucl. Phys. $\underline{A354}$ (1981) 19.

15. C.R.Bingham and M.L.Halbert, Phys. Rev. $\underline{C2}$ (1970) 2297.

16. K.Kumar et al., Phys. Rev. $\underline{C16}$ (1977) 1235.

17. A.Faessler, L.Lin and F.Wittman, Phys. Lett. $\underline{44B}$ (1973) 127.

18. S.C.K.Nair and A.Ansari, Phys. Lett. $\underline{47B}$ (1973) 200.

19. S.Das Gupta and A.Van Ginneken, Phys. Rev. $\underline{164}$ (1967) 1320.

20. P.Paradis et al., Phys. Rev. $\underline{C14}$ (1976) 835; ibid. $\underline{C20}$ (1979) 1201.

# CHAPTER V

## CONCLUSIONS

The spectra in the nuclei in the A=60-80 region of the Periodic Table are quite complex. Recent in-beam gamma-ray spectroscopy experiments have revealed multiple band structure in these nuclei. The complexity of the structure of these nuclei is related to the fact that the orbits spanning the underlying valence space do not exhibit strong sub-shell closures between the magic numbers 28 and 50.

The study of the yrast levels of doubly even Ge, Se, Kr and Sr isotopes presented in this work was motivated by a desire to assess the efficacy of the VAP method in the context of a microscopic description of the high-spin yrast levels. The results presented in Chapters II and III indicate that the calculational framework employed here can be considered fairly reliable for interpreting and correlating the available data on the yrast energies as well as intercascade E2 transition probabilities.

The results of the VAP calculations in Sr isotopes should be taken _cum grano salis_. It will be interesting to examine the effects arising from onset of non-axial deformations by invoking the cranked HFB method.

In Chapter IV we studied the available yrast spectra in Mo isotopes in the framework of the VAP method. The calculations suggested strongly the heretofore unanticipated possibility of observing the backbending effect in the yrast spectrum in $^{102}$Mo. In this connection, it will be very interesting to examine in Mo isotopes the consequences of the realignment of a $1h_{11/2}$ neutron pair along the rotation axis in the framework of the cranked HFB prescription.

## APPENDIX A

## THE ($2p_{1/2}$, $2p_{3/2}$, $1f_{5/2}$, $1g_{9/2}$) MATRIX ELEMENTS OF THE KUO INTERACTION

We tabulate here the matrix elements $V = \langle ab\ JT \mid V \mid c\ d\ JT \rangle$ of the Kuo interaction. The shell-model orbits are labelled by numbers:

| 8 | 9 | 10 | 11 |
|---|---|----|----|
| $2p_{3/2}$ | $1f_{5/2}$ | $2p_{1/2}$ | $1g_{9/2}$ |

| T | a | b | c | d | J | V | J | V | J | V |
|---|---|---|---|---|---|---|---|---|---|---|
| 0 | 8 | 8 | 8 | 8 | 1 | -0.8540 | 3 | -1.2313 | | |
| 0 | 8 | 8 | 8 | 9 | 1 | 0.0598 | 3 | 0.4201 | | |
| 0 | 8 | 8 | 8 | 10 | 1 | 0.7818 | | | | |
| 0 | 8 | 8 | 9 | 9 | 1 | 0.0638 | 3 | -0.0996 | | |
| 0 | 8 | 8 | 9 | 10 | 3 | -0.1320 | | | | |
| 0 | 8 | 8 | 10 | 10 | 1 | 0.0515 | | | | |
| 0 | 8 | 8 | 11 | 11 | 1 | 0.4642 | 3 | 0.2704 | | |
| 0 | 8 | 9 | 8 | 9 | 1 | -2.0460 | 2 | -0.9794 | 3 | -0.4176 |
| | | | | | 4 | -1.0385 | | | | |
| 0 | 8 | 9 | 8 | 10 | 1 | -0.7307 | 2 | -0.2676 | | |
| 0 | 8 | 9 | 9 | 9 | 1 | 0.7305 | 3 | 0.4284 | | |
| 0 | 8 | 9 | 9 | 10 | 2 | 0.7489 | 3 | 0.7749 | | |
| 0 | 8 | 9 | 10 | 10 | 1 | 0.5407 | | | | |
| 0 | 8 | 9 | 11 | 11 | 1 | 0.3585 | 3 | 0.0080 | | |
| 0 | 8 | 10 | 8 | 10 | 1 | -1.8867 | 2 | -1.2149 | | |
| 0 | 8 | 10 | 9 | 9 | 1 | -0.0250 | | | | |
| 0 | 8 | 10 | 9 | 10 | 2 | 0.5535 | | | | |

| T | a | b | c | d | J | V | J | V | J | V |
|---|---|---|---|---|---|---|---|---|---|---|
| 0 | 8 | 10 | 10 | 10 | 1 | 0.3185 | | | | |
| 0 | 8 | 10 | 11 | 11 | 1 | -0.3006 | | | | |
| 0 | 8 | 11 | 8 | 11 | 3 | -0.6248 | 4 | -0.5251 | 5 | 0.0265 |
| | | | | | 6 | -1.5399 | | | | |
| 0 | 8 | 11 | 9 | 11 | 3 | 0.6830 | 4 | -0.4880 | 5 | 0.1660 |
| | | | | | 6 | -0.6857 | | | | |
| 0 | 8 | 11 | 10 | 11 | 4 | -0.7682 | 5 | 0.3138 | | |
| 0 | 9 | 9 | 9 | 9 | 1 | -0.8225 | 3 | -0.3281 | 5 | -1.5049 |
| 0 | 9 | 9 | 9 | 10 | 3 | -0.7073 | | | | |
| 0 | 9 | 9 | 10 | 10 | 1 | -0.2413 | | | | |
| 0 | 9 | 9 | 11 | 11 | 1 | -0.5589 | 3 | -0.1943 | 5 | -0.1327 |
| 0 | 9 | 10 | 9 | 10 | 2 | -0.2495 | 3 | -1.3401 | | |
| 0 | 9 | 10 | 11 | 11 | 3 | -0.1623 | | | | |
| 0 | 9 | 11 | 9 | 11 | 2 | -2.6003 | 3 | -1.3009 | 4 | -0.7192 |
| | | | | | 5 | -1.0607 | 6 | -0.2775 | 7 | -1.7289 |
| 0 | 9 | 11 | 10 | 11 | 4 | -0.6607 | 5 | -0.7714 | | |
| 0 | 10 | 10 | 10 | 10 | 1 | -0.9367 | | | | |
| 0 | 10 | 10 | 11 | 11 | 1 | -0.1996 | | | | |
| 0 | 10 | 11 | 10 | 11 | 4 | -1.0293 | 5 | -0.5851 | | |
| 0 | 11 | 11 | 11 | 11 | 1 | -0.8509 | 3 | -0.2029 | 5 | -0.1742 |
| | | | | | 7 | -0.3696 | 9 | -1.4859 | | |

| T | a | b | c | d | J | V | J | V | J | V |
|---|---|---|---|---|---|---|---|---|---|---|
| 1 | 8 | 8 | 8 | 8 | 0 | -0.6518 | 2 | -0.2435 | | |
| 1 | 8 | 8 | 8 | 9 | 2 | -0.1621 | | | | |
| 1 | 8 | 8 | 8 | 10 | 2 | -0.2601 | | | | |
| 1 | 8 | 8 | 9 | 9 | 0 | -1.0695 | 2 | -0.1882 | | |
| 1 | 8 | 8 | 9 | 10 | 2 | -0.1122 | | | | |
| 1 | 8 | 8 | 10 | 10 | 0 | -0.8151 | | | | |
| 1 | 8 | 8 | 11 | 11 | 0 | -1.0621 | 2 | -0.3771 | | |
| 1 | 8 | 9 | 8 | 9 | 1 | 0.3127 | 2 | 0.2151 | 3 | 0.3185 |
| | | | | | 4 | -0.1686 | | | | |
| 1 | 8 | 9 | 8 | 10 | 1 | -0.0566 | 2 | -0.1587 | | |
| 1 | 8 | 9 | 9 | 9 | 2 | -0.1456 | 4 | -0.2365 | | |
| 1 | 8 | 9 | 9 | 10 | 2 | -0.2301 | 3 | 0.0989 | | |
| 1 | 8 | 9 | 11 | 11 | 2 | 0.3549 | 4 | 0.3686 | | |
| 1 | 8 | 10 | 8 | 10 | 1 | 0.0573 | 2 | -0.3799 | | |
| 1 | 8 | 10 | 9 | 9 | 2 | -0.3792 | | | | |
| 1 | 8 | 10 | 9 | 10 | 2 | -0.3782 | | | | |
| 1 | 8 | 10 | 11 | 11 | 2 | 0.2532 | | | | |
| 1 | 8 | 11 | 8 | 11 | 3 | -0.5447 | 4 | 0.1101 | 5 | -0.0060 |
| | | | | | 6 | 0.1767 | | | | |
| 1 | 8 | 11 | 9 | 11 | 3 | 0.3612 | 4 | 0.0435 | 5 | 0.2148 |
| | | | | | 6 | 0.0053 | | | | |
| 1 | 8 | 11 | 10 | 11 | 4 | -0.2115 | 5 | 0.3110 | | |
| 1 | 9 | 9 | 9 | 9 | 0 | -1.5783 | 2 | -0.1408 | 4 | 0.3567 |
| 1 | 9 | 9 | 9 | 10 | 2 | -0.4941 | | | | |
| 1 | 9 | 9 | 10 | 10 | 0 | -0.8355 | | | | |

| T | a | b | c | d | J | V | J | V | J | V |
|---|---|---|---|---|---|---|---|---|---|---|
| 1 | 9 | 9 | 11 | 11 | 0 | 1.9064 | 2 | 0.3505 | 4 | 0.1940 |
| 1 | 9 | 10 | 9 | 10 | 2 | −0.2321 | 3 | 0.5355 | | |
| 1 | 9 | 10 | 11 | 11 | 2 | 0.4929 | | | | |
| 1 | 9 | 11 | 9 | 11 | 2 | −0.6215 | 3 | −0.2006 | 4 | 0.0600 |
| | | | | | 5 | −0.1524 | 6 | 0.1745 | 7 | −0.8839 |
| 1 | 9 | 11 | 10 | 11 | 4 | −0.1677 | 5 | −0.4116 | | |
| 1 | 10 | 10 | 10 | 10 | 0 | −0.1462 | | | | |
| 1 | 10 | 10 | 11 | 11 | 0 | 0.6687 | | | | |
| 1 | 10 | 11 | 10 | 11 | 4 | 0.0467 | 5 | −0.2121 | | |
| 1 | 11 | 11 | 11 | 11 | 0 | −1.4203 | 2 | −0.7103 | 4 | −0.1848 |
| | | | | | 6 | 0.0072 | 8 | 0.1436 | | |